



**Paulo Alexandre
Oliveira Cardoso**

**Desenvolvimento de sistema para recuperação de
energia das ondas**

Development of a Power Take-off for wave energy
generation



**Paulo Alexandre
Oliveira Cardoso**

Desenvolvimento de sistema para recuperação de energia das ondas

Development of a Power Take-off for wave energy generation

Dissertação apresentada à Universidade de Aveiro para cumprimento dos requisitos necessários à obtenção do grau de Mestre em Engenharia Mecânica, realizada sob orientação científica de Jorge Augusto Fernandes Ferreira, Professor Associado do Departamento de Engenharia Mecânica da Universidade de Aveiro, e de António Manuel de Amaral Monteiro Ramos, Professor Auxiliar do Departamento de Engenharia Mecânica da Universidade de Aveiro.

Esta dissertação teve o apoio dos projetos UIDB/00481/2020 e UIDP/00481/2020 - Fundação para a Ciência e a Tecnologia; e CENTRO-01-0145 FEDER-022083 - Programa Operacional Regional do Centro (Centro2020), através do Portugal 2020 e do Fundo Europeu de Desenvolvimento Regional.

o júri / the jury

presidente / president

Prof. Doutor Nelson Amadeu Dias Martins

Professor Associado da Universidade de Aveiro

Prof. Doutor Daniel Gil Afonso

Professor adjunto da Escola Superior de Design, Gestão e Tecnologias da produção de Aveiro Norte

Prof. Doutor Jorge Augusto Fernandes Ferreira

Professor Associado da Universidade de Aveiro (orientador)

Agradecimentos / Acknowledgements

Em primeiro lugar, quero agradecer ao meu orientador Professor Jorge Ferreira e ao meu co-orientador Professor António Ramos, pelas opiniões que me guiaram nesta dissertação.

Aos amigos que fiz durante o meu processo académico que tornaram o estar longe de casa mais agradável.

Aos velhos amigos, que apesar de cada vez mais longe, me levam a que continue fiel a mim próprio.

E cima de tudo, obrigado aos meus pais e avós por me darem a oportunidade de continuar a estudar e por me guiarem até este momento, não os vou esquecer!

Keywords

RES, WEC, Power Take-off, Mechanical PTO, Rack and Pinion

Abstract

Currently we face an ever enlarging threat by the environment. Years of pollution have culminated in this situation. One of the biggest sectors contributing for this reality is the energy sector, this when paired up with the ever rising need for electricity can further damage our planet. Fortunately, most countries and other big organizations are aware of this situation, and thus, are providing solutions to transform the energy sector. This can be seen in the rising percentage of electricity produced by renewable sources. However, due to the uncontrollable nature of most Renewable Energy Sources (RES) this percentage may never reach 100%. For this reason it is necessary to diversify our sources. One possible expansion of our current sources might be the wave energy. This source as a very high potential, not just for the large amount of ocean in our planet, but also, due to its relative predictability when compared with most other RES. As it currently stands, this source as only been theorised and as not yet reached any marketable device, only prototypes. For this reason it is important to contribute to this field in order to make this technology more reliable and to diversify our energy sources. This dissertation shows the development of a mechanical Power Take-Off (PTO), based on a rack and pinion gear train, for Wave Energy Converters (WEC), from an initial review of current technology to a ready to produce prototype, detailing every engineering decision.

Palavras-chave

Energia Renovavel, Energia das Ondas, Conversor de Energia, Conversor de Energia Mecanico, Pinhão e Cremalheira

Resumo

Atualmente enfrentamos uma cada vez maior pressão sobre o meio ambiente. Anos continuados de poluição trouxeram-nos a este ponto. Um dos setores mais responsáveis por esta realidade é o setor da energia, que quando conjugado com a cada vez maior procura pode conduzir ao agravamento da situação atual. Felizmente, a maioria dos países e das grandes organizações são conhecedoras desta realidade e procuram solucionar o setor da energia transformando-o através do aumento das energias renováveis. No entanto, a maioria destas energias renováveis não são consistentes e por isso dificilmente vão conseguir substituir as alternativas não renováveis por completo. Dada esta limitação é necessário expandir as nossas fontes de energia. A energia das ondas mostra-se como uma potencial alternativa. Esta fonte de energia parece ter um maior potencial, não só pela larga extensão de oceanos no planeta, mas também por ser mais previsível quando comparada com as outras fontes de energia renováveis. De momento, este tipo de energia tem sido alvo de estudos, chegando até a protótipos, no entanto, nenhum dos equipamentos testados chegou ao mercado com sucesso. Por este motivo é importante contribuir para o desenvolvimento desta tecnologia a fim de diversificar as nossas fontes de energia. Nesta dissertação apresenta-se o processo de desenvolvimento de um conversor de energia mecânico, baseado num sistema de pinhão e cremalheira, desde um estudo dos métodos usados em protótipos anteriores até um protótipo pronto a produzir.

Contents

1	Introduction	1
1.1	Context	1
1.2	Objective	3
2	Current Technology Review	5
2.1	Wave Energy Prototypes	5
2.1.1	Pitch	6
2.1.2	Heave	7
2.1.3	Surge	9
2.1.4	Other	9
2.2	PTO Methods	11
2.2.1	Direct Electrical Drive	11
2.2.2	Direct Mechanical Drive	12
2.2.3	Hydraulic	12
2.2.4	Turbine	13
2.3	Movement Converters	13
2.3.1	Rack and Pinion	13
2.3.2	Ball Screw	13
2.3.3	Roller Screw	14
2.3.4	Lead Screw	15
2.3.5	Belt Drive	15
2.3.6	Magnetic Systems	15
2.4	Energy Conversion	16
3	Concept Discussion	19
3.1	Concept Platform	19
3.2	Initial concepts	20
4	Concept development	25
4.1	Generator	26

4.2	Buoy	26
4.3	Guiding System and PTO connection	27
4.4	PTO	29
4.4.1	Gears	30
4.4.2	Bearings	33
4.4.3	Shafts	35
4.5	Main Carter	37
4.6	Gearbox	40
4.7	Miscellaneous components	40
5	Conclusion and Future Work	41
	Bibliography	42
A	Plots From MDSolids	49
B	Technical Drawings	53

List of Tables

- 4.1 The Gears selected and their characteristics 32
- 4.2 The Slope values obtained from the MDSolids (Appendix A) and the confirmation the values are under the admissible by [1] (in mRad) 36
- 4.3 The Deflection values obtained from the MDSolids (Appendix A) and the confirmation the values are under the admissible by [1] (in mm) 36

Intentionally blank page.

List of Figures

1.1	Carbon equivalent emitted per energy source [2].	2
1.2	Evolution of the electricity obtained from Renewable sources in the EU 27 [3]	2
2.1	A diagram of the steps taken by a WEC equipped with a Hydraulic PTO [4].	5
2.2	Representation of the nodding duck [5].	6
2.3	A working Pelamis WEC [6].	7
2.4	A diagram of the Searev [5].	7
2.5	Representation of the Lysekil Project: a) foundation b) PTO schematics [7].	8
2.6	Two body systems: a) PowerBuoy b) Wavebob [8].	8
2.7	A representation of the AWS [5].	9
2.8	PS Frog Mk5 taking advantage of the surge motion via the paddle structure [5].	10
2.9	Representation of an OWC device [9].	10
2.10	Representation of an Overtopping WEC [10].	10
2.11	PTO devices [11].	11
2.12	Displacement variation methods: a) bent-axis b) swash-plate [4].	12
2.13	Application of a rack and pinion mechanism to WEC [12].	14
2.14	Ball screw based PTO [13].	15
2.15	A magnetic lead screw mechanism present in the Wavestar WEC [4].	16
3.1	The prototype developed in [14]	20
3.2	The three initial concepts developed with idea of a semi-rigid connection	21
3.3	The two rigid concepts	23
4.1	Final prototype.	25
4.2	The Yuzo wind turbine and controller from Tesup [15].	26
4.3	30° angled diagram of the supporting structure and the forces applied.	28
4.4	Diagram of the PTO system developed.	30
4.5	Schematic of the forces applied on one of the gears.	33

4.6	Schematic of the forces and the supports of the shaft, with the distance (in mm) from A below the shaft	34
4.7	The final Shaft designed to fulfill the rigidity and fatigue criteria, and confine the gears and bearings	35
4.8	A representation of the different parts of the carter and the parts confined in them.	39
4.9	Graphical representation of a gearbox from the same product line as the one selected [16].	40

Acronyms

AWS Archimedes Wave Swing.

CFTS Contact-less Force Transmission System.

EU European Union.

HVDC High Voltage Direct Current.

OWC Oscillatory Water Column.

OWE Oceanic Wave Energy.

PTO Power Take-Off.

RES Renewable Energy Sources.

RPM Rotation per Minute.

WEC Wave Energy Converters.

Intentionally blank page.

Chapter 1

Introduction

1.1 Context

It has reached common knowledge that we stand on an ecological crisis. Lately we have seen the effects of global warming as a result of the greenhouse effect.

Currently more than 75% of European Union's greenhouse gas emissions come from the energy sector [17]. This is due to the current reliance on non-Renewable Energy Sources, which are unsustainable and damaging to our environment (fig 1.1) [2, 18, 19]. Therefore, one of the ways to mitigate the ecological problem we face today is to change how we generate the electricity in our grids [20].

Overall the use of Renewable Energy Sources (RES) is on the rise due to the efforts to counteract the global warming and the increasing of demand for electricity (fig 1.2). Organizations like the EU and other countries have invested in ways to enlarge current technology applications and also supported researchers to find other sustainable methods to generate electricity [17, 20, 21].

One of the major problems of a full transition to RES is their intermittency. Current methods like Wind and Solar are dependent on the weather, which makes it unpractical to meet our needs in a calm overcast day. To mitigate this type of problems the current solution has been the hybrid (and smart) grid. In these grids the energy tends to be of mixed sources and implies the existence of large scale batteries to counteract the intermittency of some renewable sources [19, 22]. To decrease the necessity of large batteries and to make feasible the use of renewable energy only, it is necessary to expand our current grid and explore new renewable ways to sustain the demand of electricity.

One of the current emerging technologies is Oceanic Wave Energy (OWE). Its' development started back in 1973, in response to the oil crises. Although not in the current market, this technology is estimated to be up to 4 times more available and more predictable, indicating that it could have a larger impact in the energy produced worldwide [20].

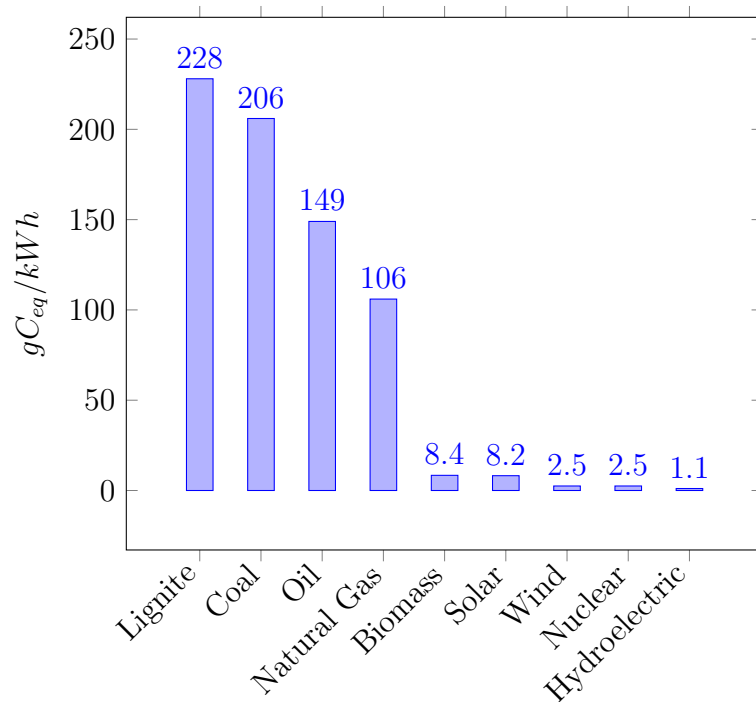


Figure 1.1: Carbon equivalent emitted per energy source [2].

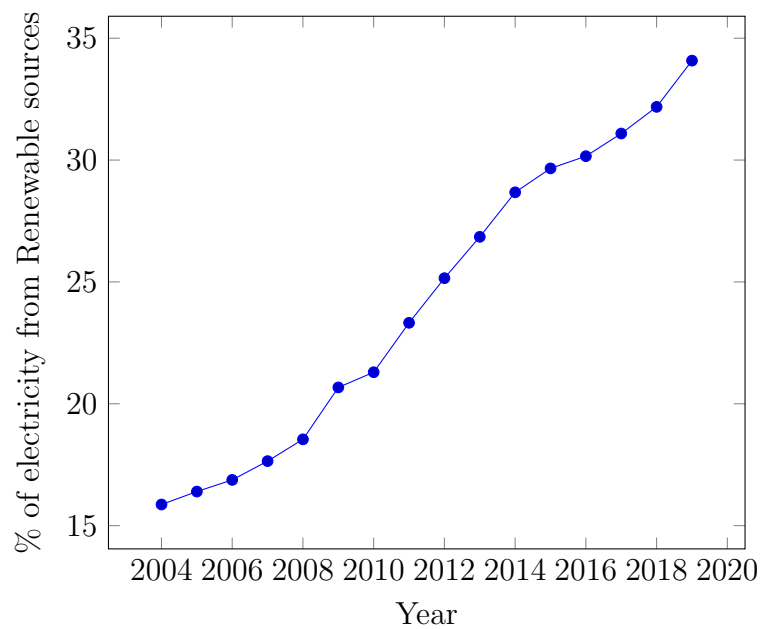


Figure 1.2: Evolution of the electricity obtained from Renewable sources in the EU 27 [3]

1.2 Objective

The main goal of this dissertation is to develop a Power Take-Off (PTO) for a small WEC prototype. With this purpose, this study presents several alternatives of PTOs and expands on, the mechanical PTO, in order to implement in the prototype.

In relation to these mechanical systems, it is prioritised addressing existing problems, such as durability and maintenance, in an attempt to make this technology more attractive for further development.

The prototype should serve to illustrate the potential of this kind of technology and to further direct its' development. In addition to this, it is crucial to develop a prototype PTO to build upon, and to possibly be integrated into, a previous developed concept . To meet this purpose the prototype developed must be comprised of two segments and take advantage of the relative movement along the vertical axis.

Targeting a future dry test and a wave tank test.

Intentionally blank page.

Chapter 2

Current Technology Review

From the waves to the grid, the energy is transformed through several steps: Absorption, Transmission, Generation and Conditioning, as demonstrated in the figure 2.1 [4]. In this chapter, a brief description of the components of each step is presented as well as an auxiliary section with extra movement converters for possible integration in a mechanical PTO, as per the objective of the thesis.

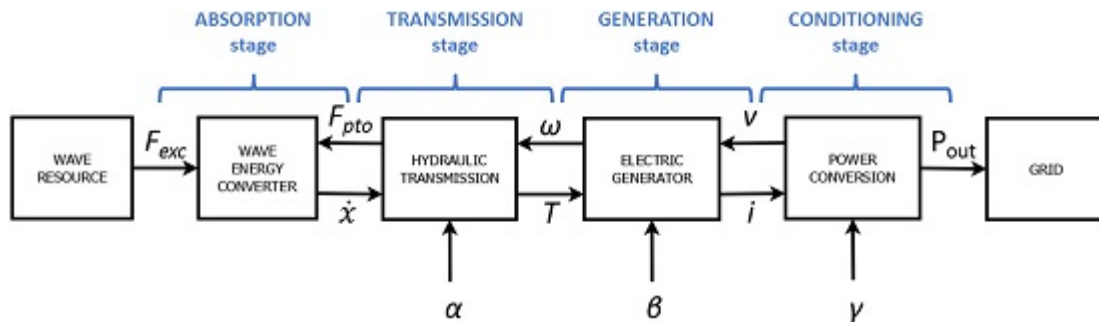


Figure 2.1: A diagram of the steps taken by a WEC equipped with a Hydraulic PTO [4].

2.1 Wave Energy Prototypes

When it comes to wave energy a standard has not been set. Thus several prototypes are currently being developed and tested. These prototypes can be split into how they are able to generate electricity, ie., from what type of motion they use to recover energy [23]. Reckoning the purpose of this dissertation, the following subsections will emphasise Oscillating-WEC. Regarding figure 2.1 the following sub-sections will mainly present several options on the **absorption** stage, with a reference to its integration with the rest of the prototype.

2.1.1 Pitch

Pitch based designs work by sourcing the difference of the surface angle i.e., the rocking motion [5, 23, 24].

The **Nodding Duck** (1974), from Edinburgh University, is one prototype built based on this concept. This cam-shaped object (fig 2.2) is composed of a static hub with a "nodding" outer shell. It is this relative movement between both parts, that is captured with the aid of a radial pistons compressor, that compress a hydraulic fluid powering a hydraulic PTO (see section 2.2.3 on Hydraulic PTOs) [25].

The same author also proposed a similar design in which the outer shell encompassed several gyroscopes and the movement used for energy recovery was in relation to these gyroscopic units [5].



Figure 2.2: Representation of the nodding duck [5].

Also in the '70s, another design was proposed, the **Raft**. This design although not successful at the time, preceded other more successful projects like the **McCabe Wave Pump** and the **Pelamis** (fig 2.3), the last one becoming the protagonist in the world's first Commercial Wave Farm, just off the coast of Portugal [5, 26]. These designs use the angle difference from each of their segments to pressurise a hydraulic fluid and, just like the **Duck**, to power a generator [5, 27].

Another way of generating power from the waves' pitch is by using this motion to power a pendulum-like structure. The **Searev** (fig 2.4) use this principle to generate hydraulic pressure to power a hydraulic PTO [5, 28, 29].

The **PS Frog MK 5** also uses the rocking motion of the waves to move an interior mass backwards and forwards but, unlike the **Searev**, the internal mass moves linearly. This movement once again is used to drive a hydraulic system [5, 24, 28, 30].



Figure 2.3: A working Pelamis WEC [6].

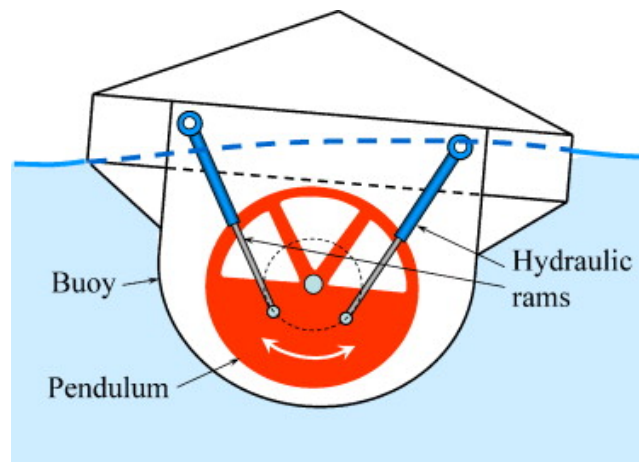


Figure 2.4: A diagram of the Searev [5].

2.1.2 Heave

Heave prototypes, on the other hand, take advantage of the up and down motion of each wave, not to be confused with tidal energy that uses the sea level rise [5,23,24].

On this topic, one of the simpler ways to recover energy from the waves' heaving motion is to attach a buoy to a static foundation in the seafloor, as used in the **Lysekil Project**, from Uppsala University. (fig 2.5) In this system, the buoy is connected to a direct electrical drive PTO (2.2.1) [7,24].

These designs have a clear limitation in terms of placement [5], the physical connection to the bottom of the ocean limits them to shallow waters and locations with minimal tidal amplitude.

With these limitations, other designs came to fruition, that instead of using one floating body linked to the seabed, use two concentric floating bodies moving with two different frequencies. Such is the case of the **PowerBuoy** (fig 2.6) from Ocean Power Technologies, in which a larger cylindrical mass floats relatively steady and guides an outer buoy around itself in a linear up and down motion powered by the heaving motion. This reciprocating action is used to power a hydraulic generator feeding an underwater battery [5,27].

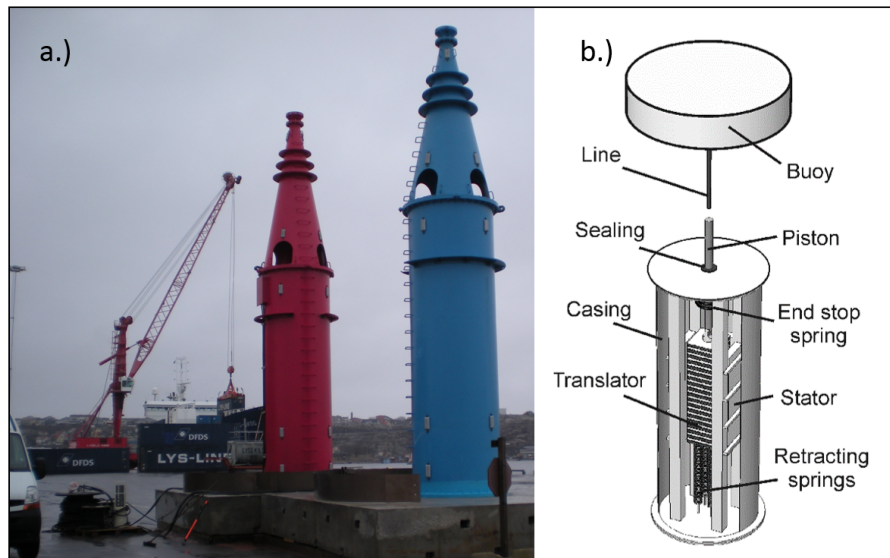


Figure 2.5: Representation of the Lysekil Project: a) foundation b) PTO schematics [7].

Like the **PowerBuoy**, the **Wavebob** (fig 2.6) is based on the same basic concept with some structural changes, more specifically on how the "static" buoy is stabilized [5, 24, 28].

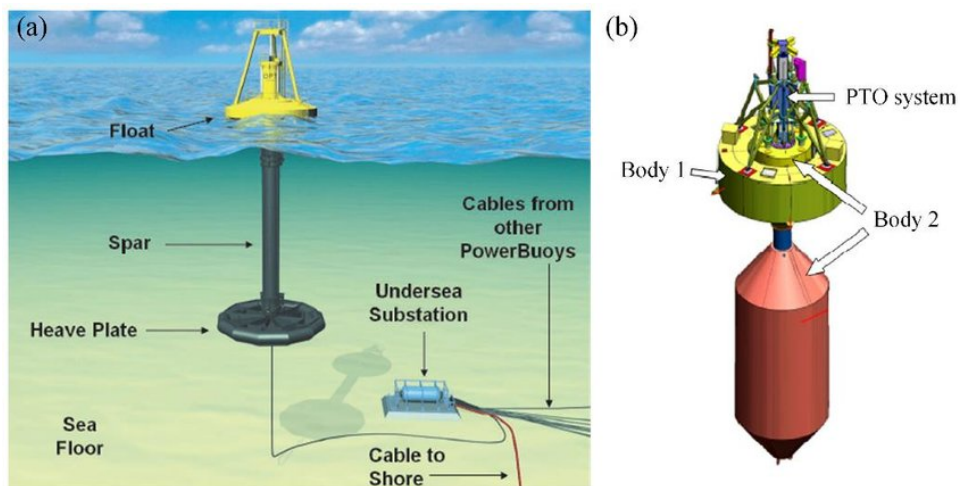


Figure 2.6: Two body systems: a) PowerBuoy b) Wavebob [8].

Another heaving prototype is the **AquaBuOY**, which also uses the same two moving objects concept, but with a considerable twist. The main body, the floating one, consists of a buoy with an internal turbine to generate energy. This turbine is powered by the relative up and down movement of the second body, which is neutrally buoyant, that forces the seawater into the upper main body to power

the turbine [5, 27, 28]. This design was heavily influenced by the **IPS** from the University of Edinburgh [5].

All of the aforementioned systems have a common similarity, they float on the waves' surface. The **Archimedes Wave Swing (AWS)** (fig 2.7) differs from this principle. This system is fixed to the seafloor with a floater attached under the waves. The **AWS** takes advantage of the pressure above the floater to move it up and down, powering a direct electrical drive PTO, like in the **Lysekil** [5, 24, 27].

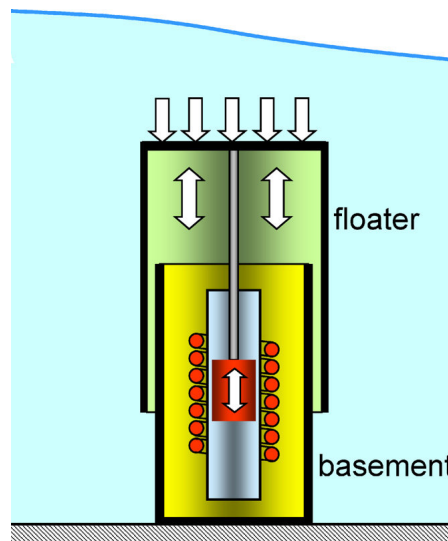


Figure 2.7: A representation of the AWS [5].

2.1.3 Surge

Surge based devices, base themselves on waves' the backwards and forwards motion [23].

This movement also features in other devices to complement the waves' heave and pitch. Such is the case in the **PS Frog MK5** (fig 2.8) with an enlarged surface area to catch the surge adding it to the tilt motion caused by the waves' pitch [30].

2.1.4 Other

Other devices have been and still are being studied that or use a mixture of the previous characteristics from the wave, or prototypes that instead of using the motion of the waves use the water from the actual waves. The latter can be Oscillatory Water Column (OWC) (fig 2.9), Oscillatory Wave Surge Converter (OWSC), Overtopping (fig 2.10) [5, 23, 24, 27, 31]...

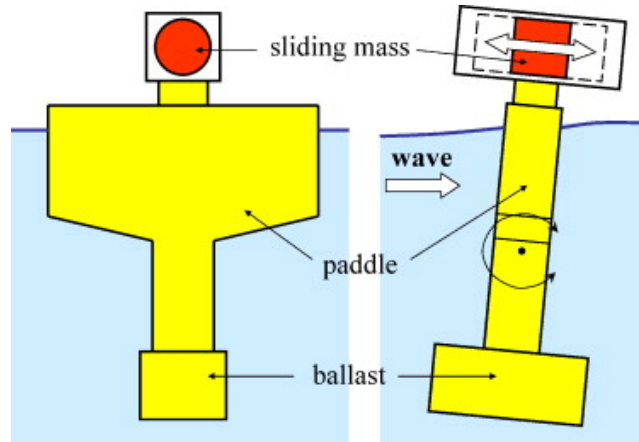


Figure 2.8: PS Frog Mk5 taking advantage of the surge motion via the paddle structure [5].

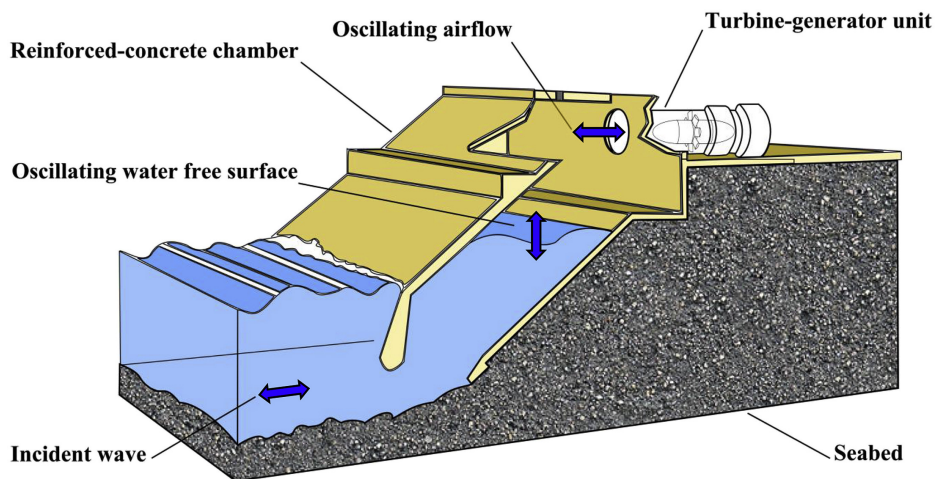


Figure 2.9: Representation of an OWC device [9].

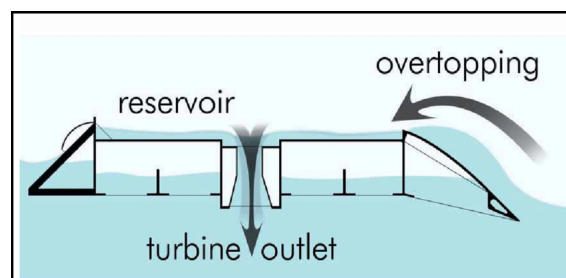


Figure 2.10: Representation of an Overtopping WEC [10].

2.2 PTO Methods

For all the designs described previously in section 2.1, the conversion of movement into electricity is done by a Power Take-Off (PTO). This is a critical component of any WEC that connects the buoy to a generator and this can be done in several ways as portrayed by figure 2.11 [5, 23, 24, 31]. Regarding the figure 2.1, this corresponds to the transmission stage and the generation stage.

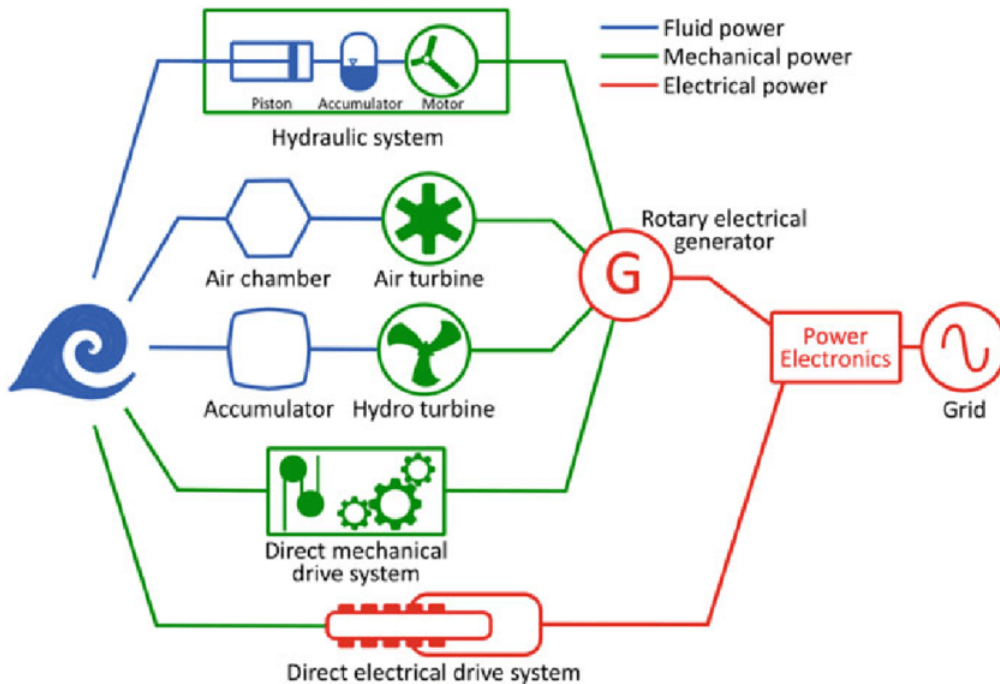


Figure 2.11: PTO devices [11].

2.2.1 Direct Electrical Drive

Unlike the other PTO systems, the generation stage on a direct electric drive does not include a rotational generator, since it connects the linear movement directly to a linear generator instead.

There are several types of linear generators in use [24,27,31] but these generators are mostly composed of a translator which moves through a stator varying the magnetic field and thus generating electricity, as seen on the side b of figure 2.5 [5, 7, 24, 27, 31].

The simplicity of the design and the lack of any intermediary system implies less need of maintenance. However these systems have no way of controlling their output and so, their erratic movement will generate an unreliable current. As a result, this PTO requires additional electric equipment [5, 27, 31].

2.2.2 Direct Mechanical Drive

A mechanical drive system consists of a series of pulleys, gears or screws... to convert the oscillating motion into rotational movement, to power a conventional generator. These systems can often be integrated with a flywheel to smooth out the waves erratic motion [11].

The potential for high efficiency is one characteristic of both direct PTO, since they offer a more direct way of transmitting power to the generator. However in the case of the mechanical PTO, the requirements for such a device are extremely high and as a result, its feasibility in the real world is yet up for debate [11, 23]. Though several smaller prototypes have been built and tested [4].

2.2.3 Hydraulic

The slow, but powerful movement of the waves is ideal for these systems. By applying the waves' motion to pressurize oil into a reservoir and only then to power an electric generator the hydraulic PTO allows the use of conventional high-speed generators [5, 23, 24, 27, 31].

These systems allow for a more carefully generated current. As the pressurized can be stored in tanks and released at a constant pressure with valves, in addition to this the hydraulic motor can have variable displacement (fig 2.12), thus providing the connected generator with a continuous motion [5, 23, 24, 27, 31].

For example, in the **Nodding Duck**, the angle of the swashplate is adjusted to balance the speed of rotation, thus allowing the generator to produce a steady stream of electricity independently of the actual wave [25].

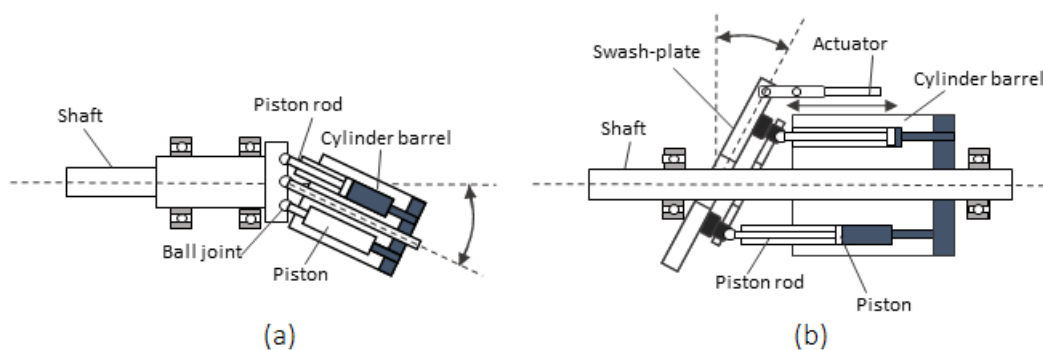


Figure 2.12: Displacement variation methods: a) bent-axis b) swash-plate [4].

As with any hydraulic system, this PTO also requires careful maintenance. Unfortunately, the conditions at sea make it very costly, in both time and money, not to mention the high level of risk of those responsible for its maintenance. Another problem with these systems is that they suffer in very harsh conditions

and can in some cases exceed the maximum displacement damaging the system. This problem is currently being mitigated by the use of radial hydraulic pistons [5, 27, 31, 32].

Overall, the hydraulic PTO seems to be a good solution on paper but it is heavily limited in the real world due to its complex systems and the difficult operating conditions.

2.2.4 Turbine

Turbine based PTO tend to be used in OWC and in Overtopping designs in which use the water or air moved by the waves to power these turbines directly. In any of these cases, the composition of the fluid in use is unknown and this can have a damaging effect on the turbine itself. Also in low-head water-based turbines, cavitation is a serious problem [31].

2.3 Movement Converters

Given the relative scarcity of direct mechanical PTO [11, 23], the following section enunciates several ways of converting the linear oscillatory motion of a buoy in regards to the waves' heave.

2.3.1 Rack and Pinion

Rack and pinion systems have long been used in the automotive industry, in elevators and in cog railways. Their application in large equipment is a known fact as they are currently being used in oilfields as part of drilling equipment and being favoured over more traditional hydraulic systems, that are harder to maintain [33].

In terms of energy recovery, these mechanical components have found themselves in prototypes of energy recovering speed breakers [34]. A small WEC prototype was built (fig 2.13) with a theoretical efficiency of 89% [12]. This prototype was able to achieve a maximum power of 100W, with a wave height of 30cm and a period of 2.5s [12].

Generally, these mechanisms are highly efficient, suffering from a short lifespan [4].

2.3.2 Ball Screw

These systems are frequently used in linear actuators due to their high precision. However several prototypes for energy recovery of linear motions are being studied

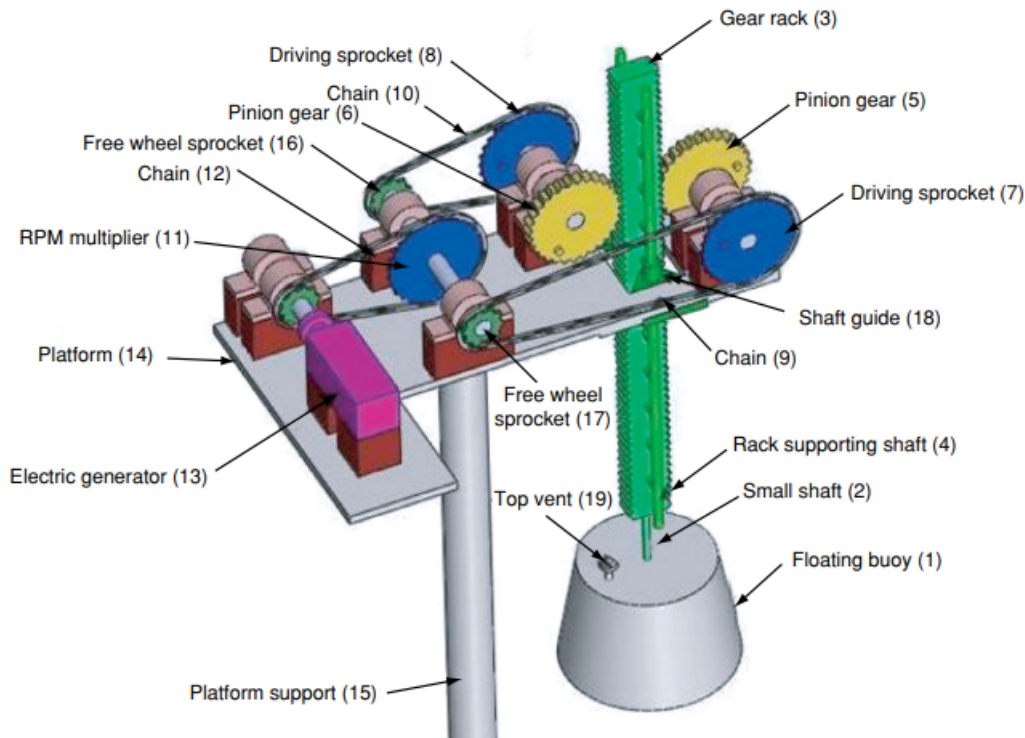


Figure 2.13: Application of a rack and pinion mechanism to WEC [12].

[13, 35].

A ball screw mechanism has been adapted for energy recovery, both on a vehicle's suspension system and on a PTO for WEC. Both prototypes work using the same principle, they take advantage of the ball screw system to generate a rotational motion and then use a pair of one-way clutches to drive a generator (fig 2.14) [13, 35].

These two systems differ in the mixed-function of the suspension recovery system that does not allow the use of a flywheel, this on the other hand is present in the WEC's PTO [13, 35]. The last one was able to achieve 62.4% efficiency in a wave tank [35].

2.3.3 Roller Screw

Similar to the Ball screw it is ideal for linear actuators and can be more precise, reach higher speeds, withstand heavier loads while having a greater life. Its drawbacks are the cost of manufacture thus it is the most expensive option in screw-based systems [4, 36].

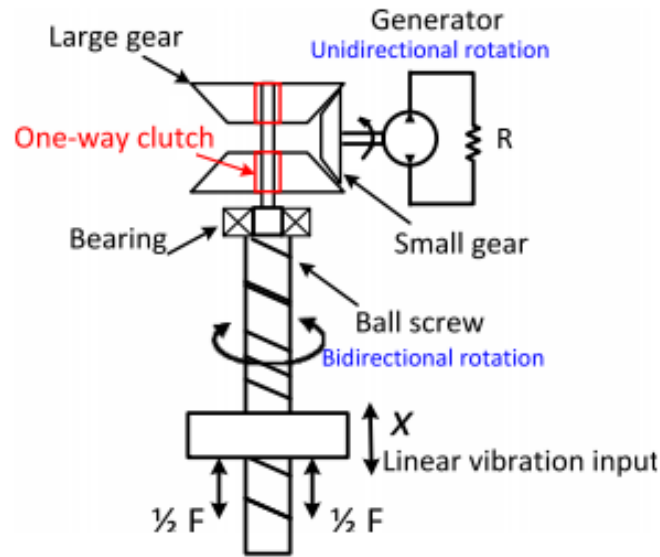


Figure 2.14: Ball screw based PTO [13].

2.3.4 Lead Screw

Currently, these systems are used as a cheaper alternative to the Ball Screw systems that are more efficient. Given the purpose of maximum efficiency prototypes with these systems have been abandoned on new prototypes [4].

2.3.5 Belt Drive

Belt driven systems connect one end of the belt to the buoy and another to a winch, thus driving a gearbox and powering a generator. These systems are limited to one direction since the winch needs to be wound back to its starting position [4].

2.3.6 Magnetic Systems

Magnetic transmissions have recently been the subject of many publications. These magnetic gears present several advantages in regards to traditional gear, mainly based on the lack of contact between gears. They have next to no maintenance and friction, thus have the capability of being more efficient, plus these systems can slip under immense stress, giving them an intrinsic overload protection. Their main disadvantages are the availability and the high manufacturing costs. Also, as relatively new systems, they are unproven, so more studies should be conducted [37].

Nevertheless, a PTO for WEC has already been designed (fig 2.15). This mechanism is based on a screw-type of linear transmission, but replacing the

contact with magnetic attraction, which with a physical separator remains a Contact-less Force Transmission System (CFTS) [4, 38, 39].

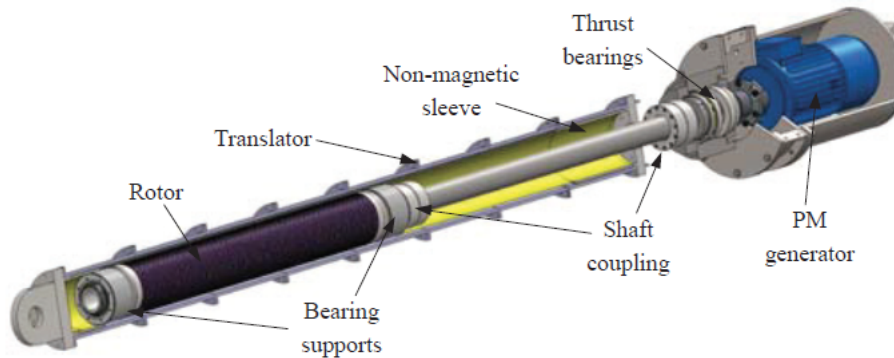


Figure 2.15: A magnetic lead screw mechanism present in the Wavestar WEC [4].

2.4 Energy Conversion

Depending on the generator of the PTO system, the energy generated from them can be very irregular, both in voltage and in current [4].

In Fixed-Speed generators, with a careful selection of the speed and the number of poles, the energy generated has the same voltage and frequency. Hence it can be directly connected to the grid and thus avoiding expensive converters, only needing a capacitor bank [4].

Nevertheless, this type of generator has its drawbacks, first of all, it requires an additional starter unit to gradually power the generator to the right speed, protecting it from power surges. In addition to their starting procedure, the fixed-speed nature of these systems implies the use of complex PTO, to convert the irregular motion into a fixed speed. Hence the common presence of these generators in hydraulic systems, that with their displacement manipulation are able to guarantee the required speed [4].

As for Variable-Speed generators, the energy produced is highly irregular and, for this reason, it is necessary to adapt and convert this irregular form of energy into regular grid energy [4,20]. To perform the conversion most systems use a combined AC to DC and DC to AC converters [4], with a possibility for an included battery on the DC circuit.

As per this type of generator, their versatility in a wider operating range of conditions is a noticeable advantage and along with DC circuit, there is the

possibility of transmitting power through High Voltage Direct Current (HVDC). A better way of power transmission for long distances [40].

Intentionally blank page.

Chapter 3

Concept Discussion

This chapter describes the full development of the concept and the conditions it must follow.

3.1 Concept Platform

The following section provides the reasoning behind several design constraints and the goals of the prototype developed.

One of the purposes of this is to continue the development of concepts in support of another masters dissertation. This other dissertation [14], written at the University of Aveiro, a concept for WEC was developed describing the process taken from an overall assessment of current technology to a very small scale prototype.

The concept developed previously comprises of a bigger semi-static body that serves as a platform for a cluster of smaller buoys moving with the heaving motion of the wave, as represented in the figure 3.1. This prototype is intended to use a **Direct Electrical Drive PTO** (view section 2.2.1) [14], however, this technology is currently more expensive and harder to apply on a larger scale due to its relative unavailability and the need of a purpose-built system, hence an alternative PTO system is required to upscale a similar version of this prototype.

As discussed earlier, there are several types of PTOs. For this application, the simpler mechanical is the better option in terms of cost, and for this reason, was the selected method to power the prototype developed in this dissertation.

To establish a scale for this new prototype it was decided to fix its capacity to 200W, this enables it to generate significant power confirming the viability of this concept and surpasses the prototype developed in [12].



Figure 3.1: The prototype developed in [14]

3.2 Initial concepts

Given the decision to develop a mechanical PTO, the initial approach was to limit the faults motioned in the section 2.2.2. Following this design principle, several concepts were developed as shown in the figure 3.2, these ideas attempt to minimize the shock from the erratic movement of the buoy.

These three systems all share the same idea of a semi-rigid connection of the PTO to the buoy, in green and blue respectively. In all of these the buoy's shaft could move and twist up to a certain limit and the guided part of the PTO system (in green) would stay on a linear path. By not resisting the lateral movements of the buoy the guiding system would ideally be under less strain, thus improving the durability of the system.

The first concept, a), is based on a loose connection between the PTO and the buoy. The shaft of the PTO is captive inside of the shaft coming from the buoy below. As evident in the figure 3.2, a), the buoy can freely move in any direction for a small distance, due to the loose nature of this connection.

Regarding the vertical axis, both the PTO's shaft and the buoy's shaft move close to sync, since the gap allowed is far inferior to the projected maximum travel distance (the idealized height for energy recovery).

Regarding other types of movement, the buoy is trapped laterally, by rollers, ensuring the buoy remains close to the centre. This enables some type of lateral movement without affecting the shaft of the PTO since the gaps in the cavity are bigger than the allowed by the rollers. Thus the PTO shaft and buoy shaft only make contact on the up and down movement.

Also, in this concept, the inner cavity could be filled with a viscose fluid to adjust the freedom of the buoy in relation to PTO, or similarly, there is also a possibility of lining the inner walls with magnets to provide a magnetic buffer and further minimize shock.

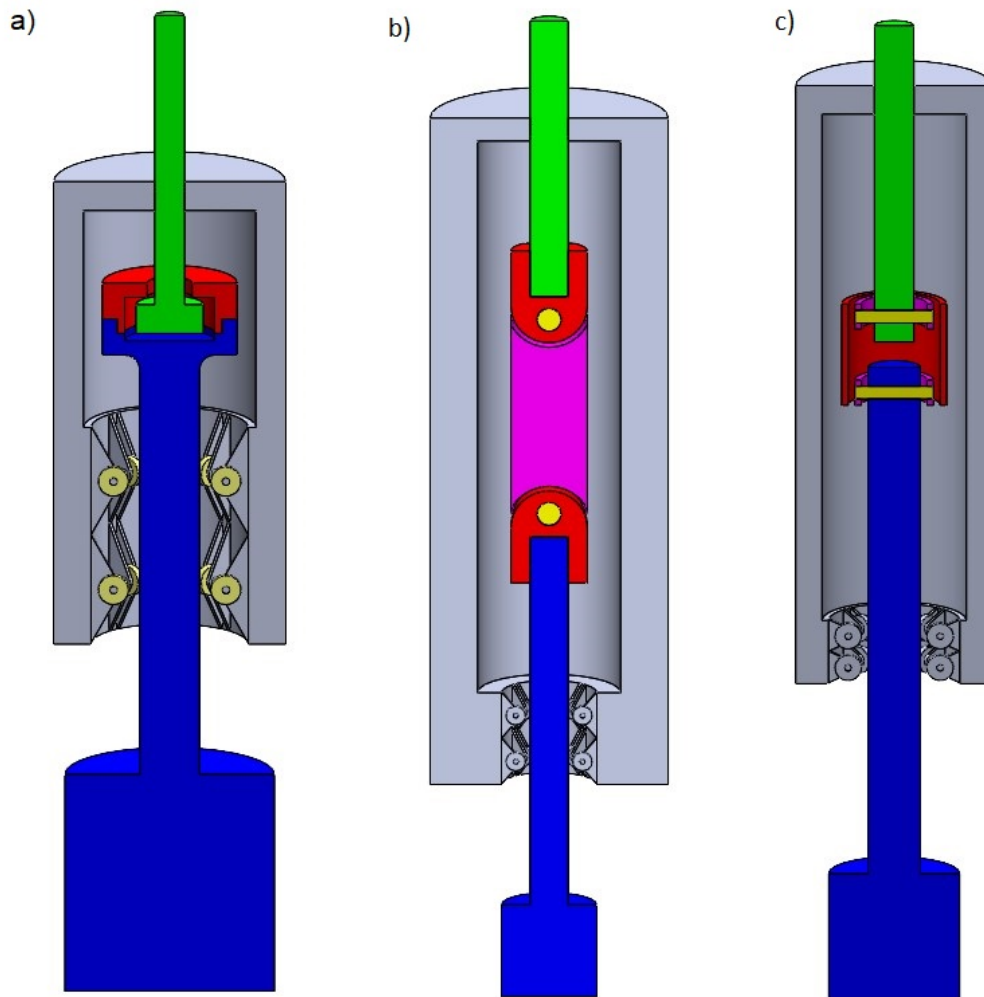


Figure 3.2: The three initial concepts developed with idea of a semi-rigid connection

The second design, b), follows the same principle, but replaces the cavity with a permanent flexible connection, thus eliminating the collisions of both shafts. On this design, both shafts are connected through rotating elements (in red) that pivot on a common element (in pink).

As for the third, c), it is a development of the second, which in practice would work in the same way except in not allowing any rotation of the shaft. In this concept both shafts connect to a separate ring that is allowed to pivot, these rings are then connected to a common larger piece through a pivoting connection at 90 degrees to the previous one. This would then enable the buoy to lean in all directions.

In the end, all of these designs have the same flaws mostly related to the

Semi-rigid concept. The lateral movement of the buoy would eventually force it to touch the limiting rollers (as intended), however, this will introduce extra drag, limiting the efficiency of the system, and depending on the shaft's angle to the roller, could even lock the system entirely. Additionally, all of the ideas above would need a lot of moving parts and, due to their position, it would be hard to separate them from the harsh environment of the sea.

Considering the shortcomings of the Semi-Rigid concept, a more traditional approach was taken. This new concept is based on guiding the buoy and the PTO shaft, making it one of the same. In this concept the relative placement of the supports regarding the PTO is critical. As such, two designs were conceived, shown in figure 3.3, in order to study and compare both possibilities.

These two designs mainly differ in the position of the linear bearings (in red) holding the shaft in place. On the first the rack for the PTO (in yellow) is located in between both bearings, this forces the distance of the bearings to be greater, reducing the forces applied in them. However, this system also offers a lot of difficulties in aligning both bearings.

In comparison, the second model has its bearings (both) under the PTO, this enables it to have a separate part of the shaft for the buoy and another for the rack since the upper part does not suffer from lateral forces. Regarding the alignment required, this second prototype as all its bearing in the same place thus reduces the number of parts that must fit concentrically. Other advantages of the second design are the enclosed upper segment that reduces complexity, as well as parts like seals, and is safer since no shaft protrudes upwards.

Given all the characteristics discussed, the second concept was developed further. A second rack for energy recovery in both ways was added, similarly to other concepts based on this technology, for instance in [12]. Expanding on this idea, the concept of a weighted buoy was conceived. This means that for the target height and period of the wave the mass of the buoy is defined as such as the maximum power is the same, both upwards and downwards. This means that the generator will ideally work on the same power range and avoids the need for a second generator for efficient generation on the downwards motion.

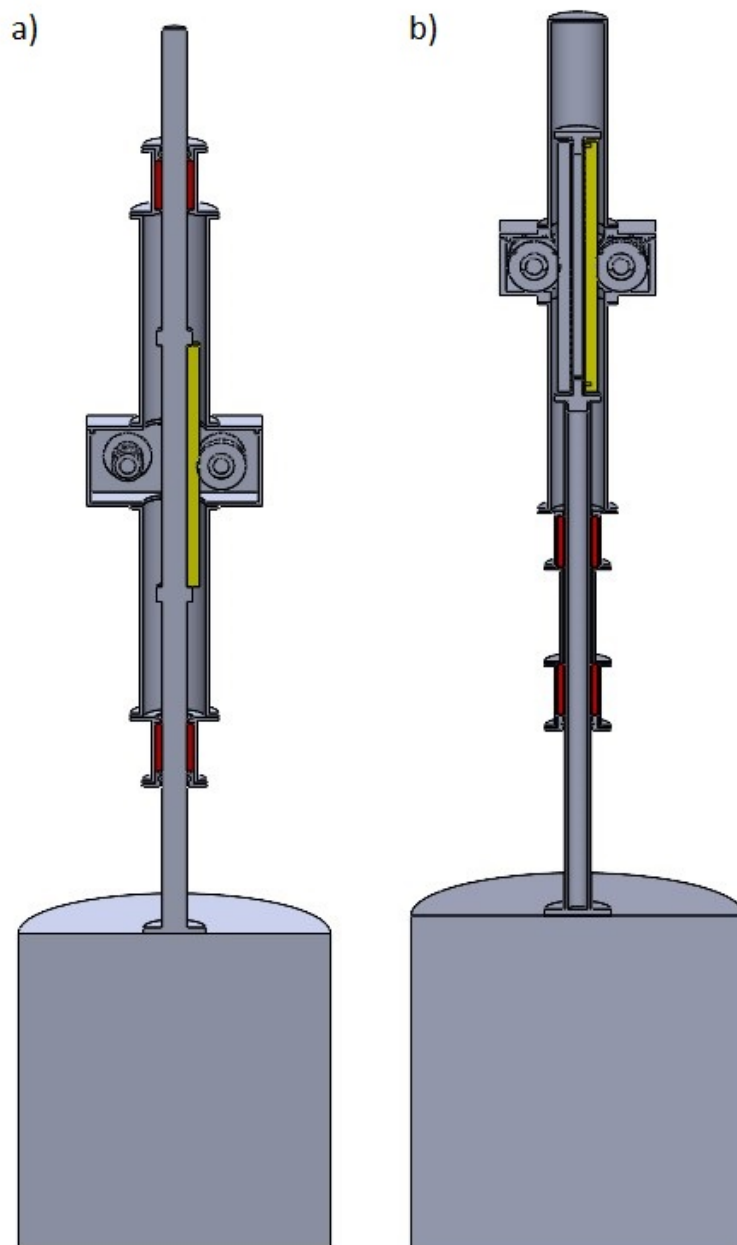


Figure 3.3: The two rigid concepts

Intentionally blank page.

Chapter 4

Concept development

This chapter is meant to explain the process of transforming the overall idea developed in the previous section to a working prototype, dividing this chapter in accordance with the main components of the final prototype (fig 4.1).



Figure 4.1: Final prototype.

Since the goal for this prototype is 200W, the prototype was engineered with a maximum capacity of 300W, thus accounting for other inefficiencies.

To generate the targeted 300W while keeping the prototype small, the movement of the buoy was limited to 0.3m, the height of a small wave in a wave tank.

4.1 Generator

For the targeted power, a generator from a small wind turbine (fig 4.2) intended for use in recreational boats was adapted. The 3-phase generator from this unit is capable of outputting 200W at 1000RPM, according to the manufacture, Tesup [15].

To convert the three phase current from the generator to a continuous current, the charge controller of the same make was used (fig 4.2).



Figure 4.2: The Yuzo wind turbine and controller from Tesup [15].

4.2 Buoy

Considering that the buoy moves 300mm relative to the main body and assuming it moves every second, to generate 300W the force (F) it had to transfer to the PTO was calculated by the equation 4.1.

$$F = \frac{P}{2 * f * h} \quad (4.1)$$

Where P is 300W of power, f the frequency of the oscillation (1Hz) and h the amplitude of the buoy (0.3m), the times two multiplier in the denominator refers to the force being generated on both directions, upwards by buoyancy and downwards by gravity. Given this equation both forces were calculated to be 500N.

With the forces established the size of the buoy was defined, firstly the weight. As it is intended to use the gravity to power the system in the down stroke, the

mass of the buoy is defined by Newton's 2nd law, resulting in the equation 4.2, where g is defined as 9.81m.s^{-2} and F is the force calculated earlier.

$$m = \frac{F}{g} \quad (4.2)$$

Lastly the volume of the buoy is provided by the equation 4.3, where F_b is the buoyancy force 500N, W is the weight, also 500N, and d is the density of the water 997kg.m^{-3} . (Note: the density varies with the salt concentration, thus it is important to rectify the calculation depending on where the prototype is tested.)

$$V = \frac{F_b + W}{d * g} \quad (4.3)$$

As a result, the ideal buoy has the following characteristics:

- Mass = 51kg,
- Volume = 0.1022m^3 ,
- Diameter = 0.5m,
- Height = 0.52m.

4.3 Guiding System and PTO connection

This section provides a brief description of the parts developed and shows the steps taken to develop them, the buoy's shaft and its connection to the PTO.

The shaft is welded to a connection plate for the buoy, on one end, and threads into the connecting segment on the other end. This shaft travels through a hydraulic wiper and two seals, while fixed in between two linear bearings.

The split connection to the PTO enables the use of a smaller shaft, easier to produce, and a purpose built connection for the two racks of the PTO. For this connection both racks are screwed to a box section tube machined parallel. To merge this tube with the buoy's shaft, an additional part was engineered. This piece threads into the buoy's shaft and fits inside of the box section fixed with screws.

The diameter of the shaft connecting to the buoy was defined in relation to the linear bearings capable of withstanding up to a maximum inclination of 30° at maximum extension, as portrayed in figure 4.3. In this instance the resisted force (F_b) by them can be described by the equation 4.4.

$$F_b = W * \sin(30^\circ) \quad (4.4)$$

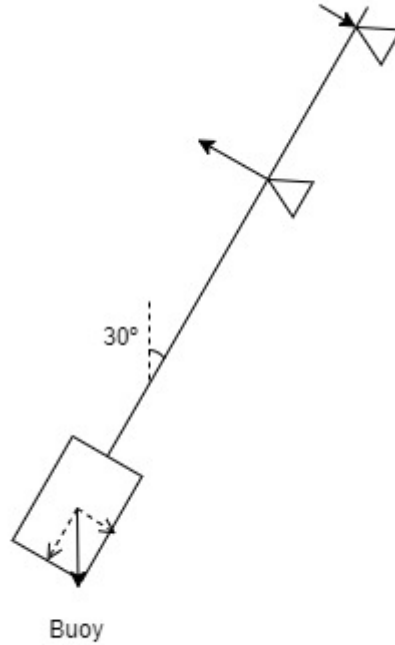


Figure 4.3: 30^o angled diagram of the supporting structure and the forces applied.

Knowing the force applied on the buoy (F_b) and its distance to the both bearings, it is possible to define the force applied on them with the equations 4.5, for the lower one and 4.6, for the higher one. Where d_t represents the total distance between the buoy and the top bearing, totaling approximately 0.963m, similarly the d_s is the distance in between both bearings supporting the shaft, 0.273m. (All distances referred were measured from the centre of every reference.)

$$F_{Bl} = \frac{F_b * d_t}{d_s} \quad (4.5)$$

$$F_{Bh} = \frac{F_b * (d_t - d_s)}{d_s} \quad (4.6)$$

In turn, these forces were used to calculate the static load (P_0), with the equation 4.7, in order to acquire a viable set of bearings. In this equation F is the force calculated earlier and the other factors f_m , related to misalignment, f_{l0} , related to the direction of the load and f_{h0} , related to the surface hardness of the shaft were considered equal to 1 as the configuration of the bearings respects the standard configuration on [41]. Thus $P_0 = F = 883\text{N}$. As a result the bearing

selected for this application is SKF's LBCD 40 D-2LS capable of $C_0 = 3350\text{N}$ and $C = 6550\text{N}$ [41]. Since the force being studied imparts a shock load on the bearings, a safety factor (S_0) of over 3 is required [41]. This was confirmed with equation 4.8.

$$P_0 = \frac{F}{f_m * f_{l0} * f_{h0}} \quad (4.7)$$

$$S_0 = \frac{C_0}{P_0} \quad (4.8)$$

Similarly to the static load, the dynamic load is equal to the force, as the factor in equation 4.9 were considered 1 for the same reason. For these condition the lifetime of the bearings was calculated with equation 4.10. Where c_1 is a factor for reliability considered 1 for 90% (standard reliability value), c_2 is a factor for the operating conditions related to the lubrication and the speed of the shaft considered to be 0.4, as a result of the high speed difference possible on the system, and f_s a factor related to the travel distance and size of the bearing, in this case this factor is also equal to 1, as the travel distance is bigger than the raceway of the bearing.

$$P = \frac{F}{f_m * f_l * f_h * f_i} \quad (4.9)$$

$$L_{ns} = 100 * c_1 * c_2 * f_s * \left(\frac{C}{P}\right)^3 \quad (4.10)$$

As a result it is safe to assume the bearings will last at least 16000Km. Inferior to the projected 21600Km for the prototype, however the bearing calculation assumed an extreme condition that, with regular use, the prototype will not be subject to. So these bearings were deemed acceptable and since these bearings have an interior diameter of 40mm the shaft's diameter was defined in accordance.

4.4 PTO

The PTO makes use of two rack and pinion gear on opposites sides to recover energy from both upwards and downwards motion. These pinions are mounted into sprag clutches (freewheel gears), so that they do not conflict with each other, as both connect to the same shaft. This system (fig 4.4) allows the exit shaft to rotate in the same direction regardless of the way the buoy moves.

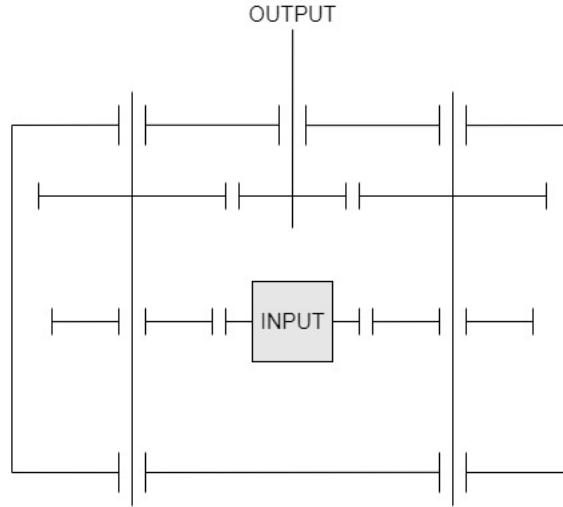


Figure 4.4: Diagram of the PTO system developed.

4.4.1 Gears

All of the gear in the PTO developed are straight cut, since when compared to the alternative, helical gears, straight gears do not produce any axial load and tend to be cheaper. The only advantage brought by helical gear would be noise reduction, but noise was not a limiting factor when designing this prototype. The material for all of these gears is C45 steel, this material was chosen because of a cost saving logic and also since size is not a critical factor at this scale.

The first part of the process began with the size of the pinion gears. Since, due to design constraints, the freewheel bearings have to fit inside of the pinions. This iterative part of the process culminated on a pinion gears with ($Z_p =$) 37 teeth and a module (m) of 2mm.

The racks connected to the buoy, as described earlier, transmit 500N to the pinions while traveling at 0.6ms^{-1} , resulting in the targeted 300W of power. To recover this energy the pinions were defined so that they verify the conditions for bending fatigue and contact fatigue in [1], equations 4.11 and 4.14 respectively. With these condition met it is safe to assume that the gears can, in fact, transfer all the power reacquired for the lifetime projected.

$$m_f \geq \sqrt[3]{\frac{1.96 * 10^4 * P * K_M * K_{bl} * Y_\epsilon}{C_L * \sigma_{blim} * n_p * K_A * Z_p * Y_F} * \frac{u + 1}{u}} \quad (4.11)$$

In this equation (4.11):

- K_M refers to the dynamic factor, which for the conditions applied was set at 1.5.

- K_{bl} is the fatigue factor calculated in 4.12, for an expected number of cycles (N_{Lh}). In this case the equivalent of 10000h.
- Y_ϵ in this case 0.8 since there was no need to correct the gear's teeth.
- C_L the width factor, considered 10.
- σ_{bLim} the tension limit for flexion. 210MPa for C45 Steel.
- n_p is the RPM of the pinion gear. The result of equation 4.13, where V_{LR} is the linear velocity of the rack and $\varnothing_p (= Z_p * m)$ is the primitive diameter of the pinion.
- K_A refers to the alignment factor, in this case 1, as the ratio $Width/\varnothing$ is inferior to 1.
- Y_F the factor for tension concentration, 0.4, due to no correction required.
- u is the multiplication between gears in this case 1, since it relates to a rack and a pinon

$$K_{bL} = \frac{\log_{10}(N_{Lh})}{8} \quad (4.12)$$

$$n_p = \frac{V_{LR} * 60}{\varnothing_p * \pi} \quad (4.13)$$

$$m_c \geq \sqrt[3]{\frac{6 * 10^4 * P * K_M}{\pi^2 * C_L * \sigma_{HLim}^2 * n_p * K_A * Z_p^2 * K_{HL} * \sin(2\alpha)} * \frac{2 * E}{1 - \nu^2} * \frac{u + 1}{u}} \quad (4.14)$$

In the equation 4.14:

- σ_{HLim} the tension limit for contact. 550MPa in this instance.
- K_{HL} is the inverse of K_{bL} .
- α is the pressure angle of the gears, in this case 20 degrees.
- E the Young's Modulus of the gears material, in this case 190000MPa.
- ν is the Poisson's ratio 0.29.

The same method of verification was applied for the other set of gears. However, this other set had to maintain the same shaft distance (d) defined by the first set of gears. Thus the number of teeth of the gears in the second set (Z_s for the smaller and Z_b for the bigger) must respect the equation 4.15.

$$d = m * (Z_s + Z_b) \quad (4.15)$$

Since the PTO is connected to a gear box (later picked with the ratio 1:5.3) the multiplication of this step ended up to be 1:1.3, achieving a maximum speed at the generator of 1077 RPM.

In summary, the gears selected for this prototype as follows in table 4.1.

Table 4.1: The Gears selected and their characteristics

Quantity	Type	Modulus	α	Size	Material
2	Gear Rack	2	20°	390mm	Ck45
2	Spur Gear	2	20°	37 teeth	Ck45
2	Spur Gear	2	20°	42 teeth	Ck45
1	Spur Gear	2	20°	32 teeth	Ck45

The gears from the second stage interact with their respective shaft through keys. To guarantee the reliability of this method they were evaluated in relation to shear stress and compression stress with the following equations 4.16 and 4.17.

$$\tau_{adm} > \frac{\tau}{l * b * \varnothing} \quad (4.16)$$

$$\sigma_{adm} > \frac{\tau}{L * \varnothing * (h - t_1)} \quad (4.17)$$

In these equation the τ is the torque transmitted, portrayed in equation 4.20, and the other constants refer to the size of the actual key: L is the length (in between the center of the rounded edges), b is the width, h is the height and t_1 the height of the key in the shaft.

From these equations were defined the following keys:

- 2 DIN 6885 A 8x7x25 for each 42 toothed gear.
- 1 DIN 6885 A 5x5x25 for the single 32 toothed gear.

Regarding the two 37 toothed gears, from the first set, they form a pressure fit with the freewheel bearing, as established in the start of this section, and this bearing also forms a pressure fit on the shaft, thus not requiring any keys.

4.4.2 Bearings

In this PTO prototype there are 2 equal shafts that include 2 gears each. The other gear is mounted directly on the gearbox's input shaft.

To properly engineer the shafts and to pick the bearings it is necessary to define the forces applied on each gear. In this case, since the gears are straight no axial force is applied, thus all of the force can be split into tangent forces (F_t) and radial forces (F_r), as represented in figure 4.5. These forces can be calculated using the equations 4.18 and 4.19. In which τ refers to the torque transmitted by the gear, and is defined by the equation 4.20, while ω is the rotational velocity ($\text{rad}\cdot\text{s}^{-1}$).

$$F_t = \frac{2 * \tau}{m * Z} \quad (4.18)$$

$$F_r = F_t * \tan(\alpha) \quad (4.19)$$

$$\tau = \frac{P}{\omega} \quad (4.20)$$

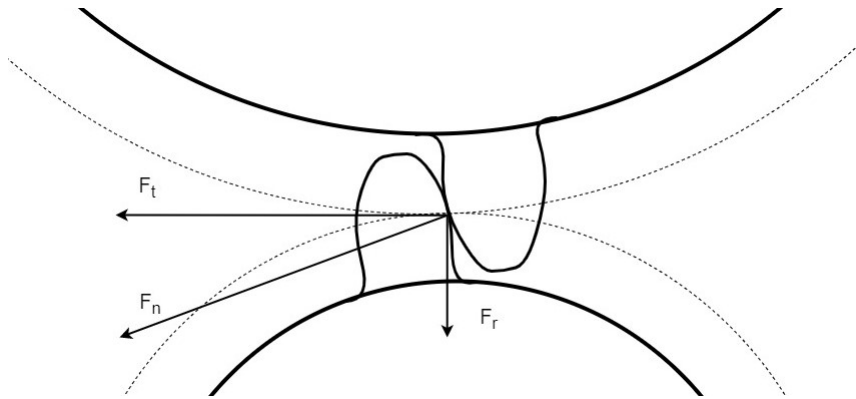


Figure 4.5: Schematic of the forces applied on one of the gears.

By describing the forces this way its possible to organize them in two separate orientations (Y and Z), as portrayed in the figure (fig 4.6). For each orientation we can define the reaction forces of the supports (the bearings) with the equations 4.21 and 4.22. By combining both components (Y and Z) with equation 4.23, the static and dynamic loads can be calculated through equations 4.24 and 4.25 [1].

$$F_A = \frac{F_1 * d_{1-B} + F_2 * d_{2-B}}{d_{A-B}} \quad (4.21)$$

$$F_B = \frac{F_1 * d_{1-A} + F_2 * d_{2-A}}{d_{A-B}} \quad (4.22)$$

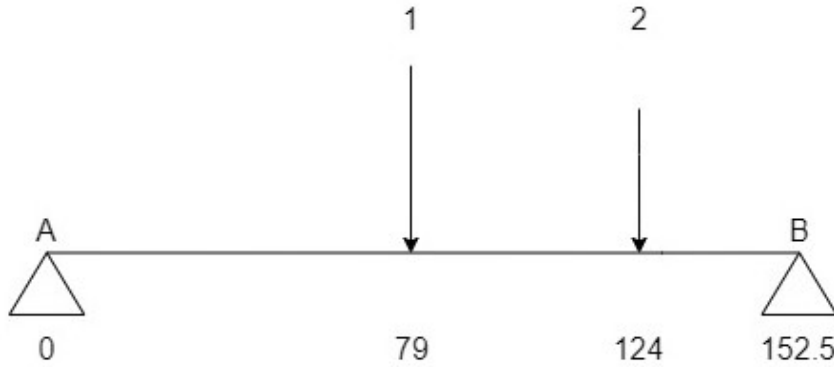


Figure 4.6: Schematic of the forces and the supports of the shaft, with the distance (in mm) from A below the shaft

$$F = \sqrt{F_Y^2 + F_Z^2} \quad (4.23)$$

$$C_0 = f_s * F \quad (4.24)$$

$$C = \frac{f_l}{f_n * f_t} * F \quad (4.25)$$

In these equations:

- f_s is a safety factor applied to equivalent static load, in this case 1.5.
- f_l is a stress factor depending on the type of application, in this instance 3, similar to the value labeled for a naval gear train in [1].
- f_n is a factor for rotation, considered 0.405, value obtained from [1] for 500RPM.
- f_t is a factor for temperature, set as 1, since the prototype is projected to work in a low temperature environment.

In the case of the freewheel bearing, the force (F_n) that is responsible for its load results directly of the forces applied on the pinion gear, thus resulting in the equation 4.26.

$$F_n = \sqrt{F_t^2 + F_r^2} \quad (4.26)$$

This culminated in the following results:

- Bearing SKF 61804 [42] for side A
 - $C = 2615\text{N} < 4030\text{N}$
 - $C_0 = 320\text{N} < 2320\text{N}$
- Bearing SKF 16005 [43] for side B
 - $C = 4800\text{N} < 8060\text{N}$
 - $C_0 = 585\text{N} < 4750\text{N}$
- GMN Freewheel Clutch FPD 437 M [44] for the gears in the position 1
 - $C = 4960\text{N} < 9200\text{N}$
 - $C_0 = 480\text{N} < 8140\text{N}$

4.4.3 Shafts

The shaft (fig 4.7) was modeled in MDSolids [45] and analyzed using the "Bending Deformation" of the "General Analysis Module". This approach was used due to the added complexity a variable diameter shaft brings. From this analysis 8 plots resulted, shown in appendix A.

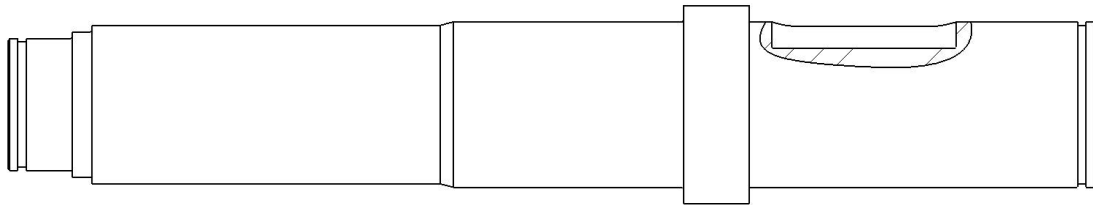


Figure 4.7: The final Shaft designed to fulfill the rigidity and fatigue criteria, and confine the gears and bearings

From these plots is possible to use the values of the slope (tab. 4.2) and deflection (tab. 4.3) from the critical points, i.e., gears and bearings, and guarantee the shaft meets the criteria for rigidity set in [1].

Following this verification, the fatigue strength was verified with the Solderberg method described in [1], throughout all the critical stress points, i.e., changes of diameter and keyway section.

Using the same plots from appendix A is possible to know the bending moment (M_b) by combining the moments from both directions, as in equation 4.27, and with it and the diameter of this section (\varnothing) it is possible to calculate the alternate tension (σ_a) (equation 4.28).

$$M_b = \sqrt{M_{b_y}^2 + M_{b_z}^2} \quad (4.27)$$

Table 4.2: The Slope values obtained from the MDSolids (Appendix A) and the confirmation the values are under the admissible by [1] (in mRad)

	Y Direction	Z Direction	$\sqrt{Y^2 + Z^2}$	Admissible
Bearing A	0.11	0.30	0.32	3
Gear 1	0.00	0.02	0.02	0.5
Gear 2	0.09	0.25	0.27	0.5
Bearing B	0.12	0.32	0.34	3

Table 4.3: The Deflection values obtained from the MDSolids (Appendix A) and the confirmation the values are under the admissible by [1] (in mm)

	Y Direction	Z Direction	$\sqrt{Y^2 + Z^2}$	Admissible
Gear 1	0.0055	0.0148	0.0158	0.02
Gear 2	0.003	0.009	0.0095	0.02
Maximum	0.0055	0.0148	0.0158	1.525

$$\sigma_a = \frac{32 * M_b}{\pi * \varnothing^3} \quad (4.28)$$

Similarly, the alternate torsion, represented by τ_a is a result of equation 4.29, where M_t is the torque transmitted trough the shaft/gears.

$$\tau_a = \frac{16 * M_t}{\pi * \varnothing^3} \quad (4.29)$$

Both o these values are corrected by multiplying them with the factor of concentration (K_f), like in equation 4.30 and 4.31.

$$\sigma_f^{max} = K_f * \sigma_a \quad (4.30)$$

$$\tau_f^{max} = K_f * \tau_a \quad (4.31)$$

While K_f is defined by the equation 4.32. Where q is an index for sensibility for the material in relation to the radius of the geometry change and K_t a function of scale of the radius and its relation to overall size of change (both values used were captured from charts in [1])

$$K_f = 1 + q * (K_t - 1) \quad (4.32)$$

The σ_f^{max} and τ_f^{max} are then used to calculate the equivalent static tension (following Soderberg), equations 4.33 and 4.34.

$$\sigma_{static}^{equiv} = \sigma_f^{max} * \frac{\sigma_y}{\sigma_e^c} \quad (4.33)$$

$$\tau_{static}^{equiv} = \tau_f^{max} * \frac{\tau_y}{\tau_e^c} \quad (4.34)$$

Where σ_y and τ_y are the yield strength for normal and shear loads respectively, in this case considered 305MPa and 153MPa, σ_e^c and τ_e^c are the equivalent limits for fatigue considering the size and manufacture of the component, conditions represented by K_S and K_{AS} (equation 4.37) in the following equations 4.35 and 4.36, in which σ_e and τ_e are the theoretical limits for fatigue from [1].

$$\sigma_e^c = K_{AS} * K_S * \sigma_e \quad (4.35)$$

$$\tau_e^c = K_{AS} * K_S * \tau_e \quad (4.36)$$

$$K_{AS} = 1.189 * \phi^{-0.097} \quad (4.37)$$

From the Soderberg, equations 4.30 and 4.31, its possible to apply the von Mises yield criteria, resulting in equation 4.38.

$$\sigma_{VM} = \sqrt{(\sigma_{static}^{equiv})^2 + 3 * (\tau_{static}^{equiv})^2} \quad (4.38)$$

Which when compared with yield strength can provide the safety factor (SF) for this component to perform 10^8 cycles (equation 4.39), above the required $9.3 * 10^7$.

$$SF = \frac{\sigma_y}{\sigma_{VM}} \quad (4.39)$$

On the prototype developed the most critical point, located on the transition from 30mm diameter to 25mm, was verified with an SF of 6.2.

4.5 Main Carter

This structure (fig 4.8) holds most of the mechanical components and shields them from the outside environment. It is mostly constructed out of welded aluminum segments bolted together. This segments can be split by function.

One section of the carter is responsible for containing the buoy's shaft in place and prevent the ingress of water into the system, for this it holds both bearings and seals, one at each end and a wiper to clear any big debris. This section then screws into a spacing segment.

This section serves to allows the racks to move 300mm down from the pinions and connects the guiding system on the previous section to the PTO. Similarly, there is another section for the top of the prototype, this section is lighter, since it

serves a non structural role only doubling as a lid. Between the spacing elements fits the main part of the carter.

This last section holds all of the gears and locks the whole system to the table in which is mounted. This section is made out of aluminum plates welded together, forming an open box and then machined to provide smooth surfaces to fix the bearings, two large holes on one side for the purpose of mounting the shafts, an hole on the bottom to fit the inferior spacing segment enabling it to receive the buoy's shaft and lastly another for the gearbox to hold the final gear and seal the system.

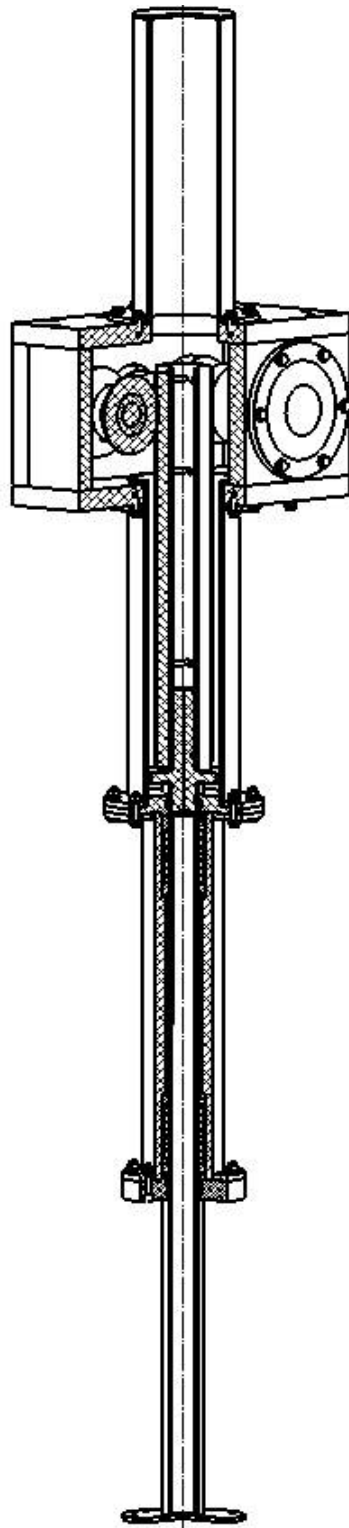


Figure 4.8: A representation of the different parts of the carter and the parts confined in them.

4.6 Gearbox

For the selection of the gearbox several requirements were established along with its ability to transmit the necessary torque. An initial range of multiplication from 1:4 to 1:7, this range was based on the ability to alter the second set of gear of the PTO to match the targeted 1000RPM at the exit of the selected gearbox. Also, this gearbox had to have a long input shaft to enter the PTO.

These criteria culminated in a gearbox from STM (fig 4.9) with a ratio of 1:5.3 and capable of 26.8Nm of torque [16].



Figure 4.9: Graphical representation of a gearbox from the same product line as the one selected [16].

4.7 Miscellaneous components

In addition to all the components above, other components are part of this system, this includes the supporting material such as an aluminium profile from which the table supporting the entire system is made of, a coupling that connects the exit from the gearbox to the generator and additional O-Rings that seal the static connections between every part of the main carter including the two side lids.

Chapter 5

Conclusion and Future Work

In conclusion, in this dissertation was developed a concept of a PTO, intended for a WEC, based on a rack and pinion system. In this concept, the buoy is connected to two racks, on opposing sides, that transmit power to pinion gears. These pinions have a freewheel bearing inside stopping them from transmitting power to the shaft at the same time, this means one pinion is capable of recovering the force from the rack on the upstroke and the other on the downstroke.

This system thus allows energy capture both ways, and given the orientation of the gears means that the generator rotates in the same direction, so no energy is lost when the buoy reaches the top or the bottom of its oscillation. This constant state of energy recovery allows for a future implementation of a flywheel to smooth the erratic motion of the buoy.

Unfortunately, due to the current pandemic situation, the prototype was not built. This current situation impacted the arrival time of the material and given the timeline of this dissertation the materials would not arrive before its presentation. Hence testing it was not possible. Therefore it is dependent on future construction and application to truly know the efficiency of the PTO developed and the extent of the goals meet.

Upon the development of the prototype, several other possibilities were noted and unfortunately not explored. These other possibilities are as follows.

One design that could have been analysed prior to the decision to follow a traditional approach was one with two different connections, one shaft for guidance that would be responsible for withstanding all the lateral forces and the other would connect to the PTO. This design would separate the two systems enabling them to be designed separately, thus reducing its complexity and also reducing the height of the prototype when compared to both in the figure 3.3.

Another possibility, in relation to the prototype that was developed, is to instead of fixing the last gear of the PTO to the gearbox used, to use an exit shaft and have the last gear of the PTO permanently fixed to the actual PTO.

This would open the possibility of using a coupling to connect to the gearbox, thus allowing future changes to the multiplication, by changing the gearbox, in order to adapt to other types of waves.

Regarding the future of this prototype, it is necessary to reevaluate the current work and the possibility of integration of the idea described in the previous paragraph. Depending on the results of said analysis actually built the prototype to confirm its feasibility.

In the likelihood of this prototype being built, it would be interesting to perform two sets of tests.

An initial test to evaluate the dynamics of the prototype when acted upon the buoy shaft. This would likely involve moving the shaft up and down at different speeds and reaching different heights, with the idea of simulating the movement of the buoy under the various waves. A study like the one described would make it possible to determine the efficiency for the different conditions and establish a preferred operating range, without the interference of the buoys dynamics.

And a test of the buoy's dynamics, using the prototype as a platform to make some connection between the wave height and frequency, and the actual movement of the buoy. This could define the ideal buoy shape and size for added efficiency.

With these results, it would be possible to define a relationship between the wave size and the PTO's requirements. A crucial step in transforming this technology to full scale.

In addition to the tests, transforming the prototype here developed to produce alternating current (similar to the grid) could prove interesting and will possibly raise other points to improve on the current design. Another possible point for future improvement would be the addition of a flywheel before the generator to smooth the energy recovered, allowing a more constant curve of electricity produced.

Bibliography

- [1] António Completo and Francisco Q. Melo. *Introdução ao Projeto Mecânico*. Booki - Conteúdos Especializados, Lda., 03 2019.
- [2] Joseph Spadaro, Lucille Langlois, and B. Hamilton. Greenhouse gas emissions of electricity generation chains: Assessing the difference. *IAEA Bulletin*, 42:19–24, 01 2000.
- [3] Eurostat. Share of energy from renewable sources. https://ec.europa.eu/eurostat/databrowser/view/nrg_ind_ren/default/table?lang=en, 2021. Accessed: 04-03-2021.
- [4] Markel Penalba and John Ringwood. A review of wave-to-wire models for wave energy converters. *Energies*, 7:506, 06 2016.
- [5] António F. de O. Falcão. Wave energy utilization: A review of the technologies. *Renewable and Sustainable Energy Reviews*, 14(3):899–918, 2010.
- [6] EMEC: European Marine Energy Centre. Pelamis wave power. <http://www.emec.org.uk/about-us/wave-clients/pelamis-wave-power/>. Accessed: 18-03-2021.
- [7] Linnea Sjökvist, Remya Krishna, Magnus Rahm, Valeria Castellucci, Hagnestål Anders, and Mats Leijon. On the optimization of point absorber buoys. *Journal of Marine Science and Engineering*, 2(2):477–492, 2014.
- [8] Siming Zheng, Yongliang Zhang, and Gregorio Iglesias. Concept and performance of a novel wave energy converter: Variable aperture point-absorber (vapa). *Renewable Energy*, 01 2020.
- [9] I. Hashem, H.S. Abdel Hameed, and M.H. Mohamed. An axial turbine in an innovative oscillating water column (owc) device for sea-wave energy conversion. *Ocean Engineering*, 164:536–562, 2018.

-
- [10] Qing Li, Abayomi Obisesan, • Tsz, Hang Wong, N Fernandez, S Kim, Z Morsy, V Novak, K Shiraishi, Maria Cusano, Q Li, Jorge Urrego-Blanco, T Wong, and Philip Wilson. *Coastal City and Ocean Renewable Energy: Pathway to an Eco San Andres Acknowledgements*. The Print Centre, University of Southampton, 10 2019.
- [11] Amelie Tetu. *Power Take-Off Systems for WECs*, pages 203–220. Springer, Cham, 01 2017.
- [12] Srinivasan Chandrasekaran and Harender Sinhmar. Power generation using mechanical wave energy converter. *The International Journal of Ocean and Climate Systems*, 3:57–70, 03 2012.
- [13] Y. Liu, L. Xu, and L. Zuo. Design, modeling, lab, and field tests of a mechanical-motion-rectifier-based energy harvester using a ball-screw mechanism. *IEEE/ASME Transactions on Mechatronics*, 22(5):1933–1943, 2017.
- [14] Daniela Valente. Mecanismos inovadores para recuperação de energia do movimento do mar. Master’s thesis, Universidade de Aveiro, Aveiro, 2019.
- [15] Tesup. Yuzo wing turbine. <https://www.tesup.co.uk/product-page/yuzo-wind-turbine-made-in-europe>. Accessed: 01-09-2021.
- [16] TM2A. Redutor em linha monoestágio stm- série ar/1. <https://www.tm2a.pt/catalogo/redutor-em-linha-monoestagio-serie-ar1/>. Accessed: 17-10-2021.
- [17] The European Commission. *The European Green Deal*. The European Commission, 2019.
- [18] A.K. Akella, R.P. Saini, and M.P. Sharma. Social, economical and environmental impacts of renewable energy systems. *Renewable Energy*, 34(2):390–396, 2009. Renewable Energy for Sustainable Development in the Asia Pacific Region.
- [19] Lanre Olatomiwa, Saad Mekhilef, M.S. Ismail, and M. Moghavvemi. Energy management strategies in hybrid renewable energy systems: A review. *Renewable and Sustainable Energy Reviews*, 62:821–835, 2016.
- [20] Omar Farrok, Koushik Ahmed, Abdirazak Dahir Tahlil, Mohamud Mohamed Farah, Mahbubur Rahman Kiran, and Md. Rabiul Islam. Electrical power generation from the oceanic wave for sustainable advancement in renewable energy technologies. *Sustainability*, 12(6), 2020.

-
- [21] Teodora Diana Corsatea and Davide Magagna. Overview of european innovation activities in marine energy technology. *JRC Science and Policy Reports*, 2013.
- [22] Yimy E. García Vera, Rodolfo Dufo-López, and José L. Bernal-Agustín. Energy management in microgrids with renewable energy sources: A literature review. *Applied Sciences*, 9(18), 2019.
- [23] John Brooke. *Wave Energy Conversion*. Elsevier, 2003.
- [24] Ehsan Enferad and Daryoush Nazarpour. Ocean’s renewable power and review of technologies: Case study waves. In Hasan Arman and Ibrahim Yuksel, editors, *New Developments in Renewable Energy*, chapter 12. IntechOpen, Rijeka, 2013.
- [25] Taylor J. R. M. Salter S. H., Jeffrey D. C. The architecture of nodding duck wave power generators, 1976.
- [26] James Bray, Ruben Fair, and K. Haran. Wind and ocean power generators. *Applied Superconductivity, IEEE Transactions on*, 24:1–7, 06 2014.
- [27] Andreas Poullikkas. Technology prospects of wave power systems. *Electronic Journal of Energy & Environment*, 01 2014.
- [28] Mohammed Faizal, M. Rafiuddin Ahmed, and Young-Ho Lee. A design outline for floating point absorber wave energy converters. *Advances in Mechanical Engineering*, 846097, 02 2014.
- [29] Ashank Sinha. Hydrodynamics of arrays of heaving point absorbers. Master’s thesis, Instituto Superior Técnico, Lisboa, 12 2015.
- [30] Robert H Bracewell. *Frog and PS Frog: a study of two reactionless ocean wave energy converters*. PhD thesis, University of Lancaster, 1990.
- [31] Benjamin Drew, Andrew Plummer, and Mehmet Sahinkaya. A review of wave energy converter technology. *Proceedings of The Institution of Mechanical Engineers Part A-journal of Power and Energy - PROC INST MECH ENG A-J POWER*, 223:887–902, 12 2009.
- [32] Mohd Afifi Jusoh, Mohd Zamri Ibrahim, Muhamad Zalani Daud, Aliashim Albani, and Zulkifli Mohd Yusop. Hydraulic power take-off concepts for wave energy conversion system: A review. *Energies*, 12(23), 2019.
- [33] Katie Mazerov. Multifunctional rack and pinion technology takes shape in oilfield as versatile, mobile rigs. *Drilling Rig Equipment*, pages 32–39, 2008.

- [34] Tanzila Younas, Muhammad Saadat, Imran Hussain, and Zubair Rashied. Energy recovery using ratchet mechanism: An experimental study. *Energy Procedia*, 118:104–109, 2017. 2017 2nd International Conference on Advances on Clean Energy Research (ICACER 2017), Berlin, Germany April 7-9, 2017.
- [35] Xiaofan Li, ChienAn Chen, Qiaofeng Li, Lin Xu, Changwei Liang, Khai Ngo, Robert G. Parker, and Lei Zuo. A compact mechanical power take-off for wave energy converters: Design, analysis, and test verification. *Applied Energy*, 278:115459, 2020.
- [36] Shangjun Ma, Tao Zhang, Geng Liu, Ruiting Tong, and Xiaojun Fu. Kinematics of Planetary Roller Screw Mechanism considering Helical Directions of Screw and Roller Threads. *Mathematical Problems in Engineering*, 2015:1–11, 2015.
- [37] Pushman Tlali, Rong-Jie Wang, and Stiaan Gerber. Magnetic gear technologies: A review. *Proceedings - 2014 International Conference on Electrical Machines, ICEM 2014*, 09 2014.
- [38] N. I. Berg, A. Becsei Christiansen, R. K. Holm, and P. O. Rasmussen. Design and test of a reluctance based magnetic lead screw pto system for a wave energy converter. In *2017 IEEE International Electric Machines and Drives Conference (IEMDC)*, pages 1–8, 2017.
- [39] Emmanuel B. Agamloh, Alan K. Wallace, and Annette von Jouanne. A novel direct-drive ocean wave energy extraction concept with contact-less force transmission system. *Renewable Energy*, 33(3):520–529, 2008.
- [40] Iñigo Martínez de Alegría, Jose Luis Martín, Iñigo Kortabarria, Jon Andreu, and Pedro Ibañez Ereño. Transmission alternatives for offshore electrical power. *Renewable and Sustainable Energy Reviews*, 13(5):1027–1038, 2009.
- [41] SKF. Lbc, d-series. [https://www.skf.com/binaries/pub12/Images/LBC%20D-series%20linear%20ball%20bearings%20and%20units%20-%2014058_3%20EN\(1\)\(1\)_tcm_12-252410.pdf](https://www.skf.com/binaries/pub12/Images/LBC%20D-series%20linear%20ball%20bearings%20and%20units%20-%2014058_3%20EN(1)(1)_tcm_12-252410.pdf). Accessed: 06-10-2021.
- [42] SKF. 61804. <https://www.skf.com/group/products/rolling-bearings/ball-bearings/deep-groove-ball-bearings/productid-61804>. Accessed: 11-10-2021.
- [43] SKF. 16005. <https://www.skf.com/group/products/rolling-bearings/ball-bearings/deep-groove-ball-bearings/productid-16005>. Accessed: 11-10-2021.

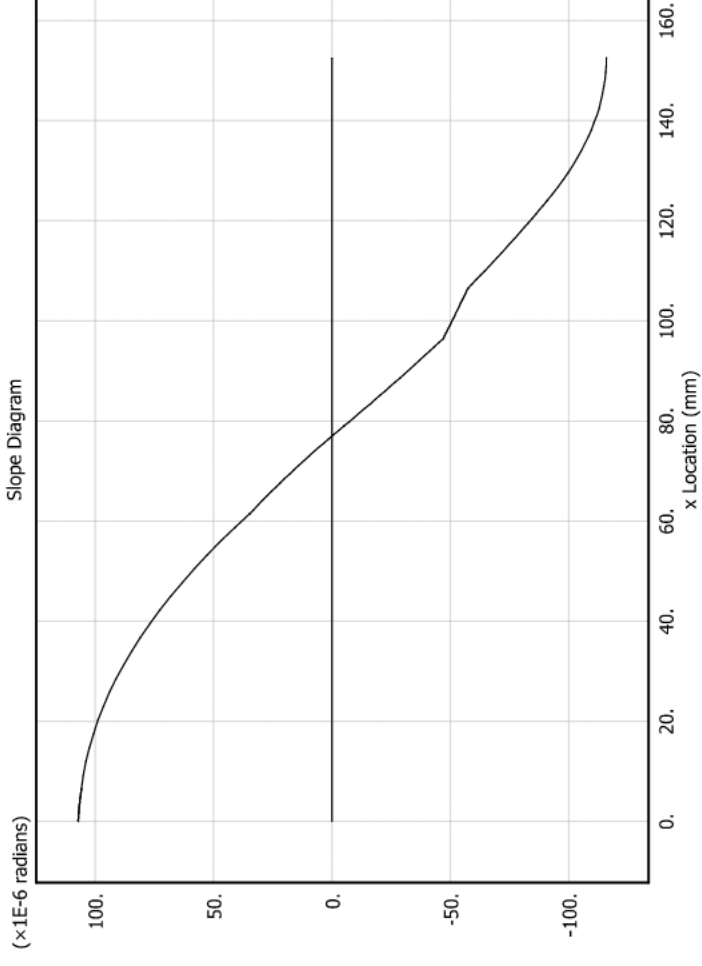
- [44] GMN. Complete freewheel clutch units. <https://www.gmn.de/en/freewheel-clutches/series/complete-freewheel-clutch-units/>. Accessed: 11-10-2021.
- [45] MDSolids. General analysis module. <https://web.mst.edu/~mdsolids/featuresSet.html>. Accessed: 12-10-2021.

Intentionally blank page.

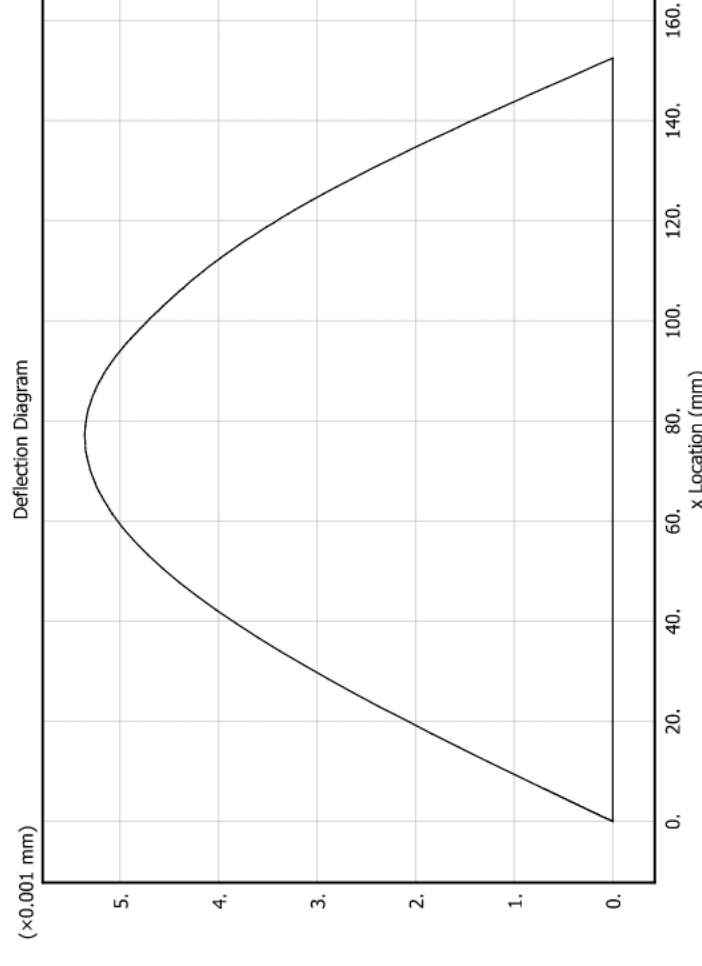
Appendix A

Plots From MDSolids

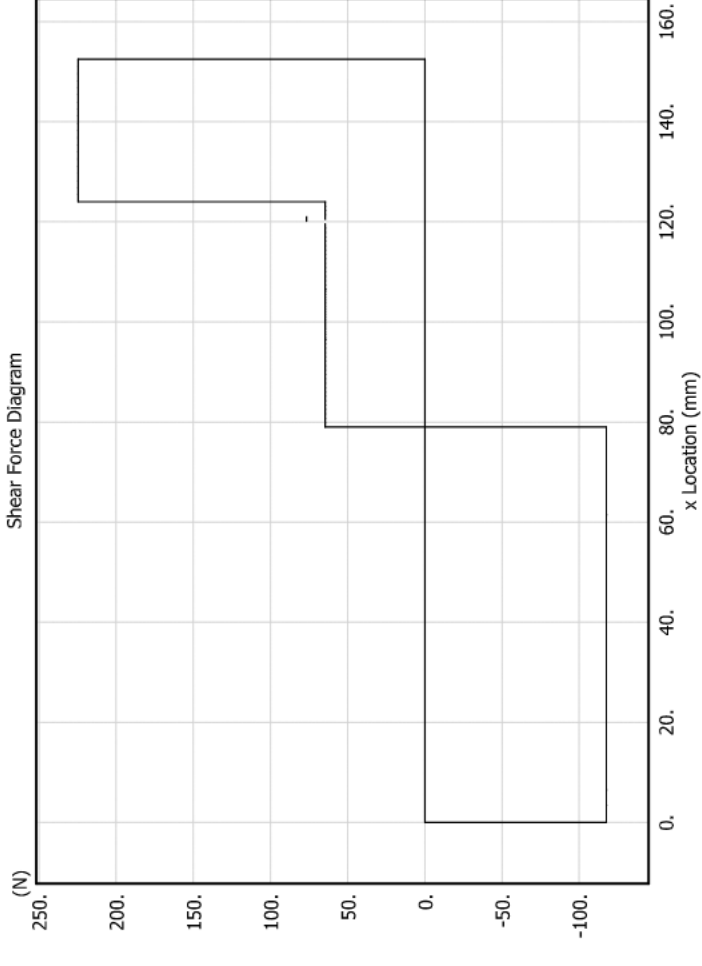
Y Direction Plot



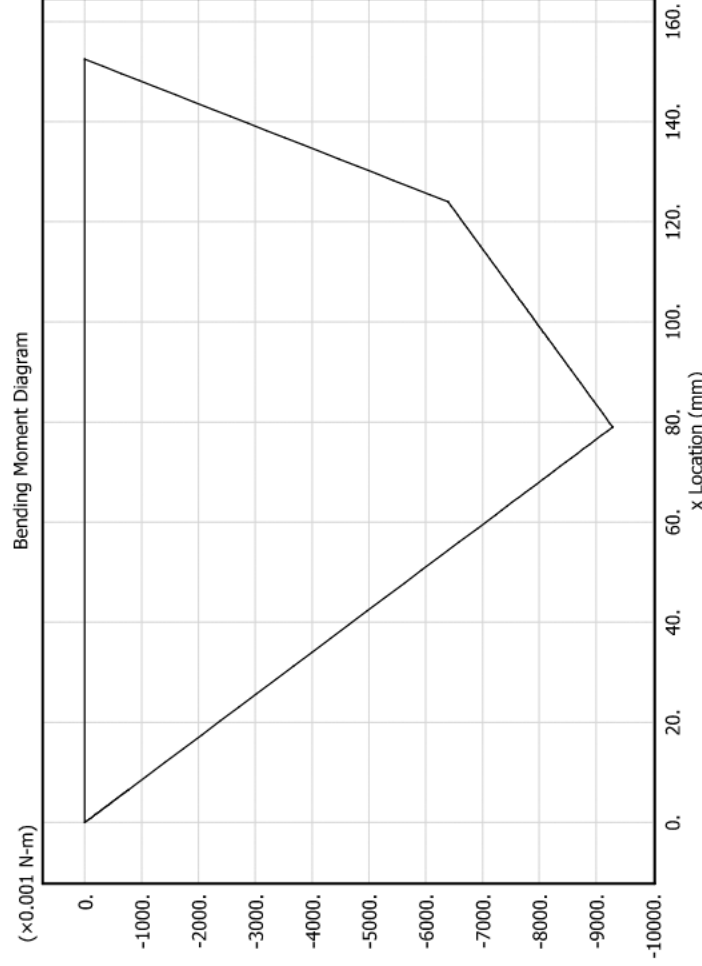
Deflection Diagram



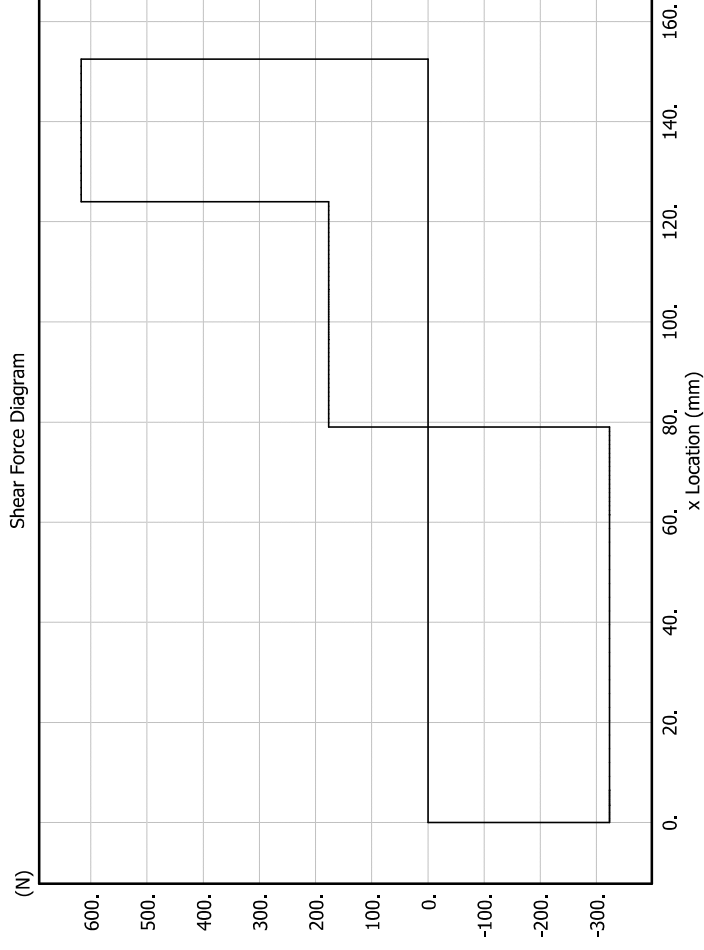
Y Direction Plot



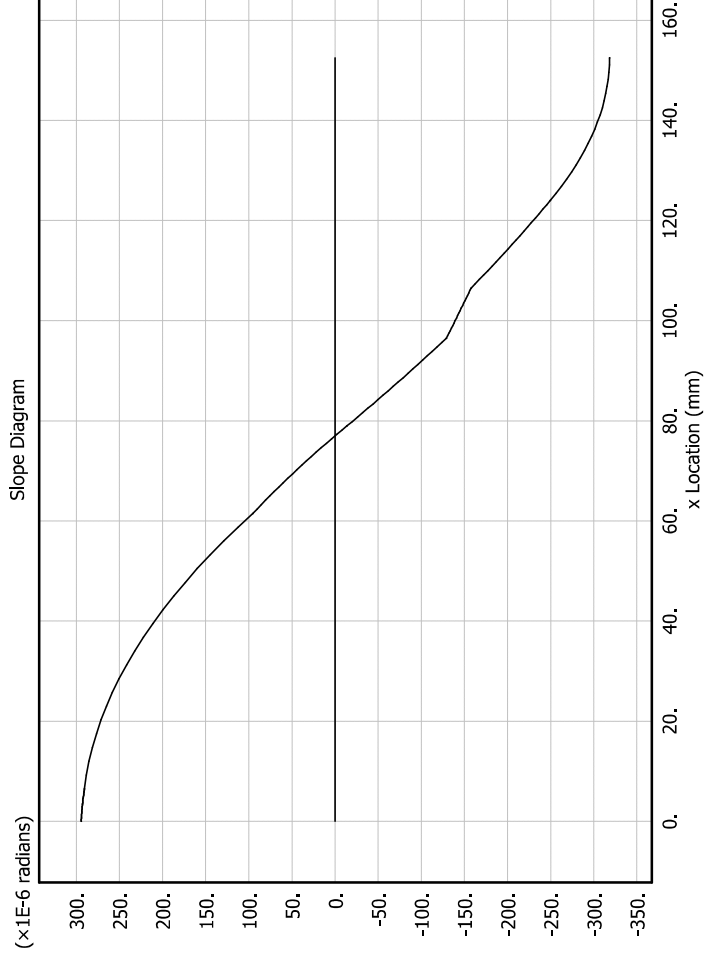
Bending Moment Diagram



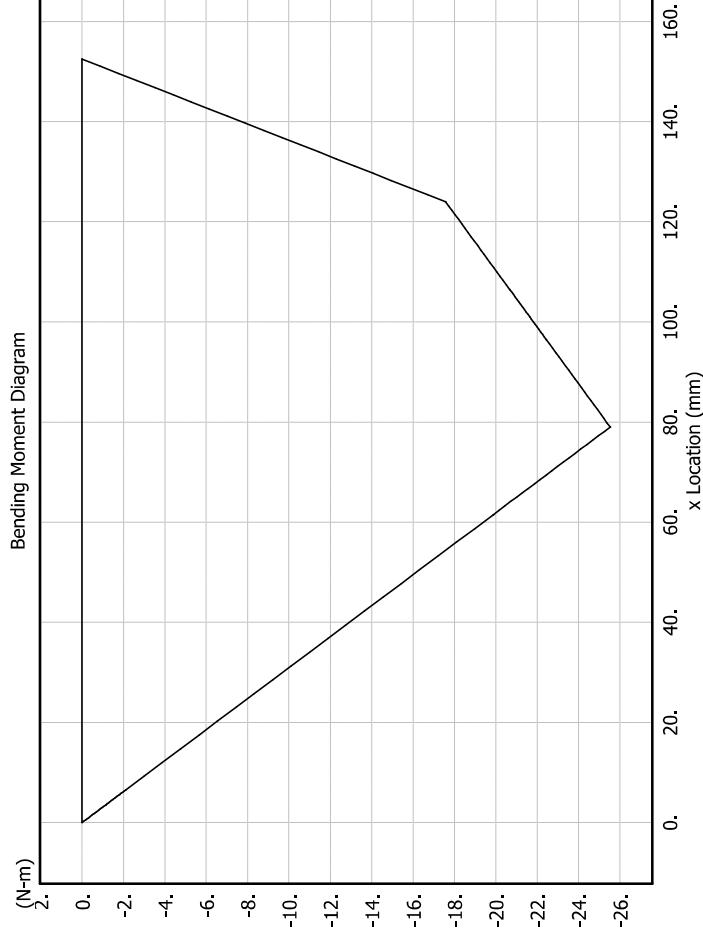
Z Direction Plot



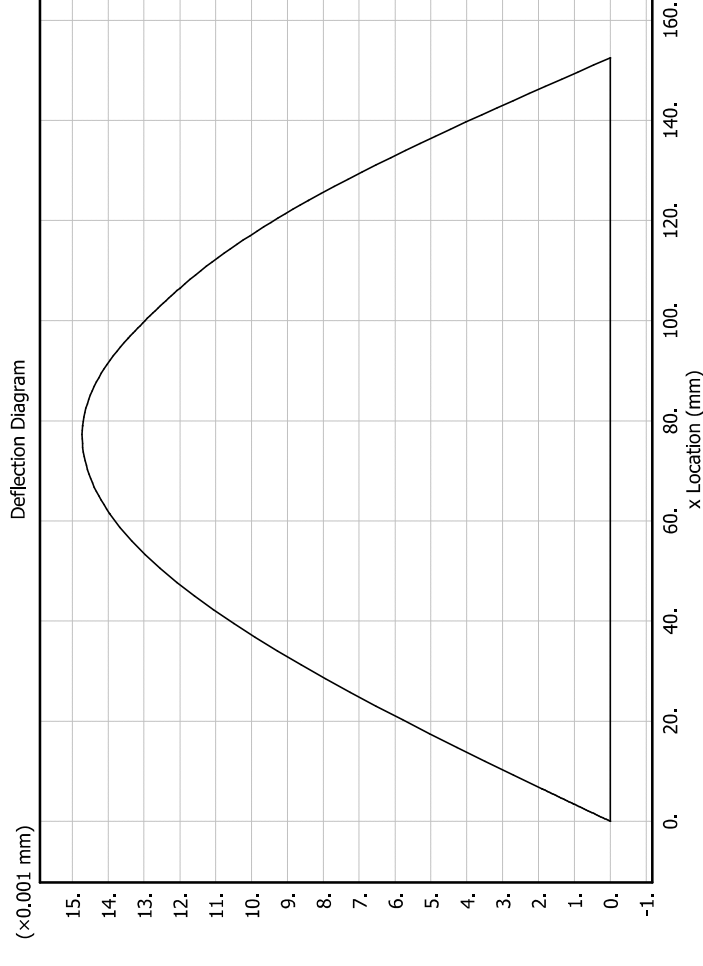
Z Direction Plot



Bending Moment Diagram



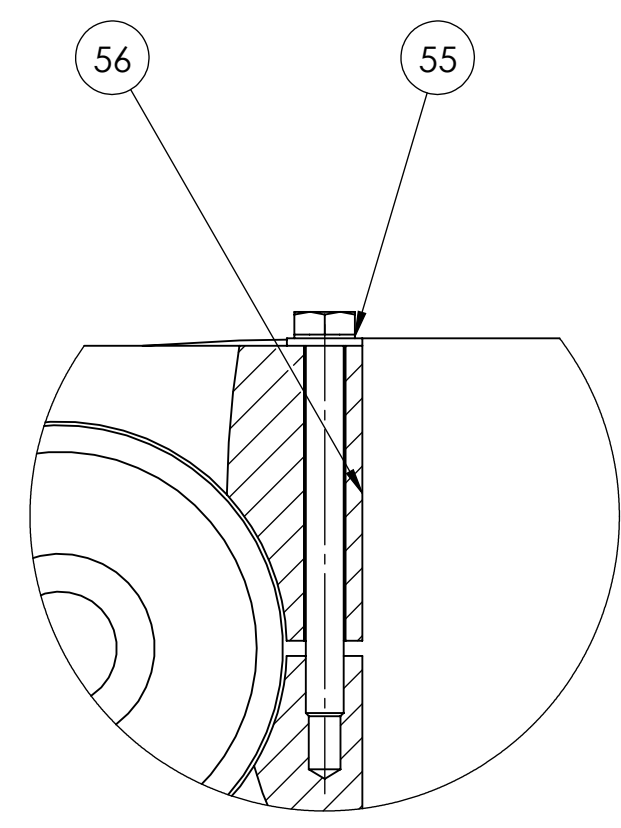
Deflection Diagram



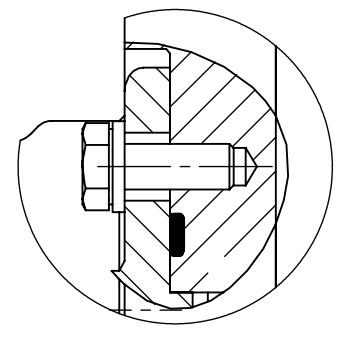
Intentionally blank page.

Appendix B

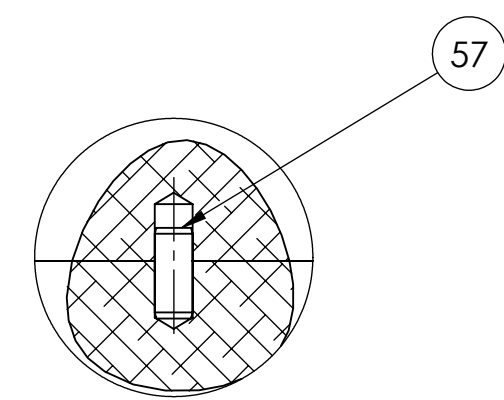
Technical Drawings



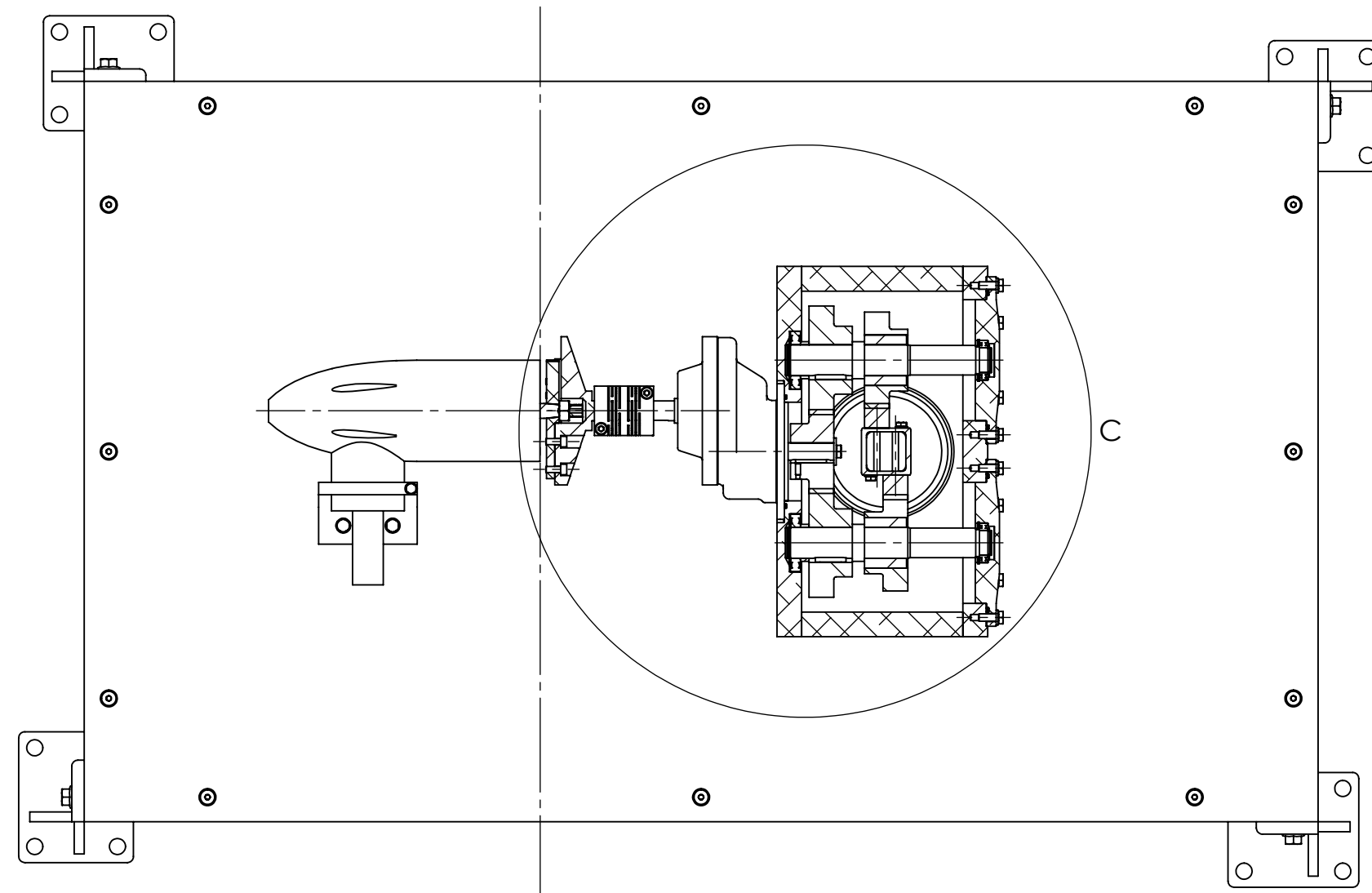
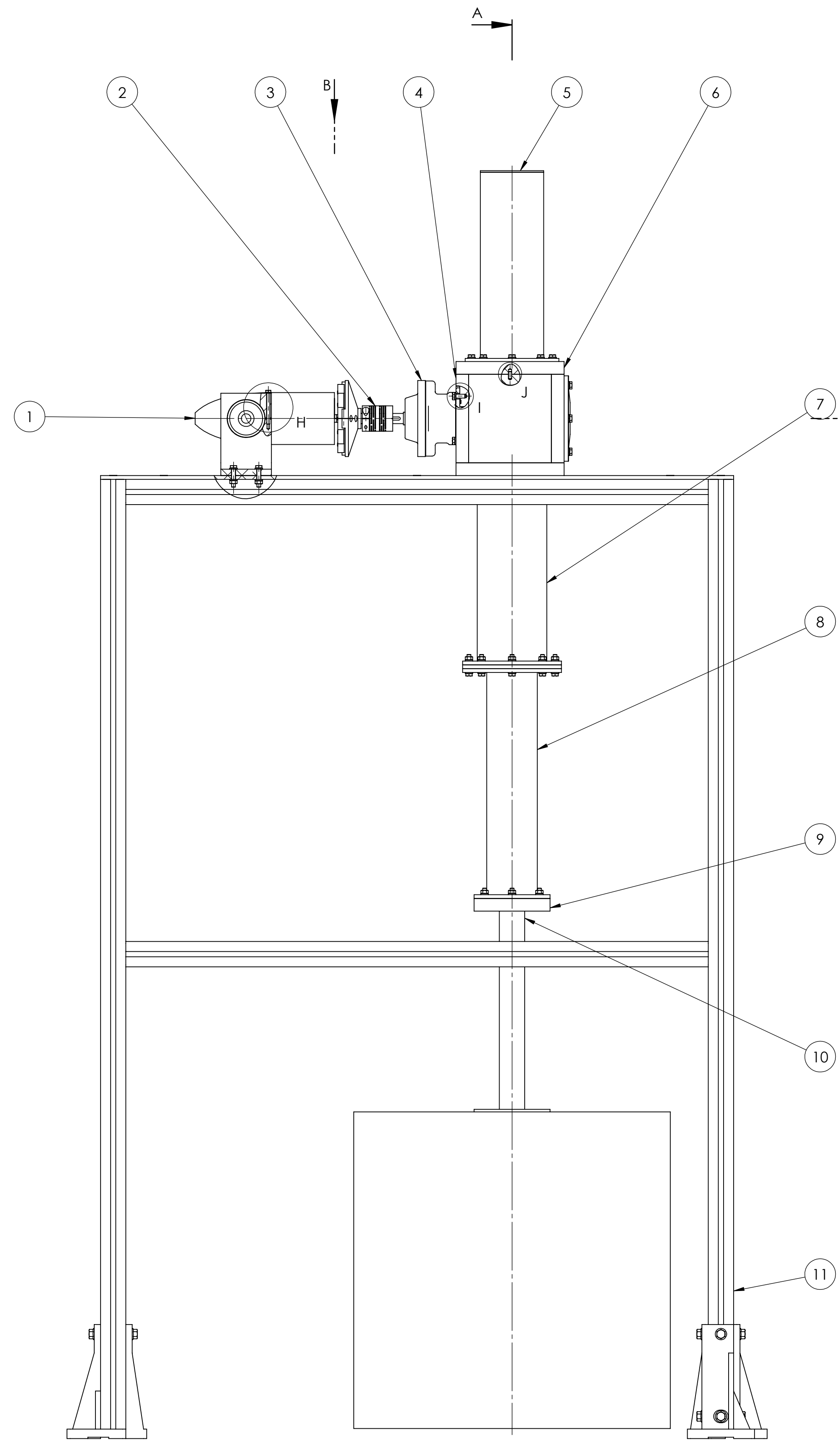
DETAIL H
SCALE 1:1



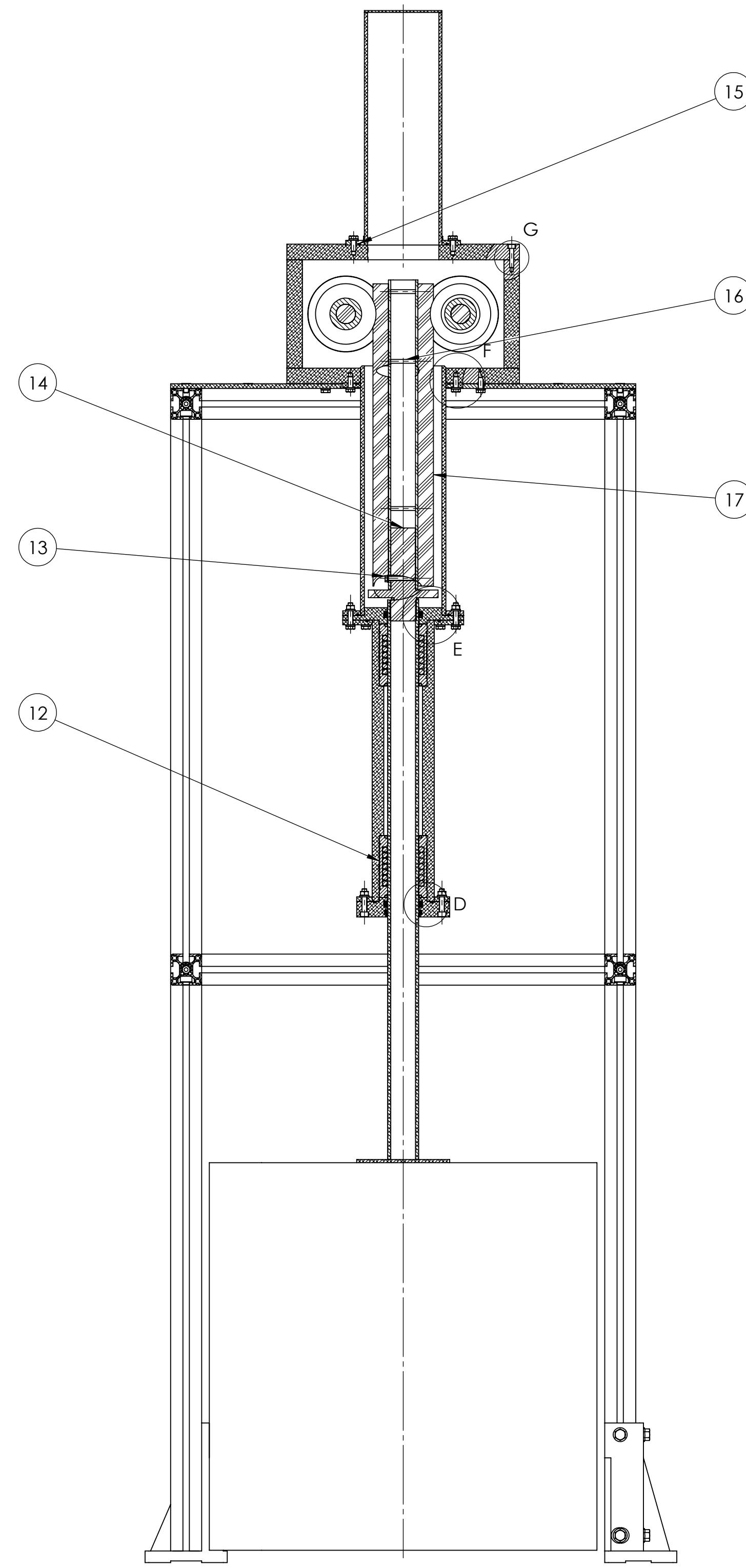
DETAIL I
SCALE 1:1



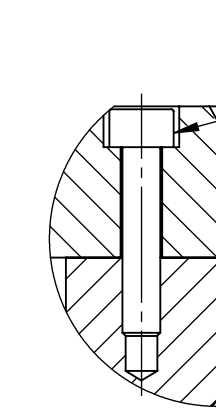
DETAIL J
SCALE 1:1



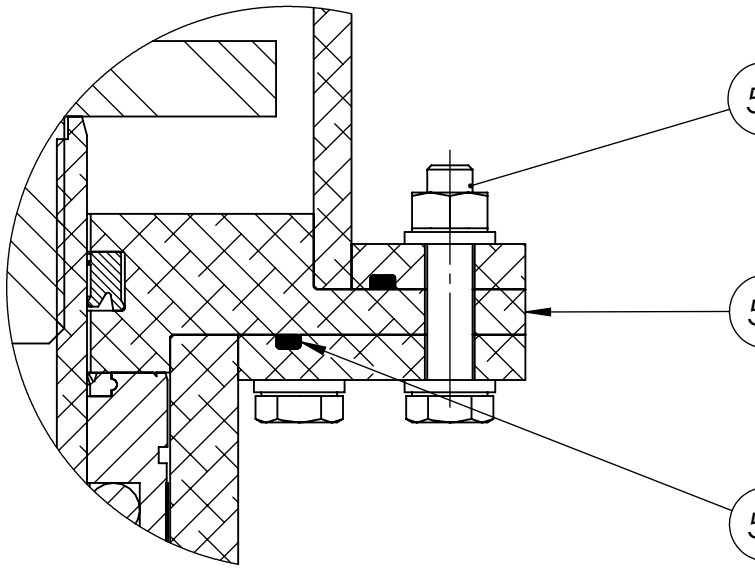
SECTION B-B



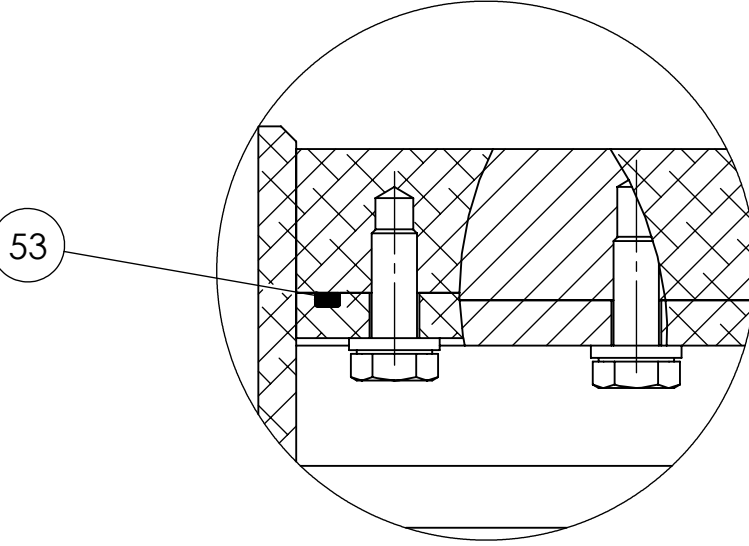
SECTION A-A



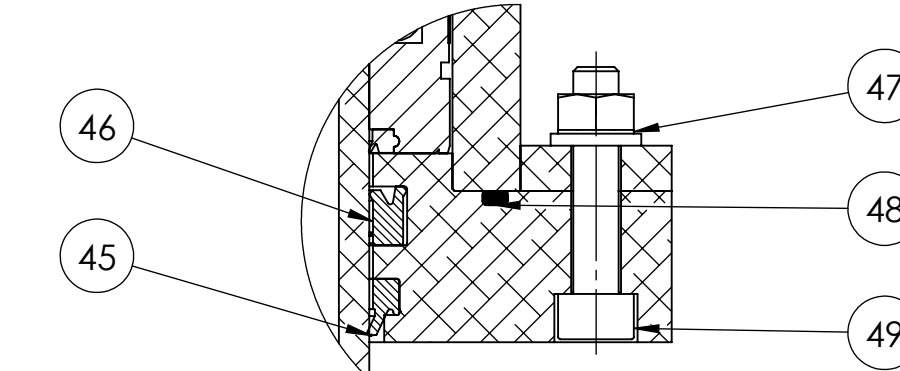
DETAIL G
SCALE 1:1



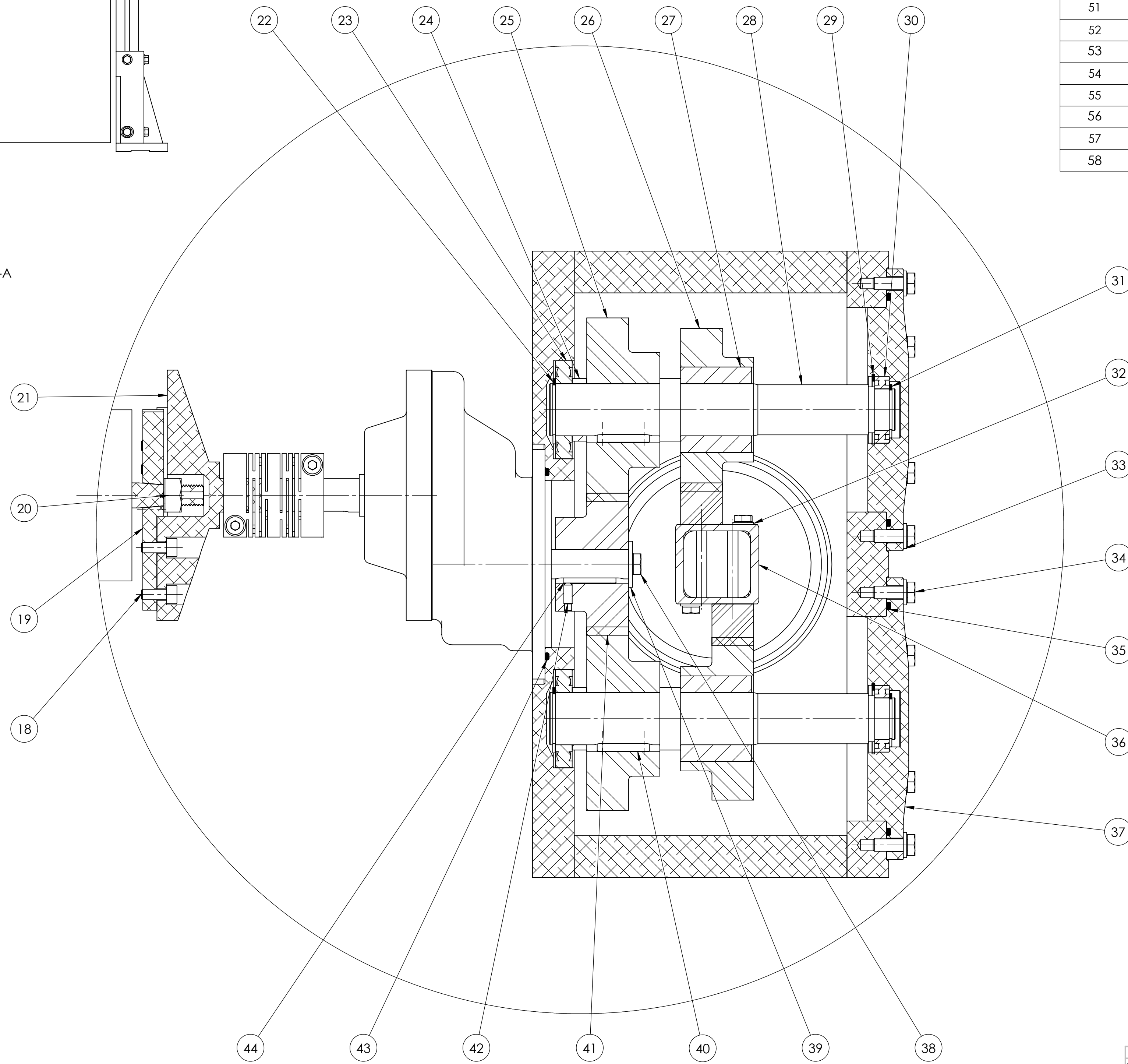
DETAIL E
SCALE 1:1



DETAIL F
SCALE 1:1



DETAIL D
SCALE 1:1



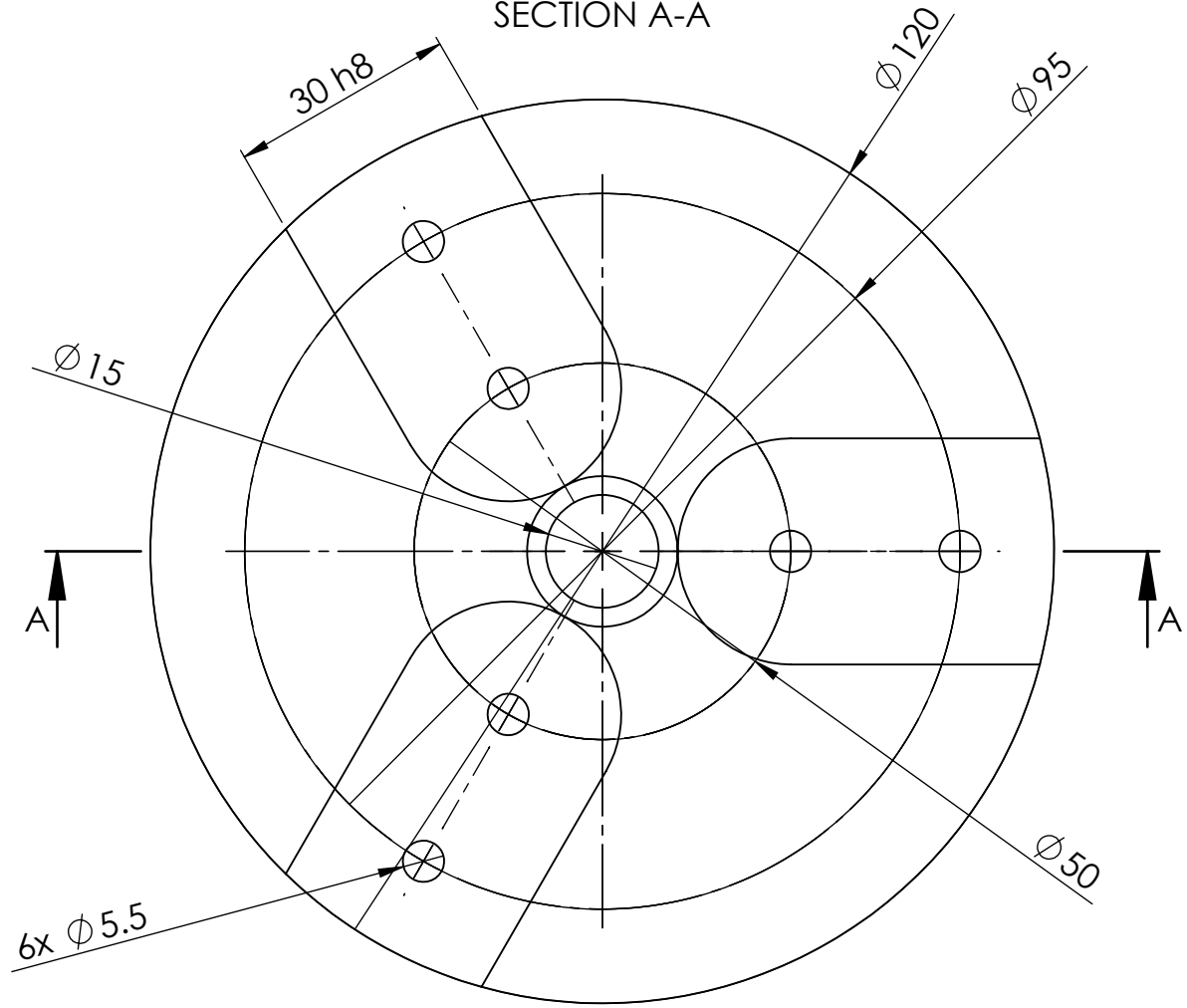
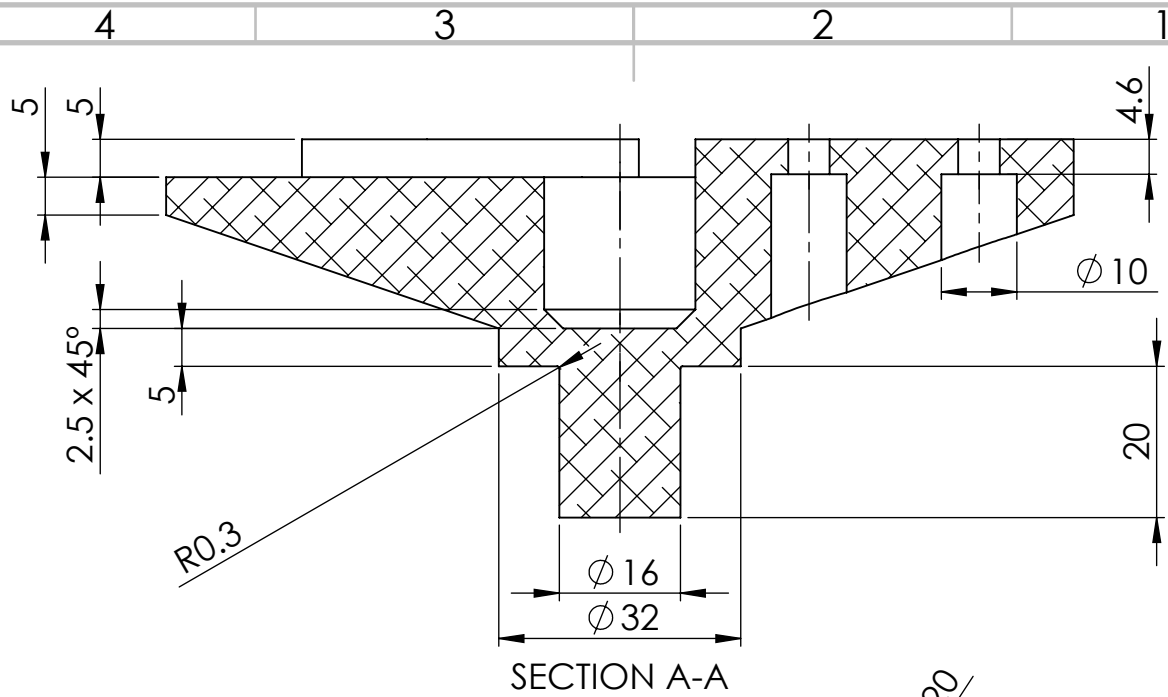
DETAIL C
SCALE 3:4

ITEM NO.	PART NUMBER	DESCRIPTION	QTY.
1	Gerador		1
2	Acoplador		1
3	Caixa_STM		1
4	Carter		1
5	TampaSup		1
6	Carter_Tampa		1
7	Espacador_Inf		1
8	Suporte_Haste		1
9	Tampa_Inf		1
10	Haste		1
11	Mesa (Perfil de Alumínio)		1
12	LBCD_40_D_2L3	Rolamentos lineares	2
13	ISO 4017 - M5 x 45-N		4
14	Juncao_Haste_Cremalheira		1
15	O-Ring110_2,5		1
16	ISO 8734 - 5 x 45 - A - S1		4
17	Cremalheira		2
18	ISO 4762 M5 x 12 - 12N		8
19	Suporte_pas		1
20	ISO - 4032 - M10 - W - N		1
21	Adaptador		1
22	Circip DIN 471 - 25 x 1.2		2
23	SKF - 16005 - 14.SI.NC.14_68		2
24	Espacador		2
25	Roda_intermedia		2
26	Roda_Entrada		2
27	GMN FPD 437 M	Freewheel Clutch	2
28	Veio		2
29	Circip DIN 472 - 32 x 1.2		2
30	SKF - 61804 - 18.SI.NC.18_68		2
31	Circip DIN 471 - 20 x 1.2		2
32	Washer ISO 7089 - 5		5
33	Washer ISO 7089 - 6		62
34	ISO 4017 - M6 x 16-N		36
35	O-Ring105_2,5		2
36	Suporte_Cremalheiras		1
37	Tampa_Lateral		2
38	ISO 4017 - M6 x 12-N		1
39	Washer ISO 7094 - 6		1
40	Parallel key A8 x 7 x 25 DIN 6885		2
41	Roda_Saida		1
42	DIN 916 - M4 x 10-N		1
43	O-Ring85_2,5		1
44	Parallel key A5 x 5 x 25 DIN 6885		1
45	DTW-40x48x50-J2G	Raspador	1
46	SIL 40x50x8	Vedante_Haste_SKF	2
47	ISO - 4032 - M6 - W - N		16
48	O-Ring70_2,5		1
49	ISO 4762 M6 x 30 - 30N		6
50	O-Ring90_2,5		1
51	Juncao_Suporte_Haste		1
52	ISO 4017 - M6 x 30-N		10
53	O-Ring115_2,5		1
54	ISO 4762 M5 x 25 - 25N		12
55	ISO 4017 - M5 x 50-N		1
56	Suporte_Gerador		1
57	ISO 8734 - 5 x 12 - A - S1		2
58	Boia		1

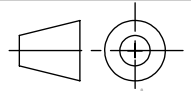
NAME	SCHAUER	DATE	TITLE
DRWEN	FRAN COELHO	20/09/2021	
CRD			
APPROV			
INFO			
GRA			

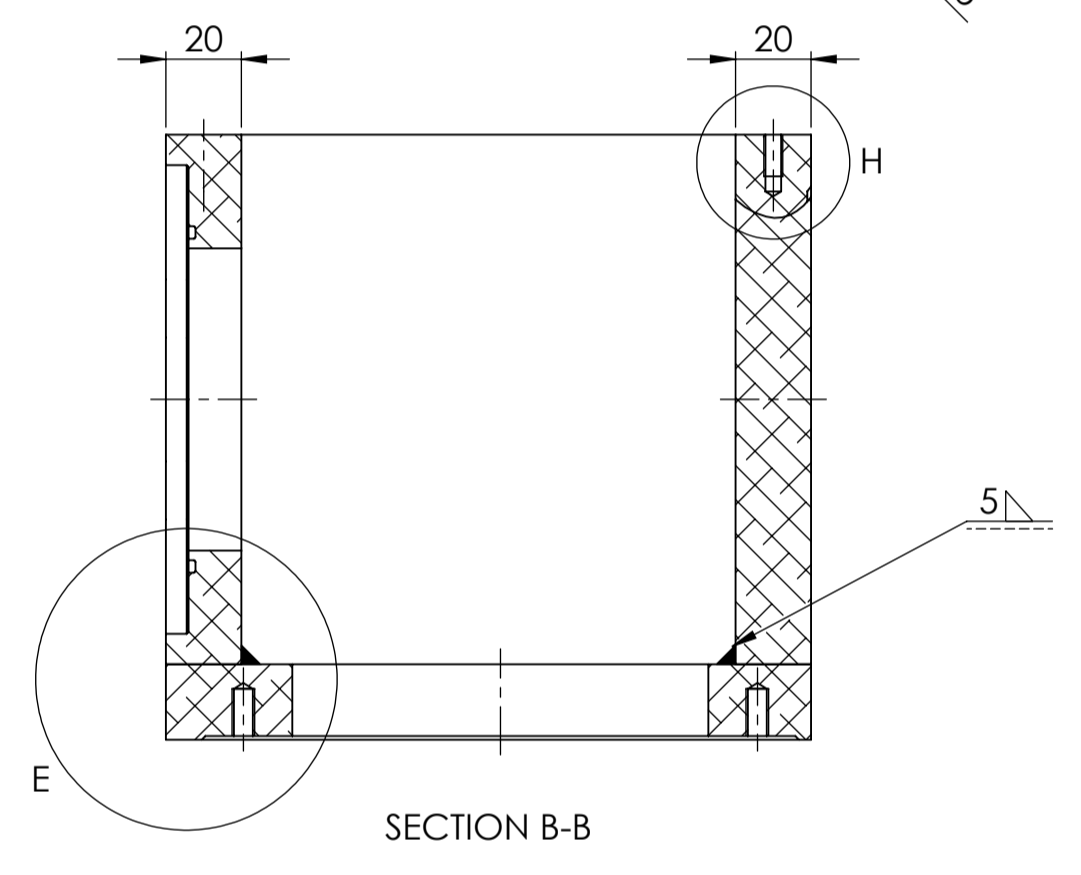
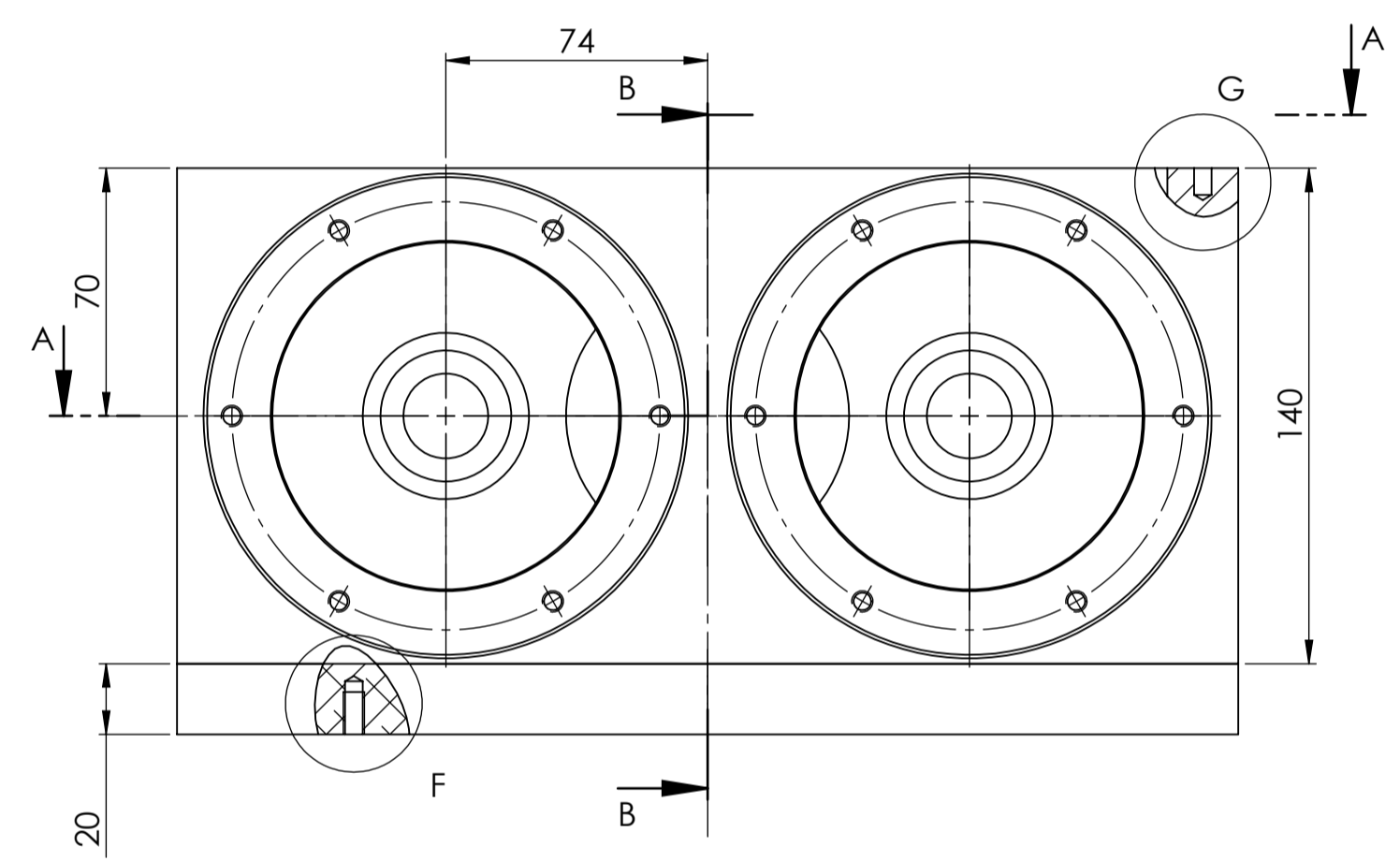
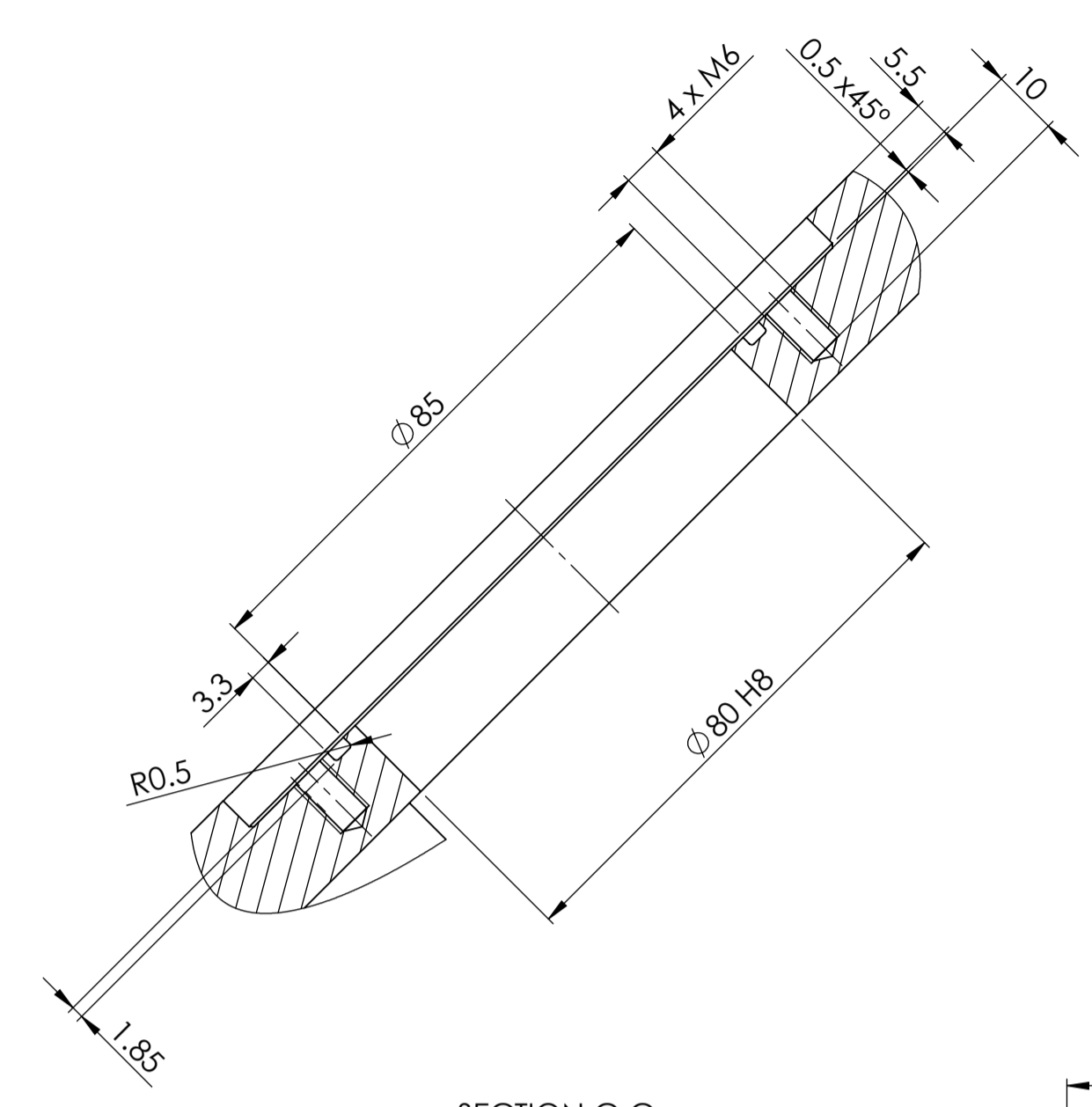
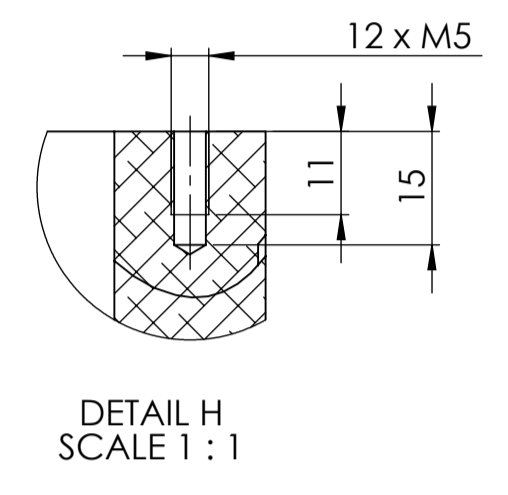
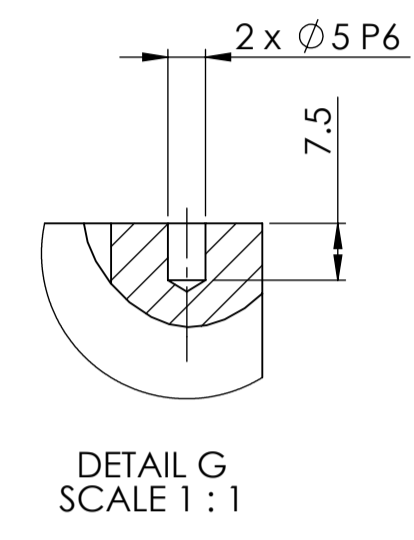
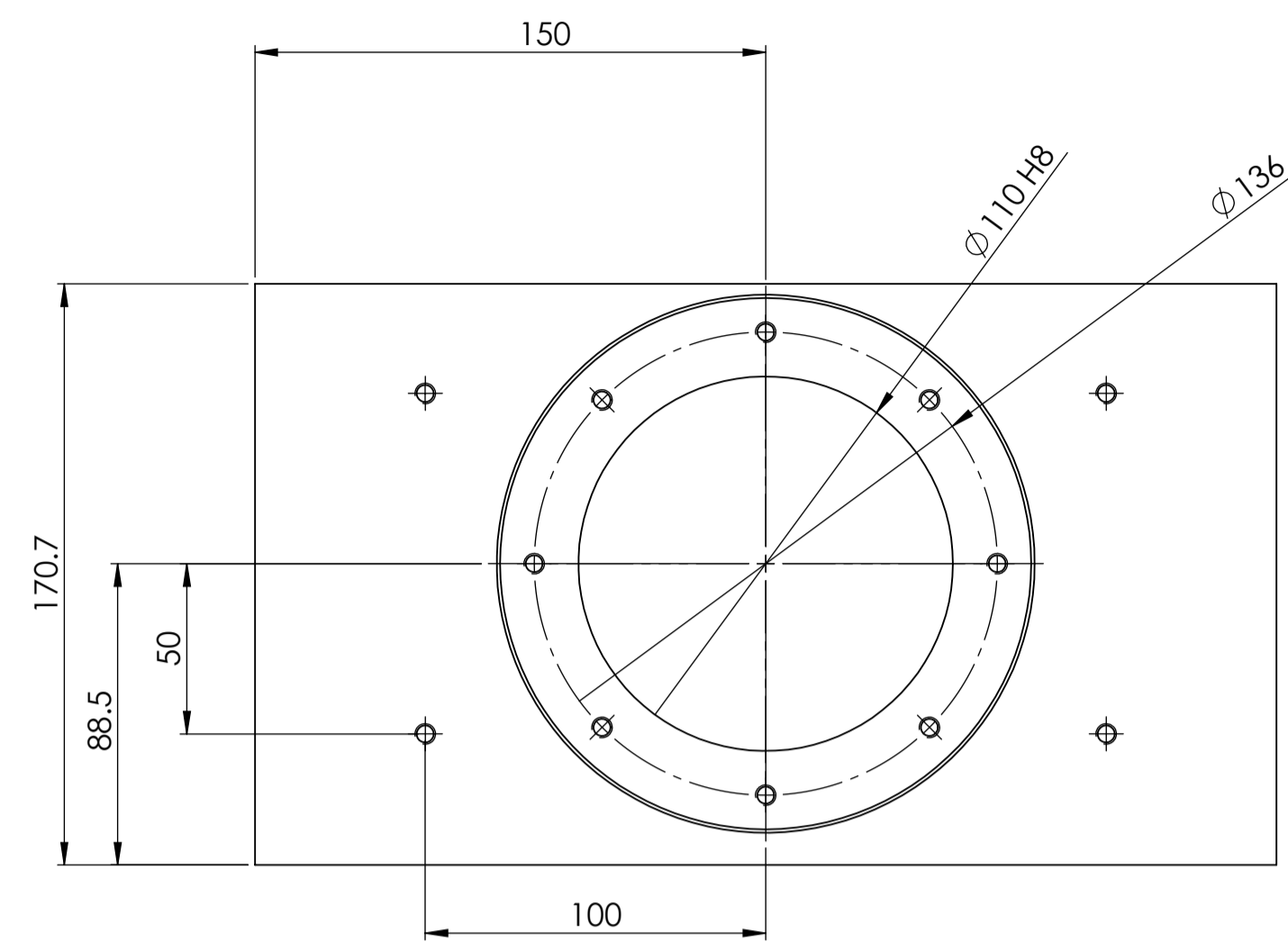
PTO_Prototype A0

SCALE: 3 SHEET OF 1

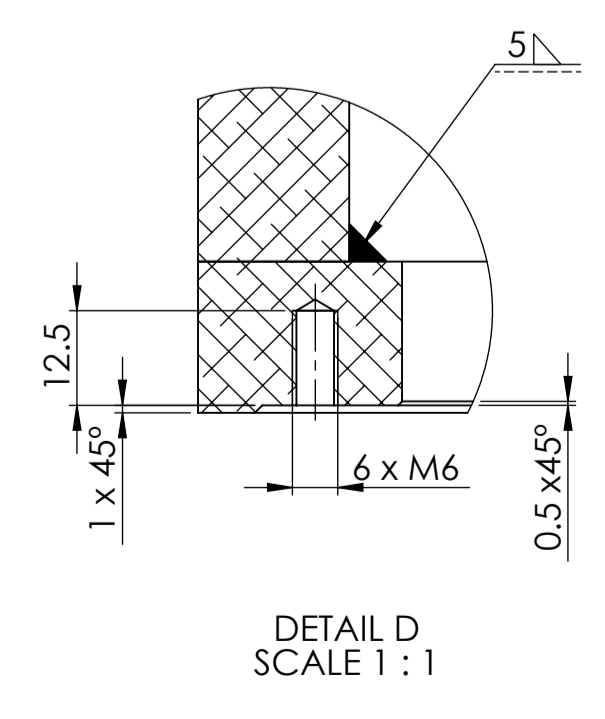
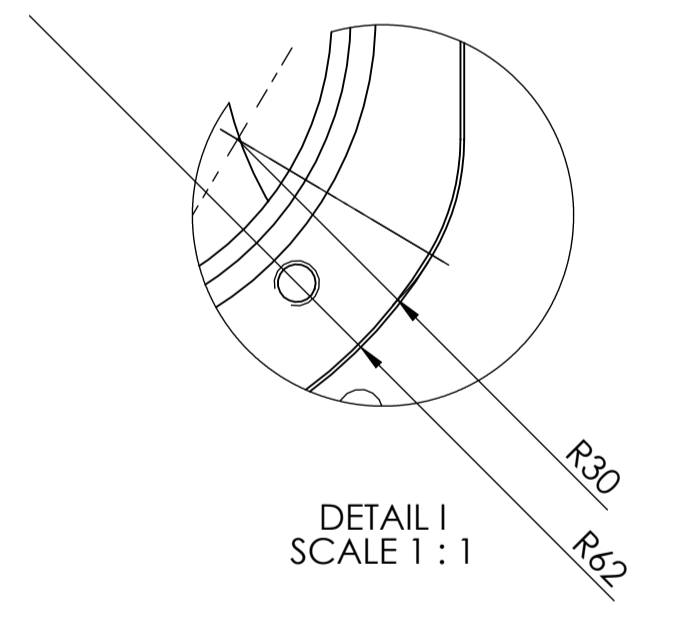
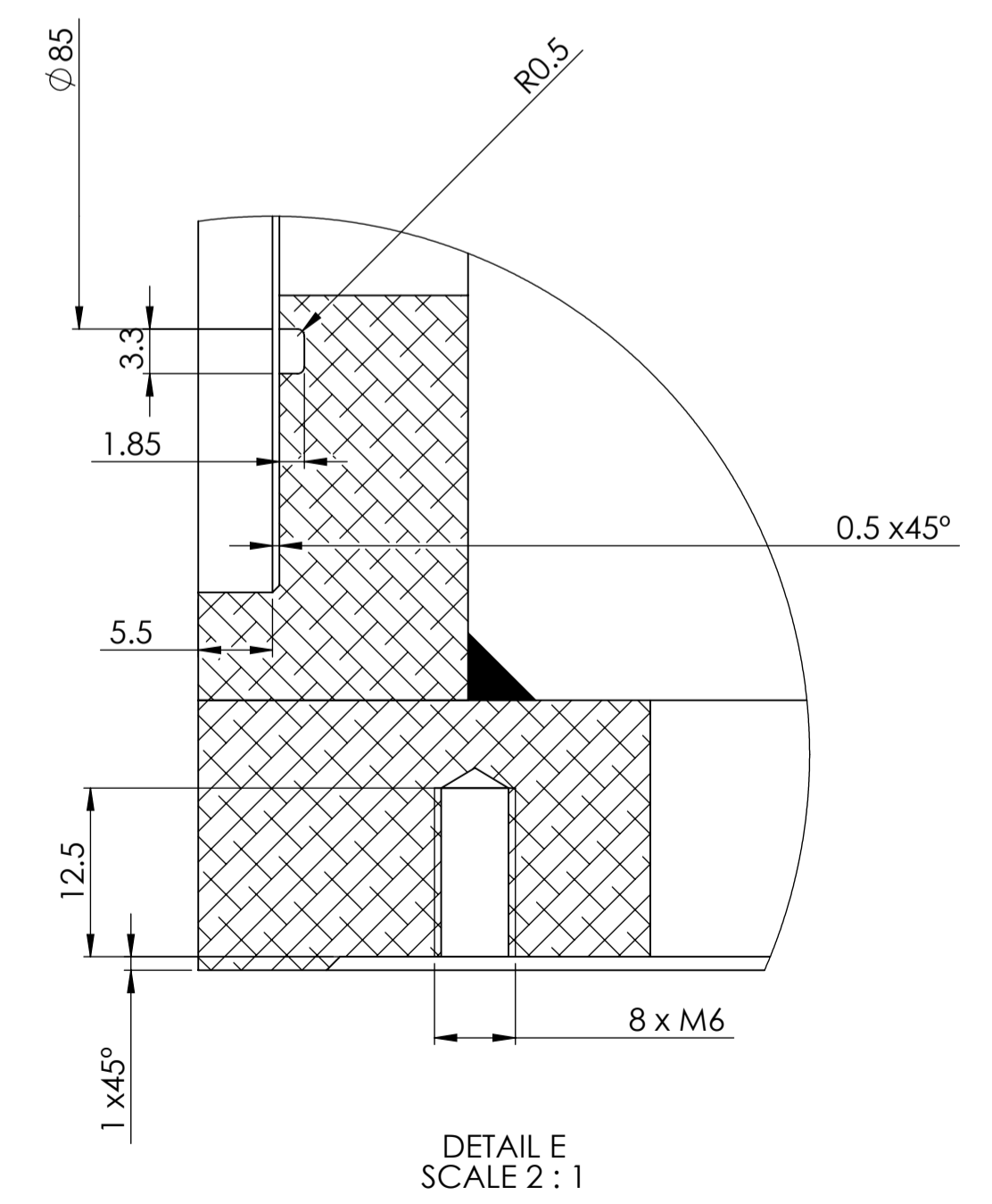
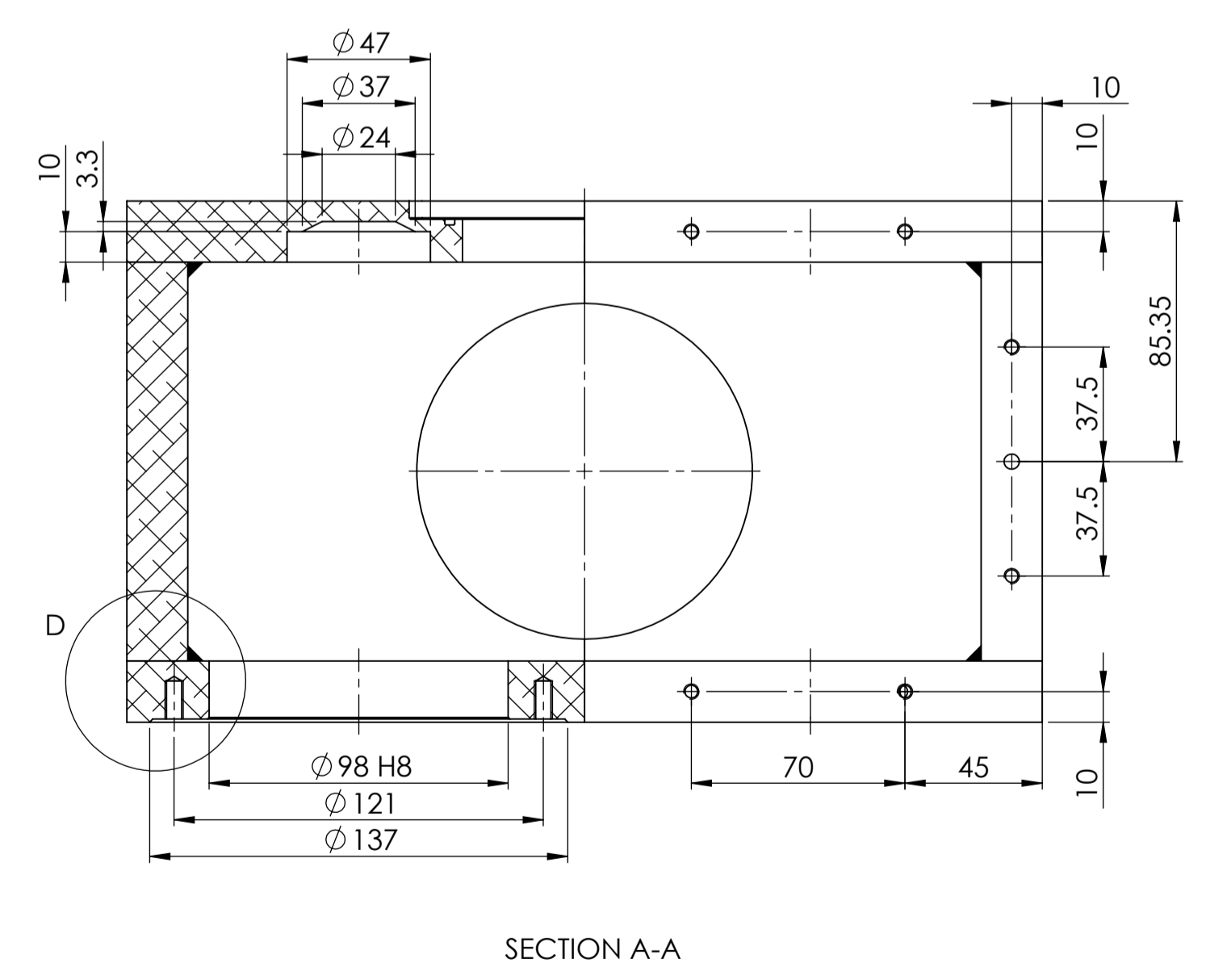
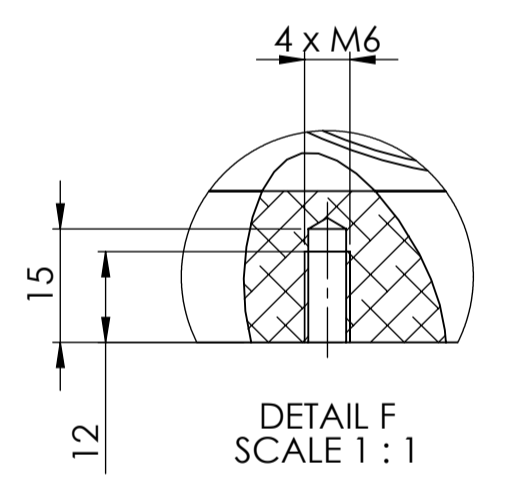
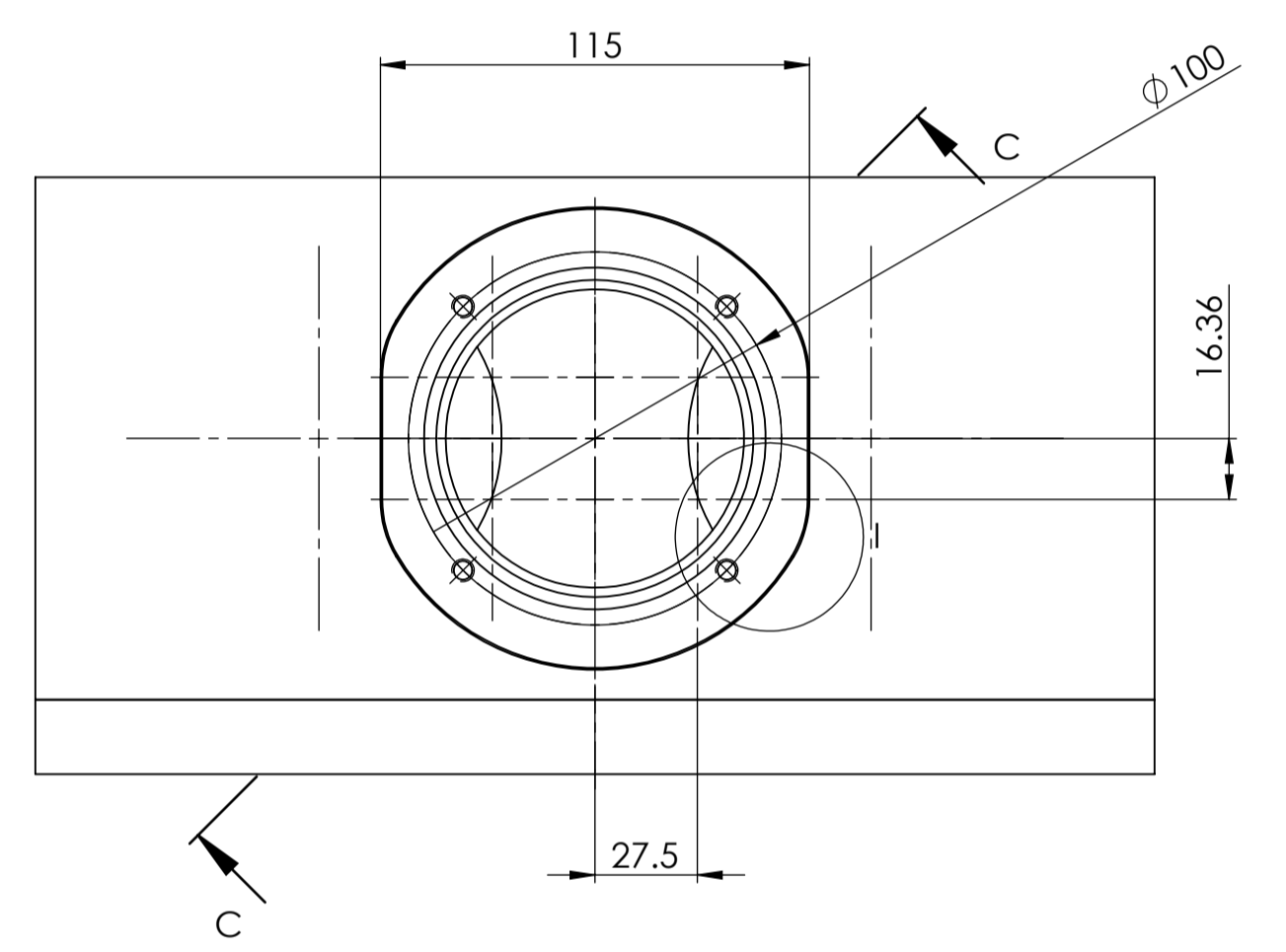


UNLESS OTHERWISE SPECIFIED: DIMENSIONS ARE IN MILLIMETERS		FINISH: ISO 8015 ISO 2768 - mK		DEBURR AND BREAK SHARP EDGES		DO NOT SCALE DRAWING		REVISION	
NAME		SIGNATURE		DATE		MATERIAL:		TITLE:	
DRAWN Paulo Cardoso				16/09/2021		AL 5xxx			
CHK'D									
APPV'D									
MFG									
Q.A									
						DWG NO.		A4	
						adaptador			
				WEIGHT:		SCALE:1:1		SHEET 1 OF 1	

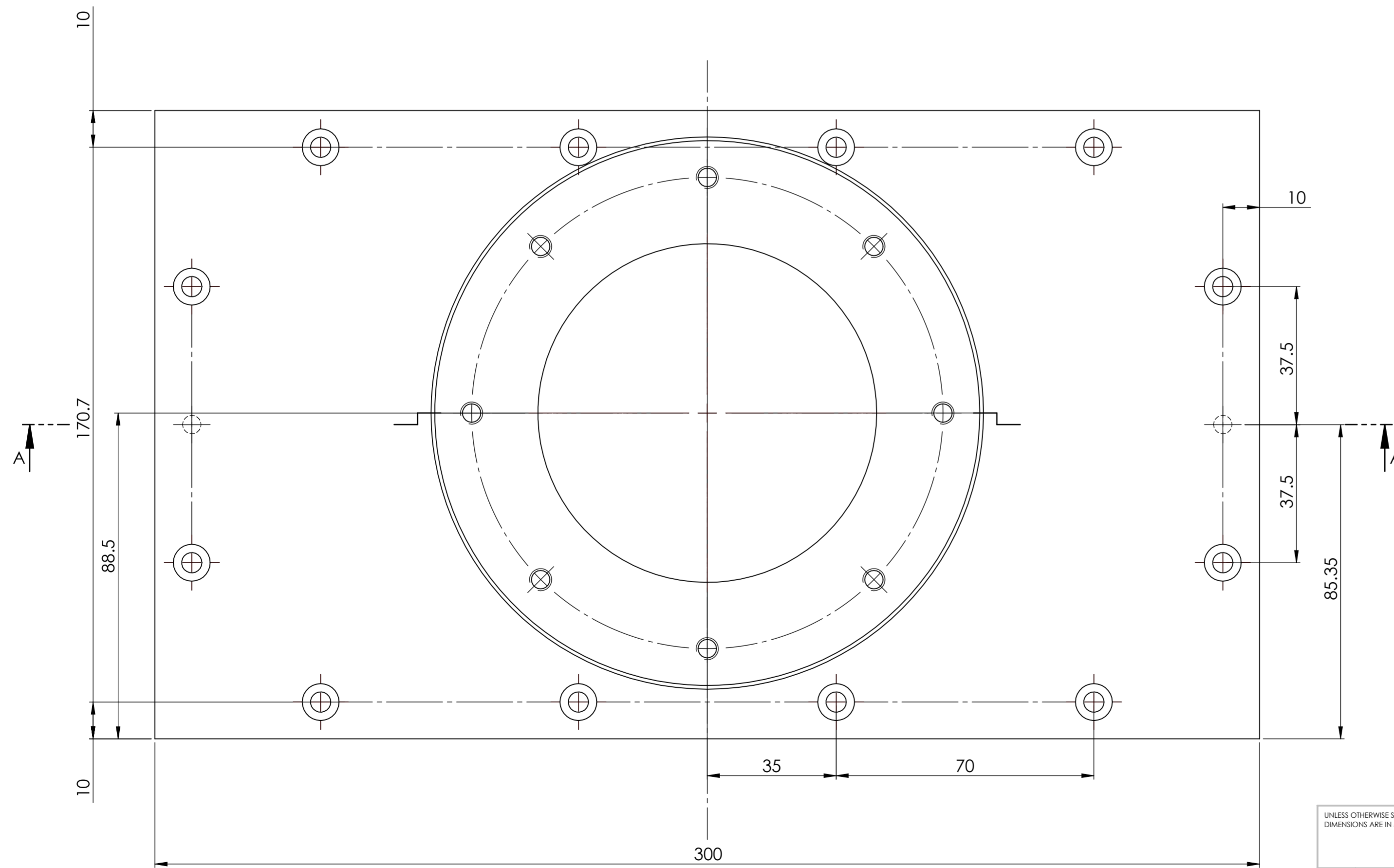
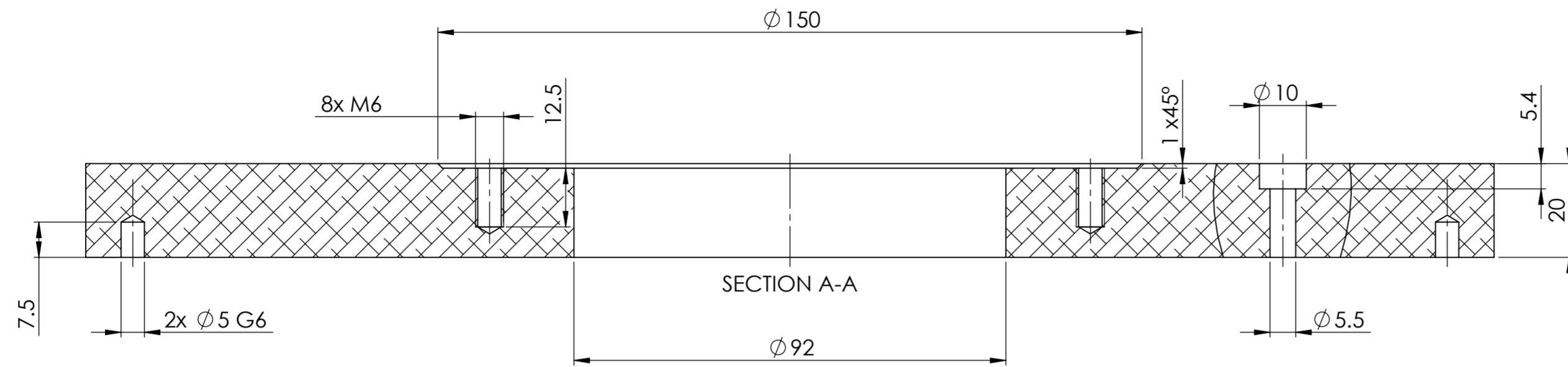




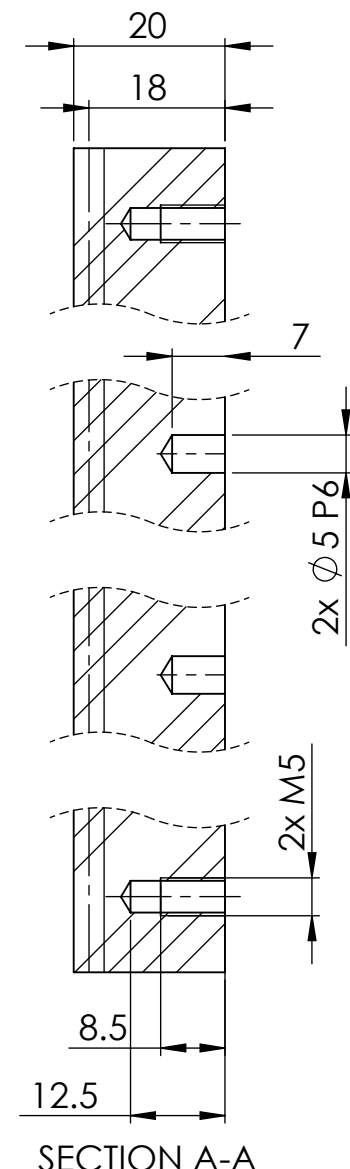
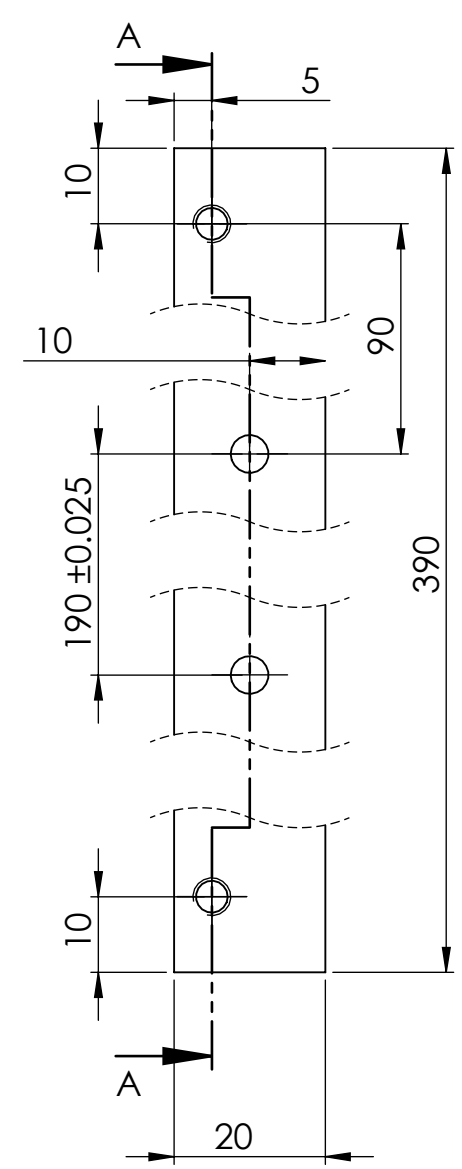
SECTION C-C
SCALE 1 : 1



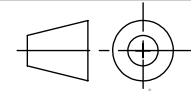
UNLESS OTHERWISE SPECIFIED: DIMENSIONS ARE IN MILLIMETERS		FINISH: ISO 8015 ISO 2768 - mK	DEBURR AND BREAK SHARP EDGES	DO NOT SCALE DRAWING	REVISION
DRAWN: Paulo Cardoso			SIGNATURE:	DATE: 17/09/2021	MATERIAL: AL 5XXX
CHECKED:			TITLE: CarterAssemb		A1
APPROVED:			DWG NO.:		SCALE: 1:2
MFG:			WEIGHT:		SHEET 1 OF 1
Q.A.:					



UNLESS OTHERWISE SPECIFIED: DIMENSIONS ARE IN MILLIMETERS			FINISH: ISO 8015 ISO 2768 - mK		DEBURR AND BREAK SHARP EDGES	DO NOT SCALE DRAWING	REVISION
NOTES: The part is simmetrical						TITLE:	
DRAWN	NAME	SIGNATURE	DATE	MATERIAL:	TITLE:		
CHKD	Paulo Cardoso		22/09/2021	AL 5xxx	DWG NO. Carter_Tampa A2		
APPVD					SCALE:1:1		
MFG					SHEET 1 OF 1		
Q.A.					WEIGHT:		



UNLESS OTHERWISE SPECIFIED: DIMENSIONS ARE IN MILLIMETERS		FINISH: ISO 8015 ISO 2768 - mK		DEBURR AND BREAK SHARP EDGES		DO NOT SCALE DRAWING		REVISION	
						GEAR RACK MODULE 2, 20° STRAIGHT TEETH			
NAME		SIGNATURE		DATE		MATERIAL:			
DRAWN Paulo Cardoso				28/07/2021		STEEL C45			
CHK'D						TITLE:			
APPV'D									
MFG						DWG NO.			
Q.A						Cremalheira			
						WEIGHT:		SCALE:1:1	
								SHEET 1 OF 1	



4 3 2 1

F

F

E

E

D

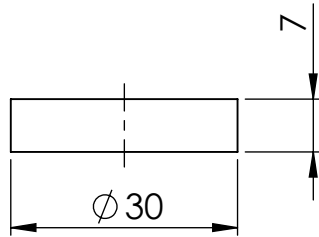
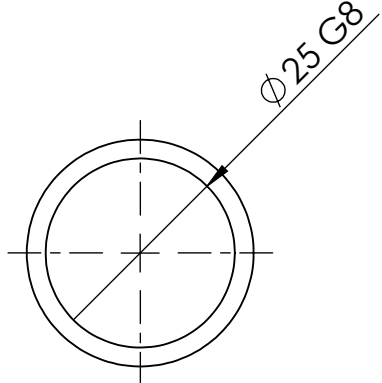
D

C

C

B

B



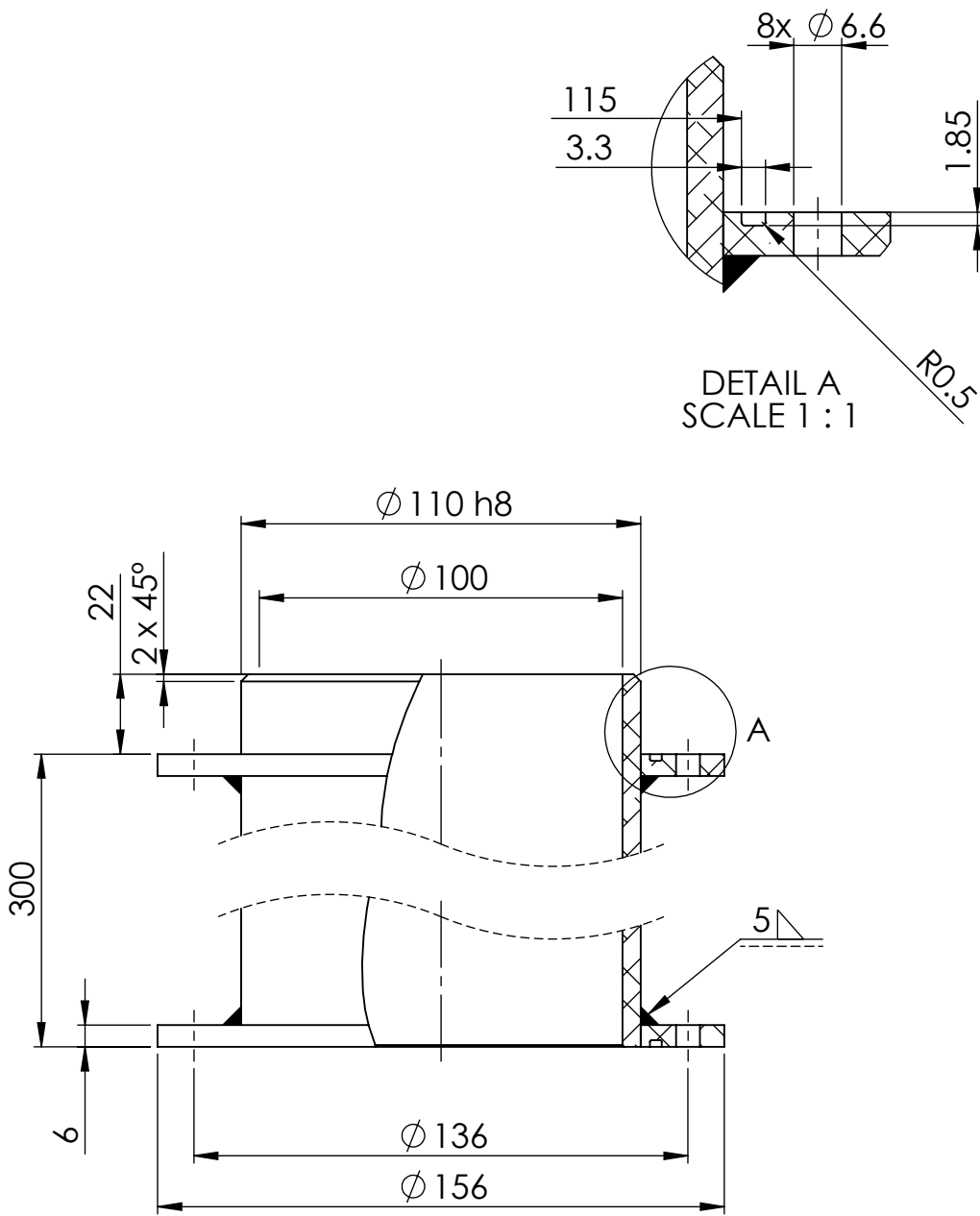
UNLESS OTHERWISE SPECIFIED: DIMENSIONS ARE IN MILLIMETERS	FINISH:	DEBURR AND BREAK SHARP EDGES	DO NOT SCALE DRAWING	REVISION
	ISO 8015 ISO 2768 - mK			

	NAME	SIGNATURE	DATE	MATERIAL:	TITLE:
DRAWN	Paulo Cardoso		07/09/2021	STEEL C45	
CHK'D					
APPV'D					
MFG					
Q.A					
				DWG NO.	Espacador
				WEIGHT:	SCALE:1:1
					SHEET 1 OF 1



A4

4 3 2 1



UNLESS OTHERWISE SPECIFIED: DIMENSIONS ARE IN MILLIMETERS	FINISH: ISO 8015 ISO 2768 - mK	DEBURR AND BREAK SHARP EDGES	DO NOT SCALE DRAWING	REVISION
--	--	------------------------------------	----------------------	----------

	NAME	SIGNATURE	DATE	MATERIAL:	TITLE:
DRAWN	Paulo Cardoso		01/08/2021	AL 5XXX	
CHK'D					
APPV'D					
MFG					
Q.A					
				DWG NO.	A4
				Espacador_Inf	
			WEIGHT:	SCALE:1:2	SHEET 1 OF 1



4 3 2 1

F

F

E

E

D

D

C

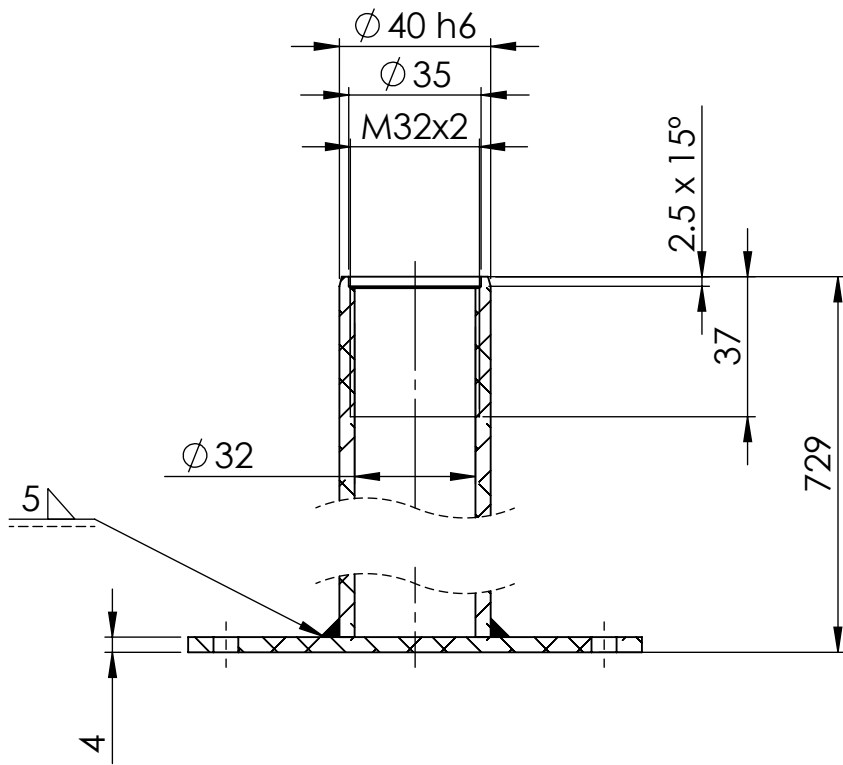
C

B

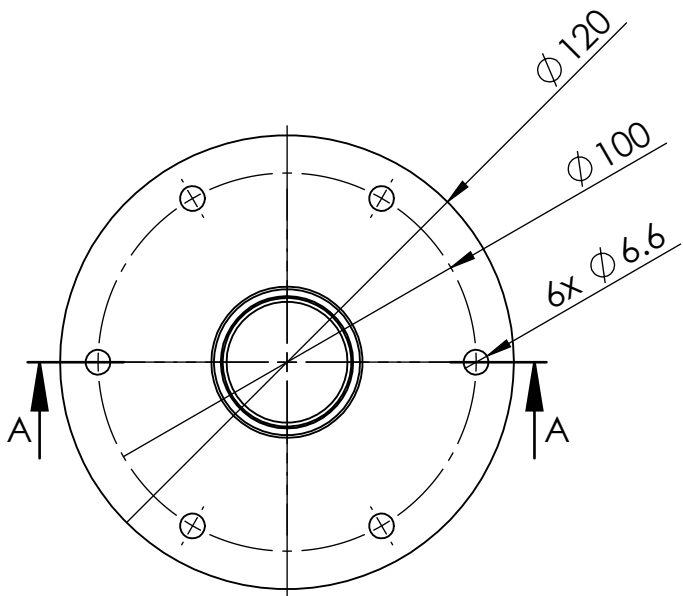
B

A

A



SECTION A-A



UNLESS OTHERWISE SPECIFIED:
DIMENSIONS ARE IN MILLIMETERS

FINISH:
ISO 8015
ISO 2768 - mK

DEBURR AND
BREAK SHARP
EDGES

DO NOT SCALE DRAWING

REVISION

	NAME	SIGNATURE	DATE	MATERIAL:	TITLE:
DRAWN	Paulo Cardoso		01/08/2021	AL 5xxx	
CHK'D					
APPV'D					
MFG					
Q.A					



DWG NO.

Haste

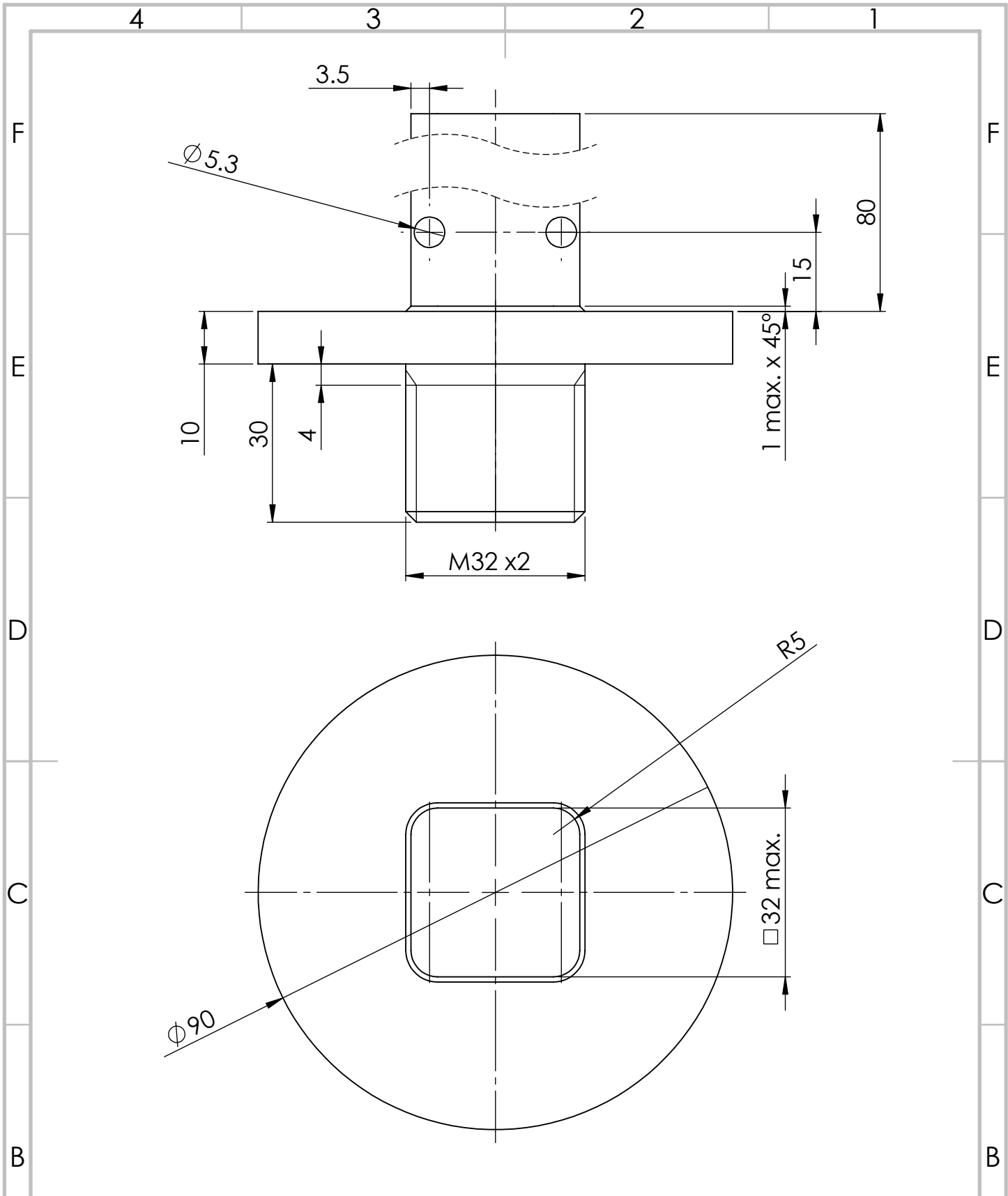
A4

WEIGHT:


SCALE:1:2

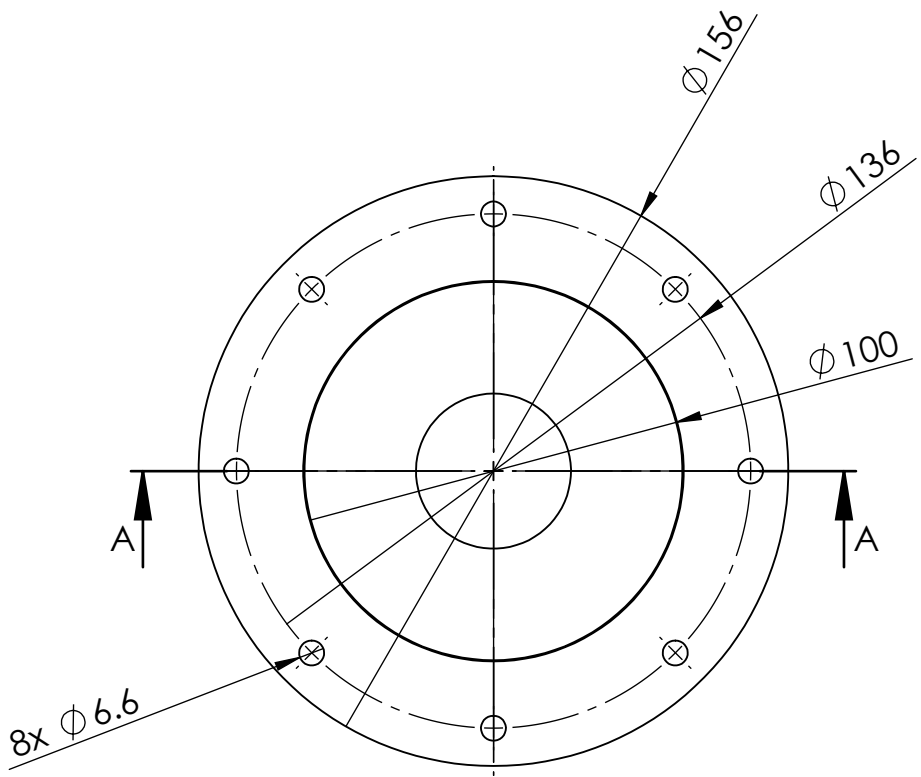
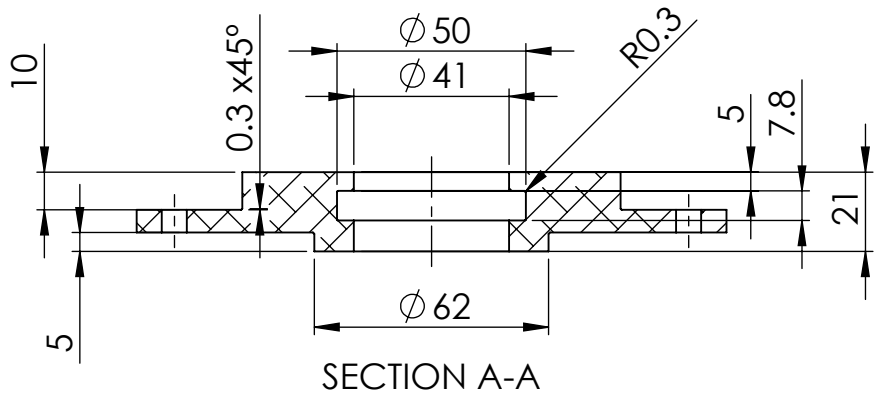
SHEET 1 OF 1

4 3 2 1



UNLESS OTHERWISE SPECIFIED: DIMENSIONS ARE IN MILLIMETERS	FINISH: ISO 8015 ISO 2768 - mH	DEBURR AND BREAK SHARP EDGES	DO NOT SCALE DRAWING	REVISION
--	--	------------------------------------	----------------------	----------

	NAME	SIGNATURE	DATE	MATERIAL:	TITLE:
DRAWN	Paulo Cardoso		22/09/2021	STEEL C45	
CHK'D					
APPV'D					
MFG					
Q.A					
					DWG NO.
					Juncao_Haste_Cremalheira
					A4
			WEIGHT:	SCALE:1:1	SHEET 1 OF 1



UNLESS OTHERWISE SPECIFIED:
DIMENSIONS ARE IN MILLIMETERS

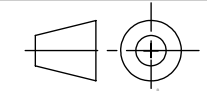
FINISH:
ISO 8015
ISO 2768 - mK

DEBURR AND
BREAK SHARP
EDGES

DO NOT SCALE DRAWING

REVISION

	NAME	SIGNATURE	DATE	MATERIAL:	TITLE:
DRAWN	Paulo Cardoso		02/08/2021	AL 5xxx	
CHK'D					
APPV'D					
MFG					
Q.A					

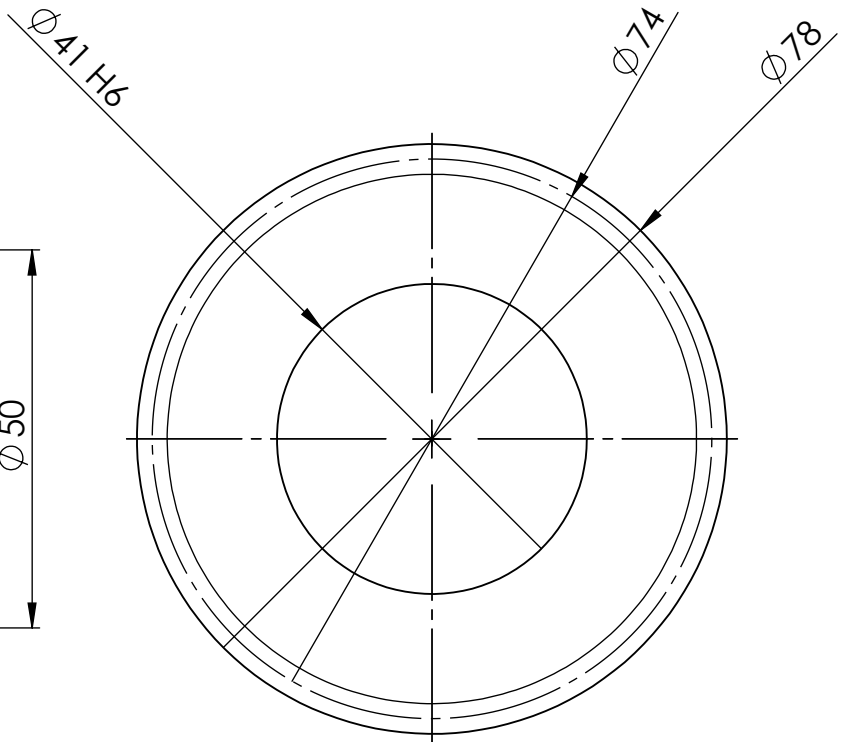
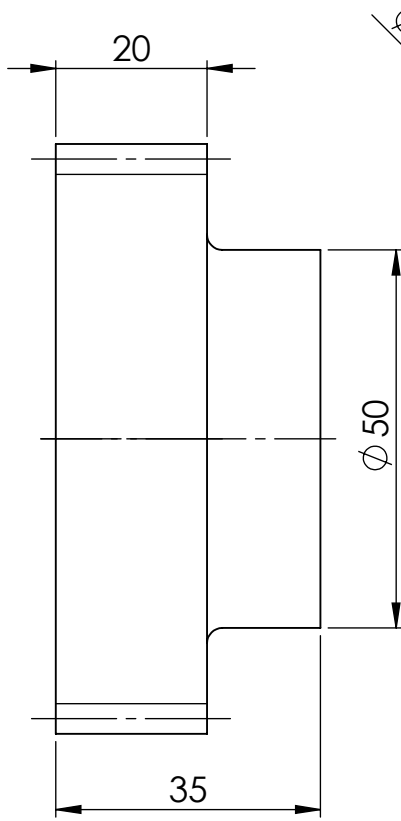


DWG NO. Juncao_Suporte_Haste A4

WEIGHT:

SCALE:1:2

SHEET 1 OF 1



UNLESS OTHERWISE SPECIFIED:
DIMENSIONS ARE IN MILLIMETERS

FINISH:

ISO 8015
ISO 2768 -mK

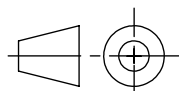
DEBURR AND
BREAK SHARP
EDGES

DO NOT SCALE DRAWING

REVISION

20° STRAIGHT TEETH SPURGEAR MODULE 2, 37 TEETH

	NAME	SIGNATURE	DATE
DRAWN	Paulo Cardoso		27/07/2021
CHK'D			
APPV'D			
MFG			
Q.A			



TITLE:

MATERIAL:

STEEL C45

DWG NO.

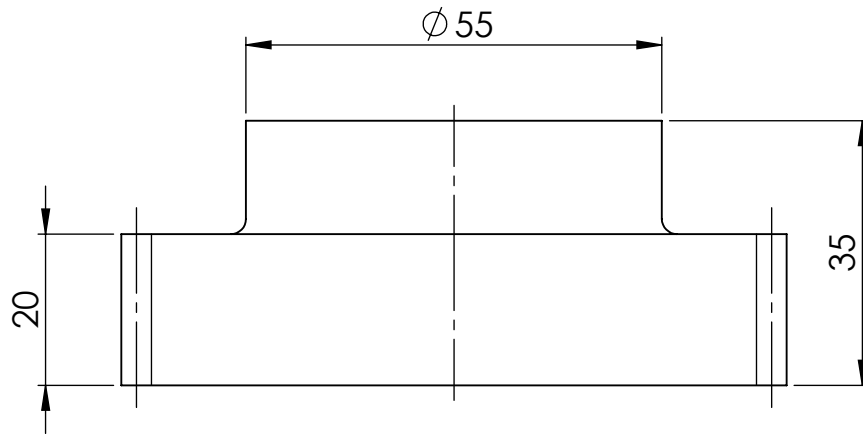
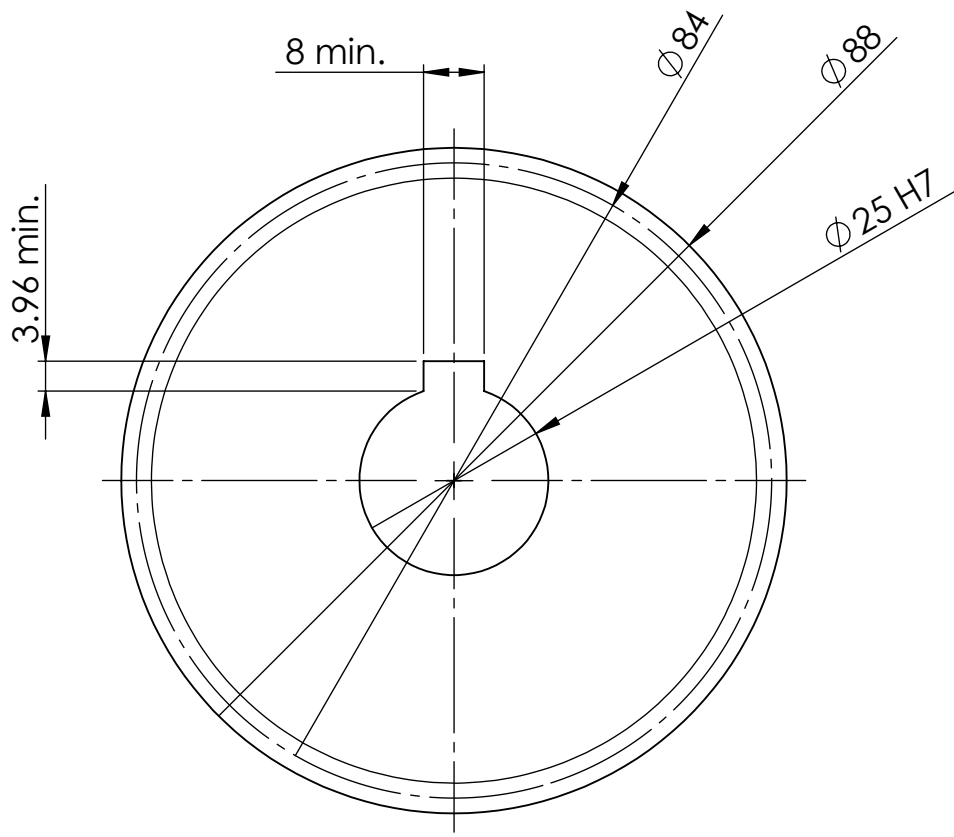
Roda_Entrada

A4

WEIGHT:

SCALE:1:1

SHEET 1 OF 1



UNLESS OTHERWISE SPECIFIED:
DIMENSIONS ARE IN MILLIMETERS
TOLERANCES: ISO 8015
GENERAL: ISO 2768 - mK

FINISH:

ISO 8015
ISO 2768 - mK

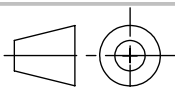
DEBURR AND
BREAK SHARP
EDGES

DO NOT SCALE DRAWING

REVISION

20° STRAIGHT TEETH SPURGEAR MODULE 2, 42 TEETH

	NAME	SIGNATURE	DATE	MATERIAL:	TITLE:
DRAWN	Paulo Cardoso		22/09/2021	STEEL C45	
CHK'D					
APPV'D					
MFG					
Q.A					



DWG NO.

Roda_Intermedia

A4

WEIGHT:

SCALE:1:1

SHEET 1 OF 1

4 3 2 1

F

F

E

E

D

D

C

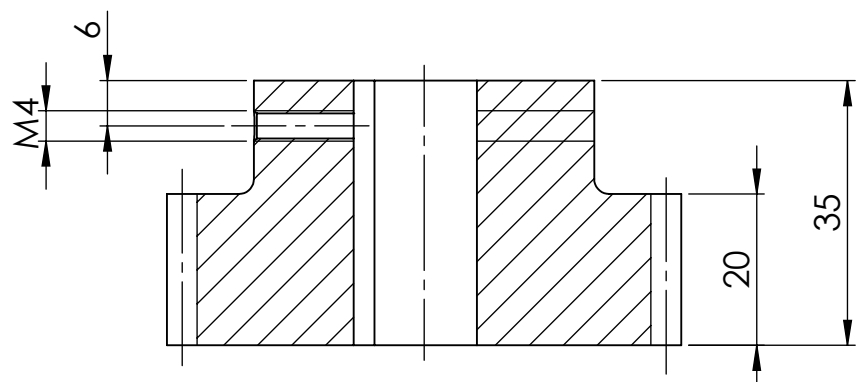
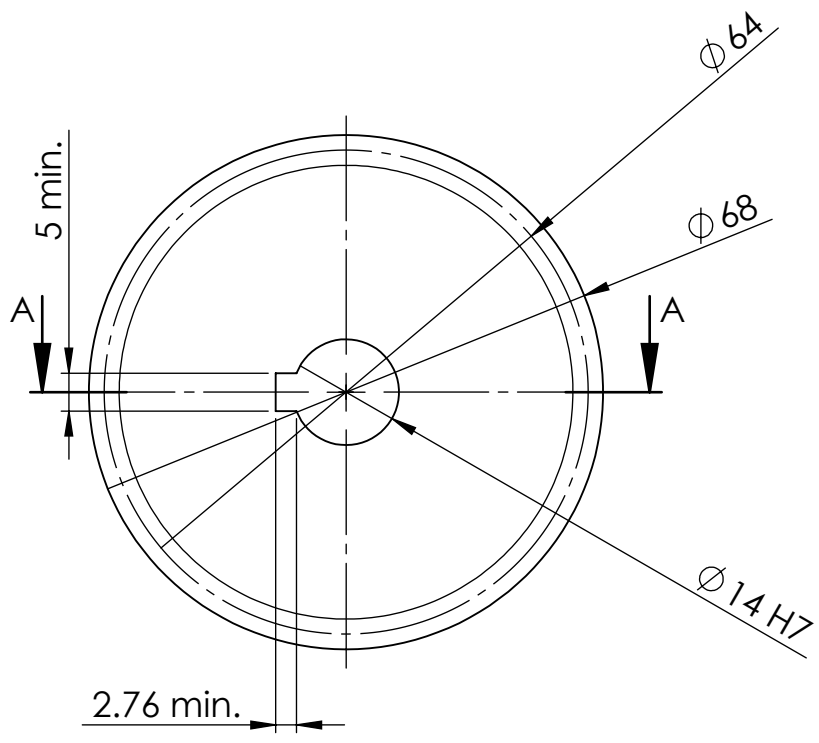
C

B

B

A

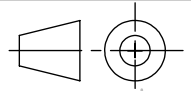
A

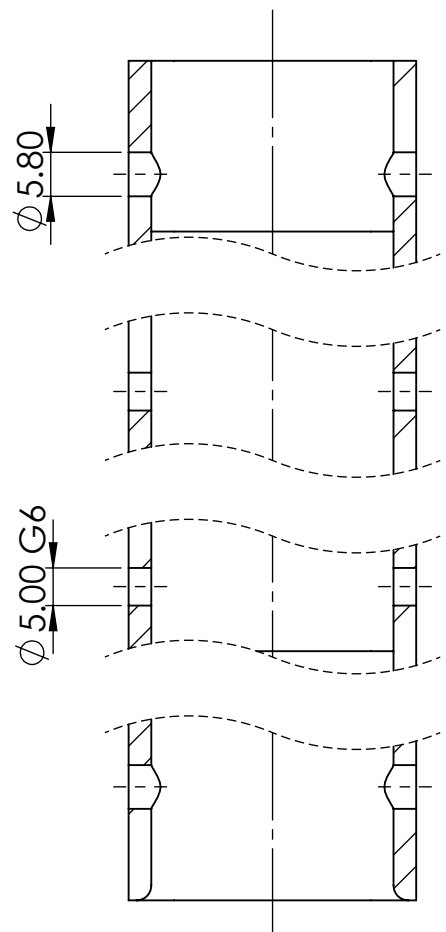
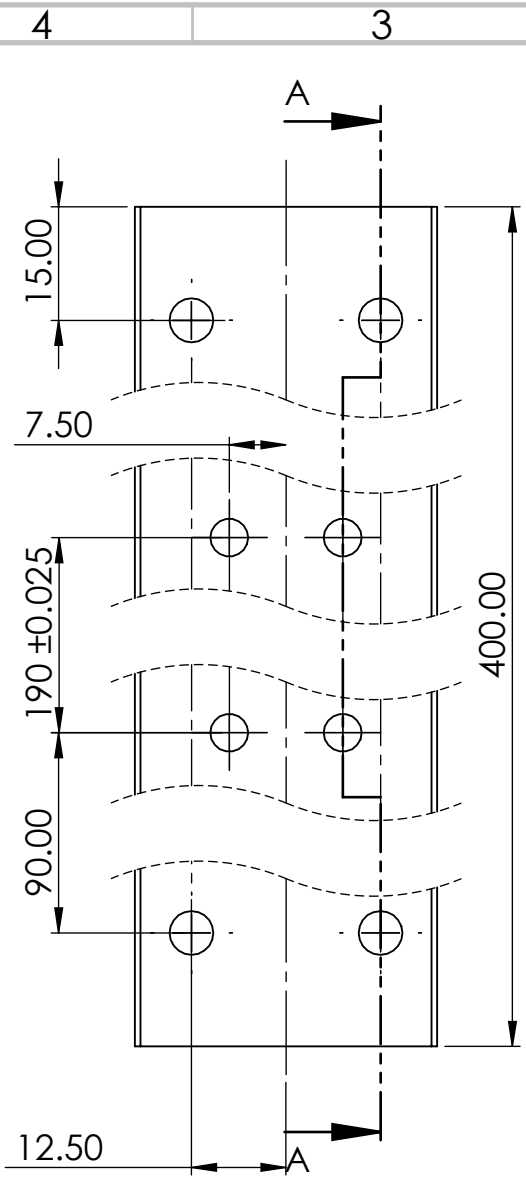


SECTION A-A

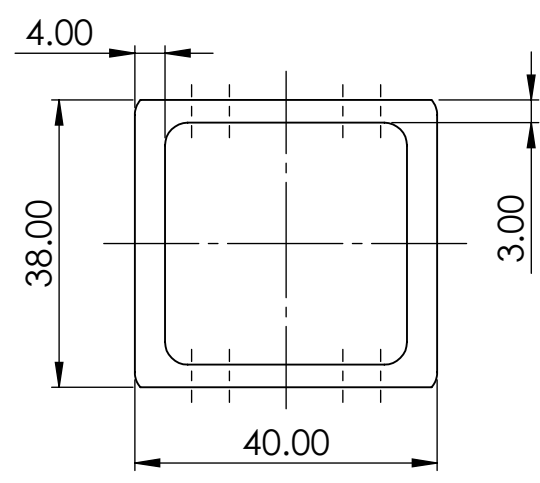
UNLESS OTHERWISE SPECIFIED: DIMENSIONS ARE IN MILLIMETERS	FINISH:	DEBURR AND BREAK SHARP EDGES	DO NOT SCALE DRAWING	REVISION
	ISO 8015 ISO 2768 - mK		20° STRAIGHT TEETH SPURGEAR MODULE 2, 32 TEETH	

	NAME	SIGNATURE	DATE	MATERIAL:	TITLE:
DRAWN	Paulo Cardoso		27/07/2021	STEEL C45	
CHK'D					
APPV'D					
MFG					
Q.A					
				DWG NO.	Roda_Saida
				SCALE:1:1	SHEET 1 OF 1



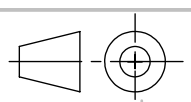


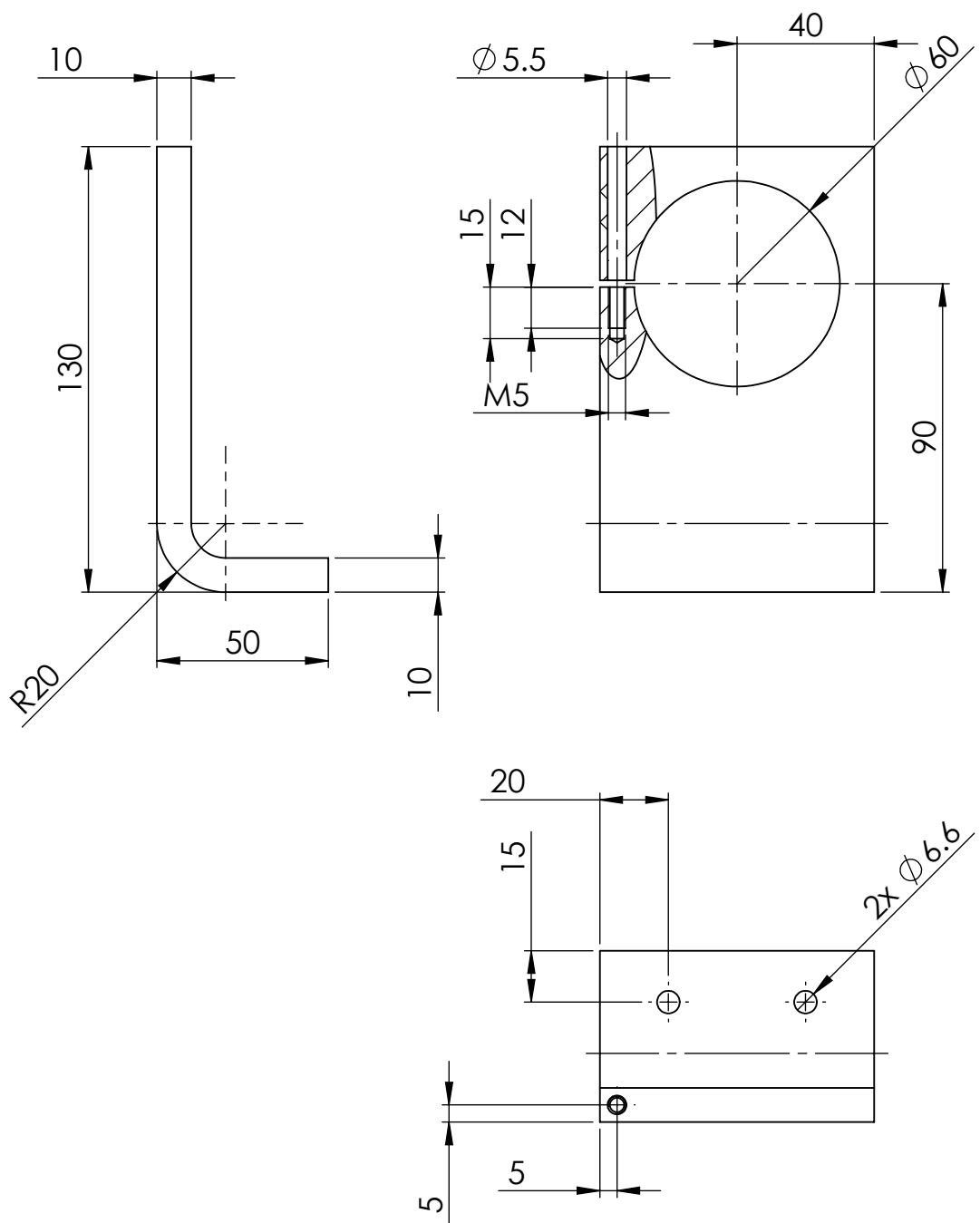
SECTION A-A



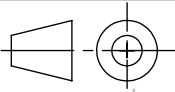
UNLESS OTHERWISE SPECIFIED: DIMENSIONS ARE IN MILLIMETERS	FINISH: ISO 8015 ISO 2768 - mK	DEBURR AND BREAK SHARP EDGES	DO NOT SCALE DRAWING	REVISION

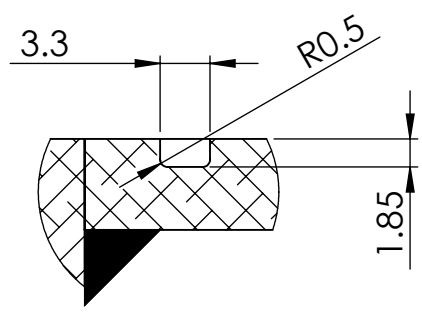
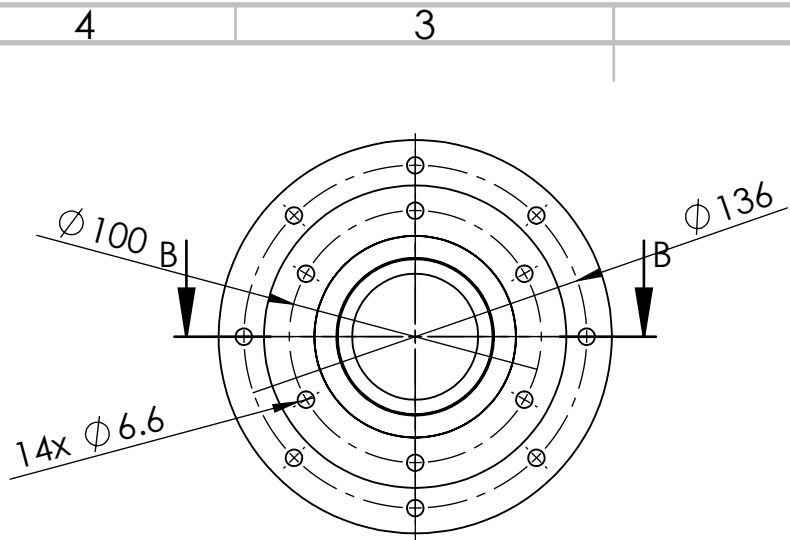
NAME	SIGNATURE	DATE	MATERIAL:	TITLE:
DRAWN Paulo Cardoso		28/07/2021	STEEL C45	
CHK'D				
APPV'D				
MFG				
Q.A				
WEIGHT:			DWG NO.	A4
			Suporte_cremalheiras	
SCALE:1:1			SHEET 1 OF 1	



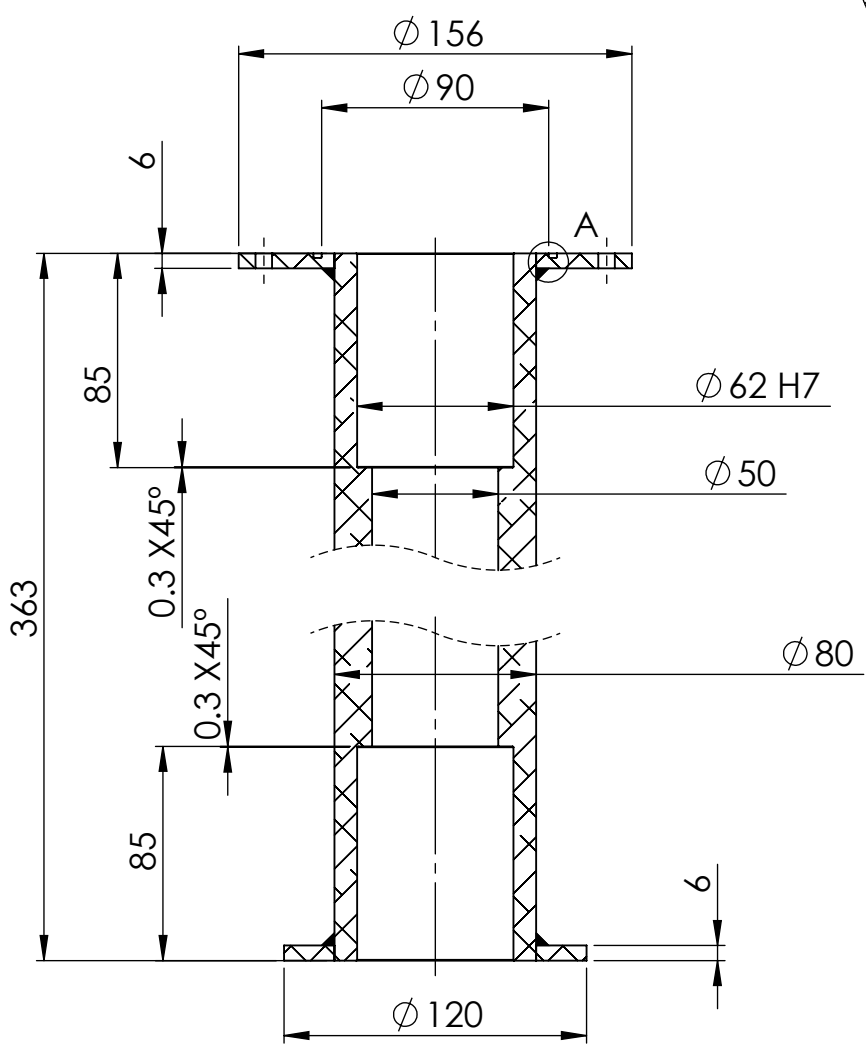


UNLESS OTHERWISE SPECIFIED: DIMENSIONS ARE IN MILLIMETERS	FINISH: ISO 8015 ISO 2768 - mK	DEBURR AND BREAK SHARP EDGES	DO NOT SCALE DRAWING	REVISION
--	--	------------------------------------	----------------------	----------

	NAME	SIGNATURE	DATE	MATERIAL:	TITLE:
DRAWN	Paulo Cardoso		18/09/2021	AL 5xxx	
CHK'D					
APPV'D					
MFG					
Q.A					
					DWG NO.
					Suporte_Gerador
				WEIGHT:	SCALE: 1:2
					SHEET 1 OF 1



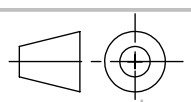
DETAIL A
SCALE 2 : 1



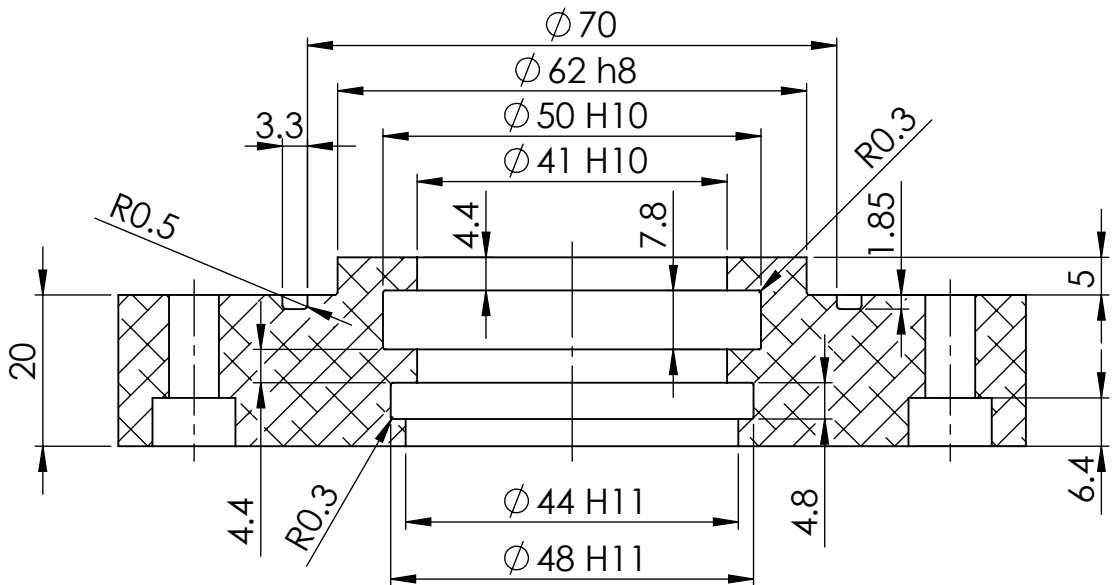
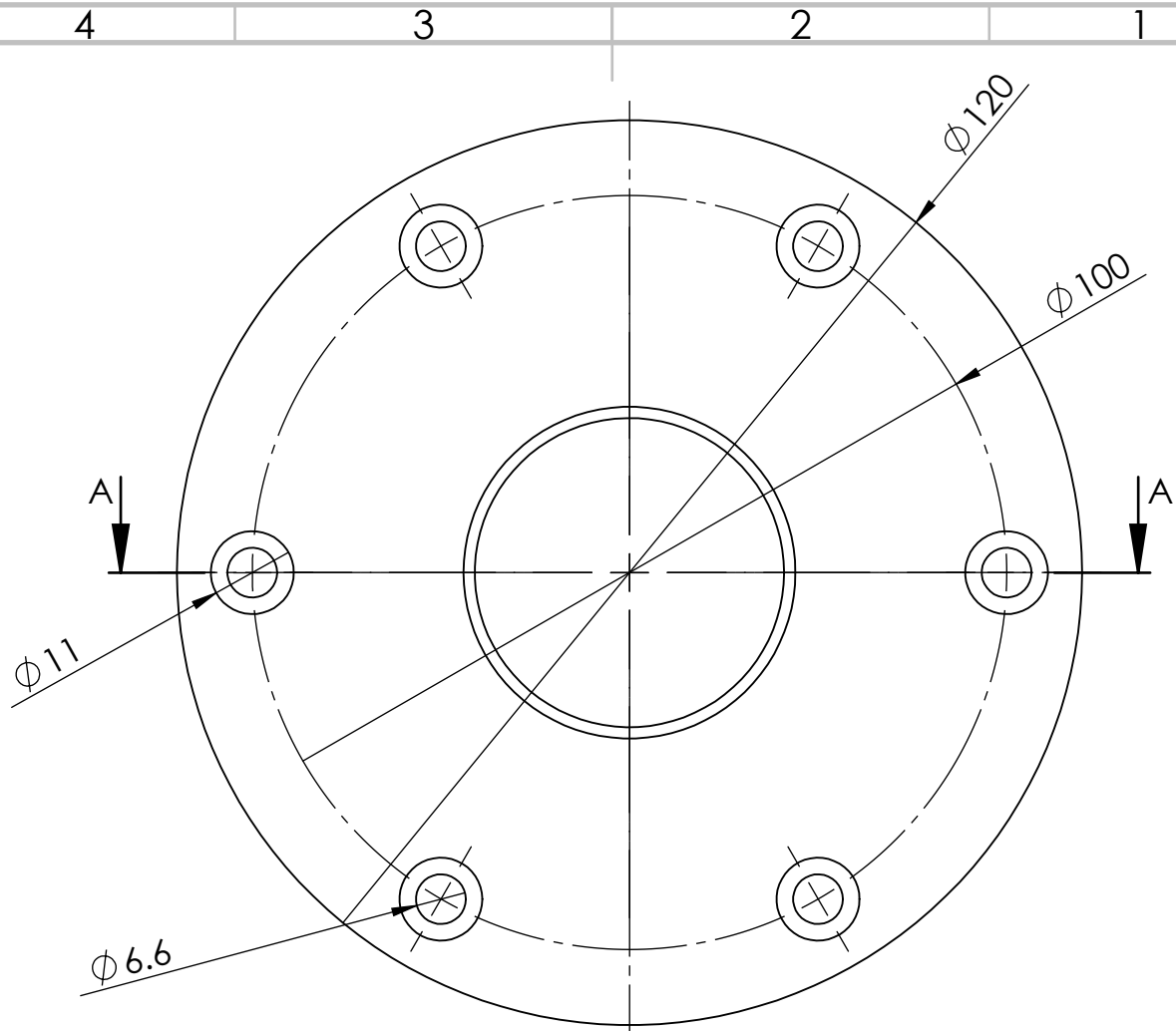
SECTION B-B

UNLESS OTHERWISE SPECIFIED: DIMENSIONS ARE IN MILLIMETERS		FINISH: ISO 8015 ISO 2768 - mK		DEBURR AND BREAK SHARP EDGES		DO NOT SCALE DRAWING		REVISION	
--	--	--	--	------------------------------------	--	----------------------	--	----------	--

NAME		SIGNATURE		DATE		MATERIAL:		TITLE:	
DRAWN Paulo Cardoso				09/09/2021		AL 5xxx			
CHK'D									
APPV'D									
MFG									
Q.A									
						DWG NO.		Suporte_Haste	
								A4	



WEIGHT:		SCALE:1:3		SHEET 1 OF 1	
---------	--	-----------	--	--------------	--



SECTION A-A

UNLESS OTHERWISE SPECIFIED:
DIMENSIONS ARE IN MILLIMETERS

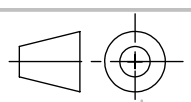
FINISH:
ISO 8015
ISO 2768 - mK

DEBURR AND
BREAK SHARP
EDGES

DO NOT SCALE DRAWING

REVISION

	NAME	SIGNATURE	DATE	MATERIAL:	TITLE:
DRAWN	Paulo Cardoso		22/09/2021	AL 5xxx	
CHK'D					
APPV'D					
MFG					
Q.A					



DWG NO.

Tampa_Inf

A4

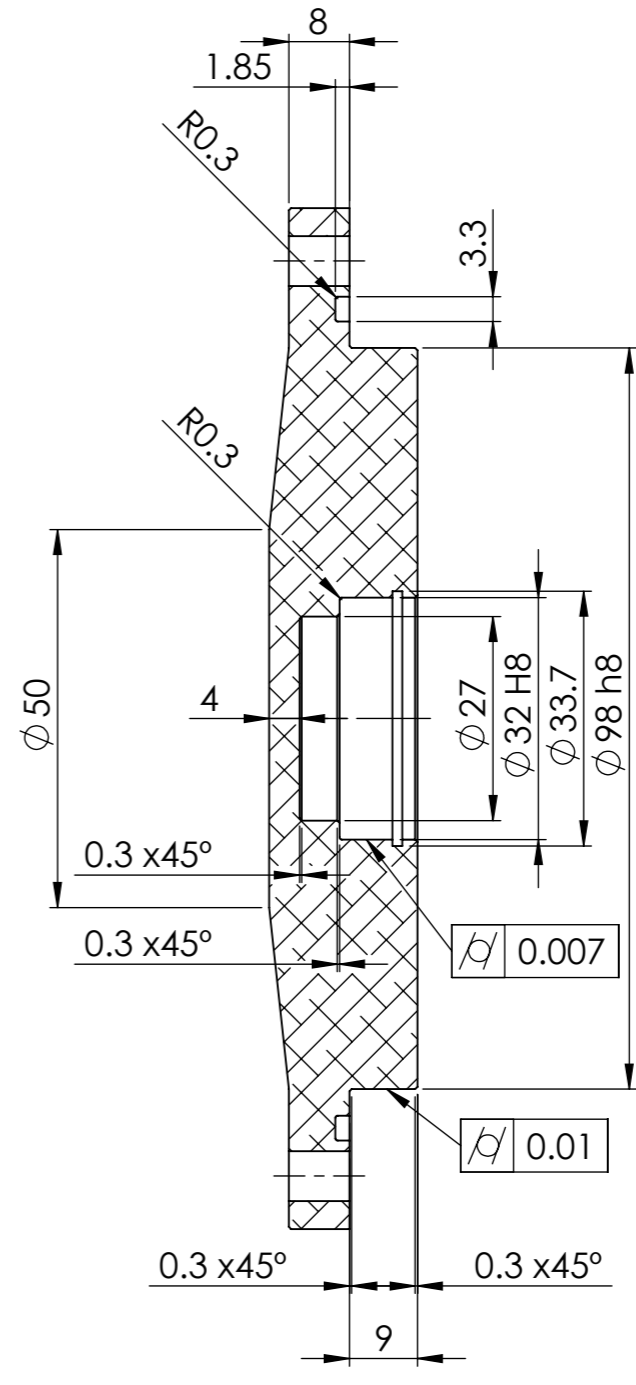
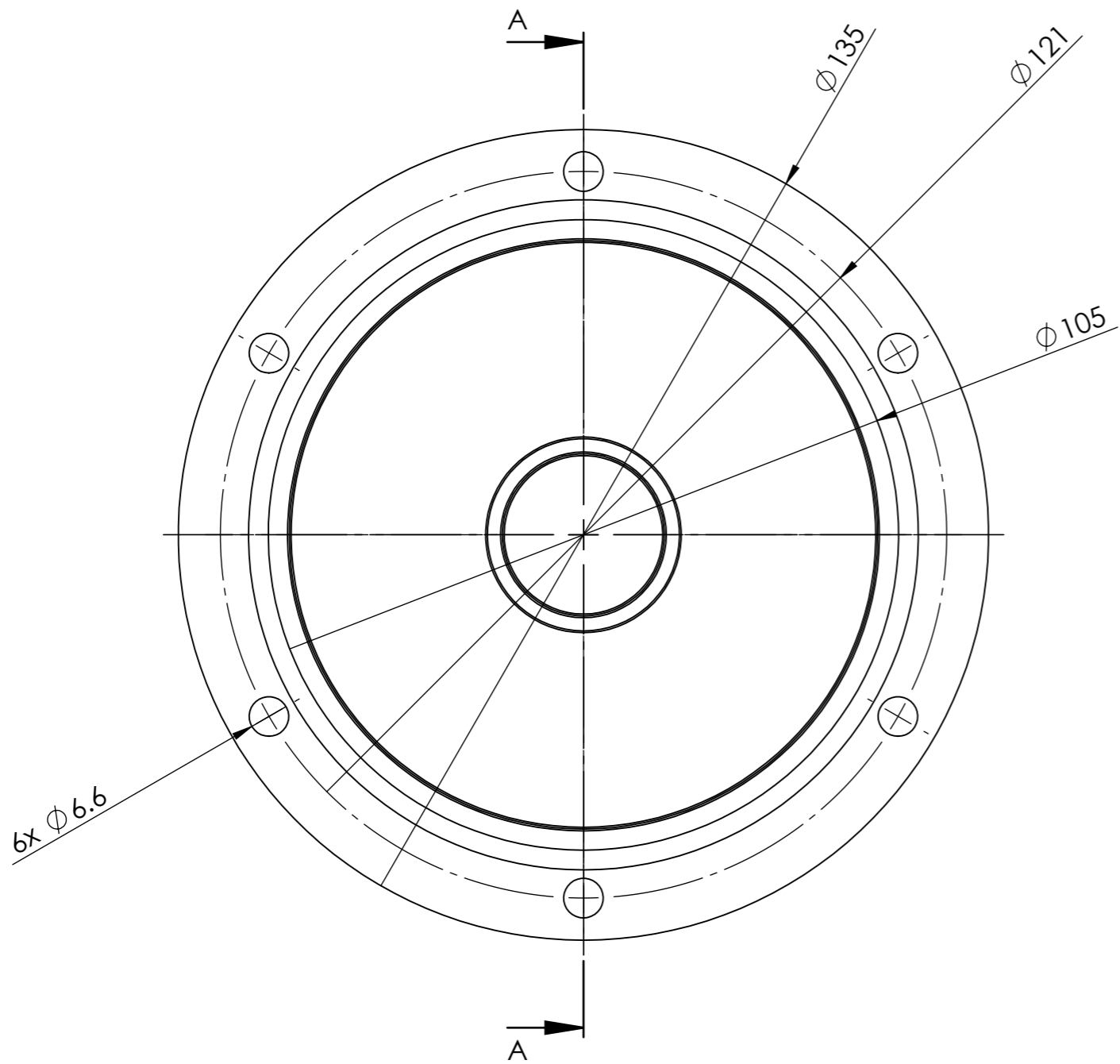
WEIGHT:

SCALE:1:1

SHEET 1 OF 1

8 7 6 5 4 3 2 1

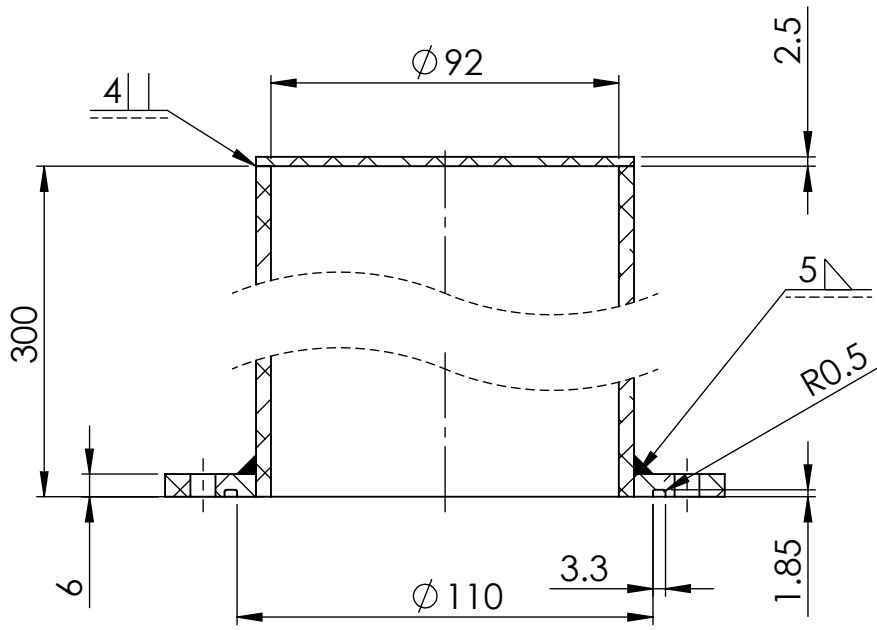
F
E
D
C
B
A



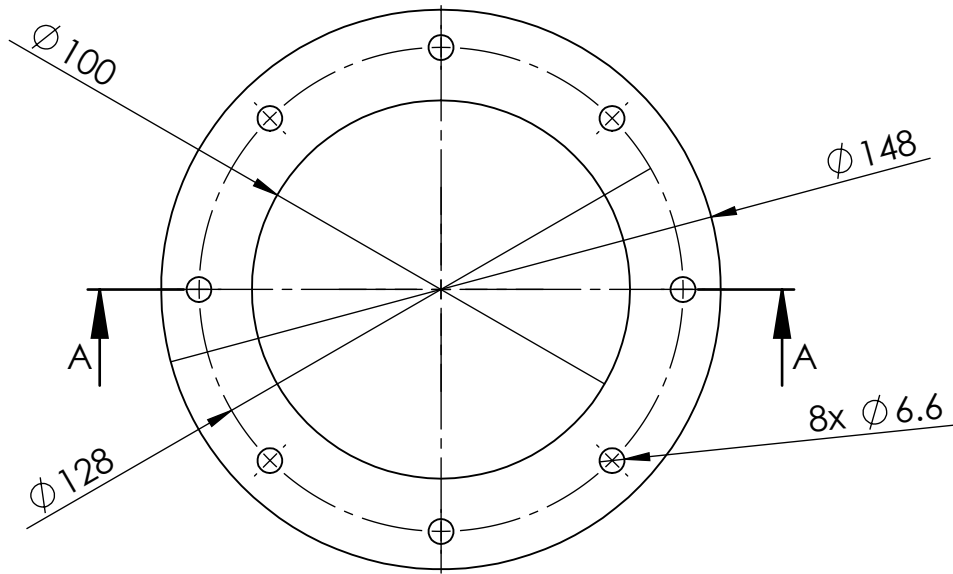
SECTION A-A

UNLESS OTHERWISE SPECIFIED: DIMENSIONS ARE IN MILLIMETERS		FINISH: ISO 8015 ISO 2768 - mK		DEBURR AND BREAK SHARP EDGES		DO NOT SCALE DRAWING		REVISION	
DRAWN Paulo Cardoso		SIGNATURE		DATE 02/08/2021		MATERIAL: AL 5xxx		TITLE:	
CHK'D		APPV'D		MFG		Q.A		DWG NO. Tampa_Lateral	
WEIGHT:		SCALE:1:1		SHEET 1 OF 1		A3			

8 7 6 5 4 3 2 1



SECTION A-A



UNLESS OTHERWISE SPECIFIED:
DIMENSIONS ARE IN MILLIMETERS

FINISH:
ISO 8015
ISO 2768 - mK

DEBURR AND
BREAK SHARP
EDGES

DO NOT SCALE DRAWING

REVISION

	NAME	SIGNATURE	DATE	MATERIAL:	TITLE:
DRAWN	Paulo Cardoso		01/08/2021	AL 5xxx	
CHK'D					
APPV'D					
MFG					
Q.A					



DWG NO.

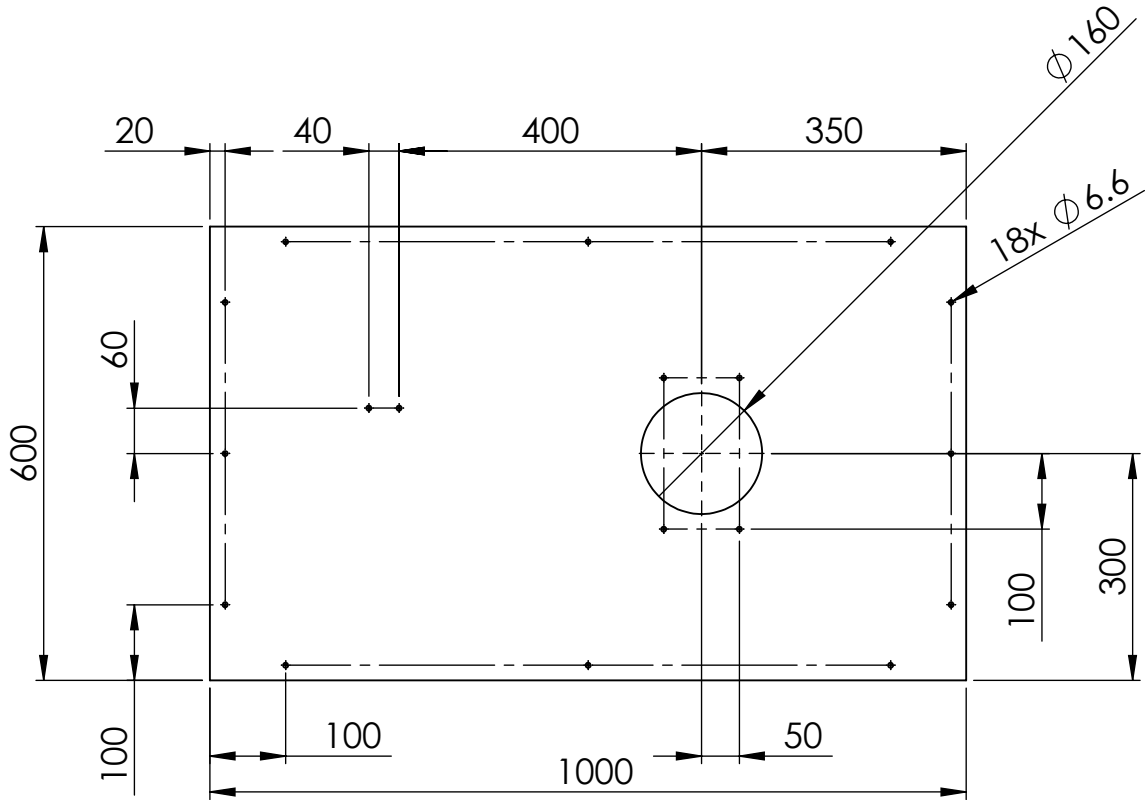
Tampa_Sup

A4

WEIGHT:

SCALE:1:2

SHEET 1 OF 1



Thickness: 6mm

UNLESS OTHERWISE SPECIFIED:
DIMENSIONS ARE IN MILLIMETERS

FINISH:

ISO 8015
ISO 2768 - mK

DEBURR AND
BREAK SHARP
EDGES

DO NOT SCALE DRAWING

REVISION

	NAME	SIGNATURE	DATE	MATERIAL:	TITLE:
DRAWN	Paulo Cardoso		20/09/2021	AL 5xxx	
CHK'D					
APPV'D					
MFG					
Q.A					



DWG NO.

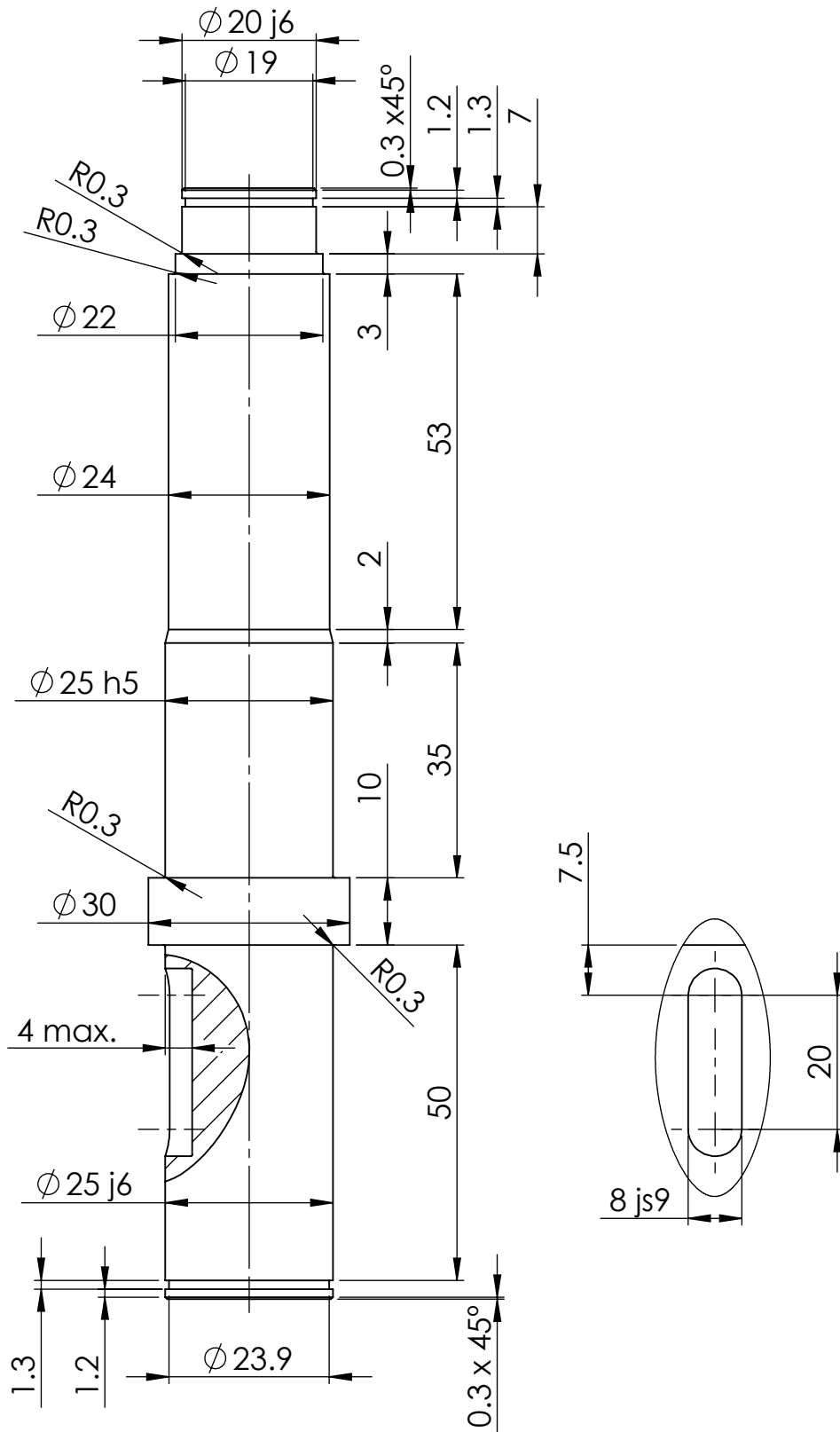
Tampo_Mesa

A4

WEIGHT:

SCALE:1:10

SHEET 1 OF 1



UNLESS OTHERWISE SPECIFIED:
DIMENSIONS ARE IN MILLIMETERS

FINISH:

ISO 8015
ISO 2768 - mK

DEBURR AND
BREAK SHARP
EDGES

DO NOT SCALE DRAWING

REVISION

	NAME	SIGNATURE	DATE	MATERIAL:	TITLE:
DRAWN	Paulo Cardoso		27/07/2021	STEEL C45	
CHK'D					
APPV'D					
MFG					
Q.A					



DWG NO.

Veio

A4

WEIGHT:

SCALE:1:1

SHEET 1 OF 1